MECHANOTRANSDUCTION AND EPIDERMAL GROWTH FACTOR RECEPTOR SIGNALING IN BLADDER EPITHELIUM

by

Elena Marie Balestreire

B.S., Carnegie Mellon University, 2001

Submitted to the Graduate Faculty of

The School of Medicine in partial fulfillment

of the requirements for the degree of

Doctor of Philosophy

University of Pittsburgh

2007

UNIVERSITY OF PITTSBURGH

SCHOOL OF MEDICINE

This dissertation was presented

by

Elena Marie Balestreire

It was defended on

June 4th, 2007

and approved by

Committee Chair: Thomas Kleyman, Professor, Department of Medicine

Lori Birder, Assistant Professor, Department of Medicine

Jeffrey Brodsky, Professor, Department of Biological Sciences

Rebecca Hughey, Associate Professor, Department of Medicine

Linton Traub, Associate Professor, Department of Cell Biology & Physiology

Dissertation Advisor: Gerard Apodaca, Professor, Department of Medicine

MECHANOTRANSDUCTION AND EPIDERMAL GROWTH FACTOR SIGNALING IN BLADDER EPITHELIUM

Elena Marie Balestreire, Ph.D.

University of Pittsburgh, 2007

In response to changes in intralumenal pressure, the urinary bladder modulates its mucosal surface to accommodate a wide range of urine volumes upon filling and voiding. During bladder stretch, umbrella cells that line the mucosal surface of the bladder undergo changes in surface area mediated by the exocytosis and endocytosis of subapical discoidal vesicles. While a number of signaling factors are required for this process, how these signals interact with each other and whether they are integrated in any manner is not known. The identification of the epidermal growth factor receptor (EGFR) as an apical receptor for stretch-induced HB-EGF signaling provides a previously unrecognized function for this versatile receptor in bladder physiology. It appears that the EGFR signaling is able to regulate protein synthesis via a MAPK signaling pathway, which is required for the late response of the tissue to prolonged stretch. The transactivation of EGFR via a metalloproteinase-dependent pathway opens the possibility that several previously recognized stretch-induced signals function upstream to stimulate EGFR activity in an integrated signaling pathway. The importance of tight regulation of EGFR activity in the bladder is highlighted by its role in bladder carcinoma pathophysiology, and future studies of this pathway may provide insights that lead to diagnostic and therapeutic advances.

TABLE OF CONTENTS

LIST OF TABLES

LIST OF FIGURES

PREFACE

First and foremost, I would like to express my gratitude to my dissertation advisor, Dr. Gerry Apodaca, for his guidance and mentorship over the past several years. Gerry taught me how to explore a new area of science and really helped me mature as a scientist. I would also like to thank my committee members, Drs. Tom Kleyman, Rebecca Hughey, Linton Traub, Jeff Brodsky, and Lori Birder, for their advice and support throughout my dissertation research.

I would like to thank the Apodaca lab members for their camaraderie. In particular, I would like to thank Asli Oztan for always being a friend in the lab. I am grateful for the wonderful group of people I worked with in the Renal Division and Department of Cell Biology & Physiology; you have created a friendly community of scientists and a wonderful workplace.

I would like to thank my family for always supporting me – you are a very important part of my life, and I am so lucky to be in Pittsburgh during these graduate years. Kristen, you are an exceptional editor. I really appreciate all of the times you've helped me by proofreading at all hours of the night, even down to my last dissertation draft! Marie, you can always bring a smile to my face. Mom and Dad, you have always encouraged me in all of my endeavors, and I cannot thank you enough for everything you've done for me. Last but not least, Matthew, thank you for making me happy. I know we can accomplish anything together - this clock never seemed so alive.

ABBREVIATIONS

ADAM	A disintegrin and metalloproteinase
ADP	Adenosine diphosphate
AMP	Adenosine monophosphate
ANGII	Angiotensin II
ATP	Adenosine triphosphate
AUM	Asymmetrical unit membrane
BFA	Brefeldin A
BSA	Bovine serum albumin
cAMP	Cyclic adenosine monophosphate
EGF	Epidermal growth factor
EGFR	Epidermal growth factor receptor; ErbB1
ERBB	Erythroblastoma virus B homology proteins
ERK	Extracellular regulated kinase
GPCR	G-protein coupled receptor
GTP	Guanosine triphosphate
HB-EGF	Heparin-binding EGF-like protein
JAK	Janus kinase

MALDI-MS/MS	Matrix-assisted laser desorption/ionization tandem mass spectrometry
MAPK	Mitogen-activated protein kinase
MDCK	Madin-Darby canine kidney
MMP	Matrix metalloprotinase
PKA	Protein kinase A
SNAP23	Synaptosome-associated protein, 23 kDa
TACE	Tumor necrosis factor alpha converting enzyme
TGF-α	Transforming growth factor alpha
TRPV	Transient receptor protein channels
UP	Uroplakin
UPIa	Uroplakin Ia
UPIb	Uroplakin Ib
UPII	Uroplakin II
UPIII	Uroplakin III
UPIIIa	Uroplakin IIIa
UPIIIb	Uroplakin IIIb
UPEC	Uropathogenic *Escherichia coli*
UTP	Uridine triphosphate
VUR	Vesicoureteral reflux

1.0 INTRODUCTION

The urinary bladder is a distensible sac situated at the end of the urinary excretory system whose main function is to store urine filtered by the kidneys until the time of voiding. The bladder is highly impermeable, which allows it to contain urine without leakage into underlying tissues. Upon micturition, the detrusor muscle, which surrounds the organ, compresses the sac and its sphincters relax to empty the bladder.

Beyond its role as a simple sac that stores urine, new data indicate that the bladder is a dynamic organ that responds to its environment through the coordinated action of its component tissue types, including the bladder epithelium (also termed the uroepithelium), smooth muscle, connective tissue, nervous tissue, interstitial cells, and vasculature. This coordination requires communication and signaling among the various cell types, and the specific molecules and pathways that are required are only beginning to be understood. The purpose of my work is to further our understanding of the signaling mechanisms that are activated in response to stretch that occurs during bladder filling and to examine how these signaling pathways may function in a coordinated manner.

During bladder stretch, various signals control the dynamic insertion and removal of membrane from the bladder's apical surface within the superficial umbrella cells of the uroepithelium. These membrane trafficking events must occur while maintaining the bladder's impermeable barrier to urine. Disruption of this barrier results in the clinical symptoms of pain,

urinary frequency, and urgency [1, 2] and is observed in several pathological states, such as urinary interstitial cystitis, noxious chemical exposure, bacterial infection, or tumor growth [3]. By studying the signaling and membrane trafficking pathways in the stretched bladder, one can begin to appreciate the complex regulation of these processes and how they are dysregulated in bladder disease states.

1.1 ANATOMY OF THE BLADDER

The human urinary bladder, a sac-shaped organ with three openings, is situated in the abdominopelvic cavity (Figure 1.1). The two ureters carry urine into the bladder from the kidneys, and the single urethra at the base of the bladder is the sphincter-controlled orifice that allows excretion of the urine during voiding. These orifices are located at the "neck" or outlet of the bladder, forming a triangular "trigone" region at the neck of the bladder. The other regions of the bladder are the "dome" region at the top of the bladder, which lies opposite the neck, and the large, central "equatorial" region, which comprises the majority of the bladder between the neck and dome [4]. The bladder is endodermic in origin, and its developmental precursor is the urogenital sinus [5]. Its general anatomy is conserved among mammals, and the bladder is comprised of several distinct tissue types, which are discussed in the following subsections.

1.1.1 Detrusor muscle

The detrusor muscle is the outermost tissue of the bladder, and it is composed of three layers of smooth muscle that surround the entire organ: inner and outer longitudinal layers and a middle

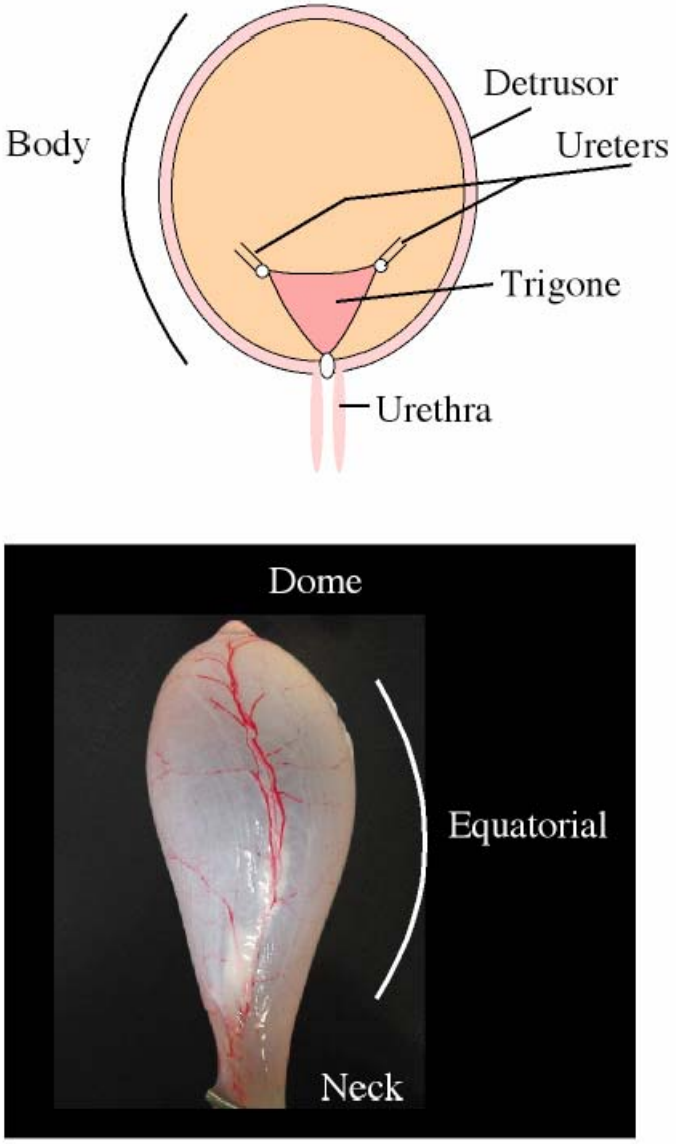

Figure 1.1: Anatomy of the bladder.

The top diagram depicts the body of the bladder, surrounded by the detrusor muscle. The trigone region between the three bladder orifices (2 ureters and urethral openings) is depicted. The bottom image is an excised rabbit bladder, demonstrating the neck (which describes the location near the urethra), opposite of the dome, with the large equatorial region in between.

circular layer of smooth muscle [4, 6]. Bladder voiding occurs upon contraction of the detrusor muscle and relaxation of the internal sphincter, which is a band of smooth muscle that surrounds the bladder neck, and the external sphincter. The latter allows the expulsion of urine over the interureteric ridge of smooth muscle between the neck region and the urethra [6]. The human bladder can hold a maximum of ~ 500 ml of urine. As it fills, the bladder unfolds and enlarges at both the tissue and cellular levels, a process that generates and relies on complex signal transduction, as described below.

1.1.2 Vasculature

The bladder receives its blood supply from a capillary bed branching off the superior and inferior vesical arteries, along with branches of the umbilical artery and vaginal artery [4]. The vesical venous plexus drains the bladder's blood supply, and its lymph drainage is to the internal and external iliac lymph nodes.

1.1.3 Innervation

The bladder has recently become appreciated as a sensory organ [2, 7], and its innervation is largely by the vesical nervous plexus. The bladder has an afferent nerve supply, as well as sympathetic and parasympathetic innervation from the thoracolumbar and sacral levels of the spinal cord [8]; in humans there are also autonomic ganglia cells present in the adventitia. The bladder "sacral reflex" describes the neuronal signaling pathway associated with voiding, which humans can voluntarily override. Upon bladder wall stretching, impulses pass from the bladder,

through the spinal cord (S2-S4), and back to the bladder, which cause concurrent contraction of the detrusor and relaxation of the sphincters, allowing the bladder to empty.

In addition to this voiding signaling pathway, nerves are located in close proximity to the uroepithelium and are thought to be involved in transmitting signals among bladder tissue types. Autonomic and afferent nerves, located in the muscle layers, in serosa, and between uroepithelial cells [9, 10], are thought to transmit signals in response to the uroepithelial release of various signals such as ATP or acetylcholine [7]. These multiple pathways of innervation set the stage for the transmission of signals arising from and among the various cell types that comprise the bladder.

1.1.4 Interstitial Cells

There are several types of interstitial cells, located beneath the uroepithelium, that contribute to the overall function of the bladder. These cells are present in the underlying adventitia, which is rich in fibroelastic connective tissue, and each has distinct roles. These cells include mast cells, fibroblasts, and myofibroblasts, and each has distinct roles that contribute to the overall function of the bladder. Mast cells are immune cells that reside in loose connective tissue. In the bladder, they play an important protective role against pathogens. Upon activation, they are able to secrete molecules such as histamine, proteoglycans, serine proteases, prostaglandins, leukotrienes, and cytokines, which cause a variety of effects on surrounding tissue. Another cell type, fibroblasts, synthesize and maintain the extracellular matrix by producing connective tissue, providing the structural stroma for other tissue types. Myofibroblasts are a type of fibroblast that have differentiated toward a smooth muscle phenotype and synthesize the small

rests of smooth muscle cells that underlie the uroepithelium. It is proposed that myofibroblasts may have a role in neuromodulation [11].

1.1.5 Uroepithelium

The inner surface of the bladder is lined by the uroepithelium, a stratified epithelial tissue comprised of three layers: umbrella, intermediate, and basal cells (Figure 1.2) [12, 13]. The umbrella cell layer is the most superficial layer of cells, and its apical surface interfaces with the urine. Below the umbrella cells are 1–3 layers of intermediate cells. These smaller cells are able to differentiate into umbrella cells during injury. The deepest layer of uroepithelium is the basal cell layer, which resides on a basement membrane. Basal cells are undifferentiated uroepithelial cells with capacity to regenerate [12, 13].

1.1.5.1 Apical surface

The apical membrane of umbrella cells, along with their tight junctions, forms the primary barrier that retains urine. The specialized plaques that comprise much of the surface of the uroepithelial mucosal plasma membrane are important for this function. Each plaque has a thick lumenal leaflet relative to its thin cytoplasmic leaflet, described as the asymmetrical unit membrane (AUM); at ~ 12 nM thickness, they are thicker than typical plasma membrane [14] (Figure 1.3A). Plaques have a hexagonal crystalline structure comprised of the five known transmembrane uroplakin (UP) proteins: Ia, Ib, II, IIIa, and IIIb [15, 16], which assemble into specific heterodimer pairs [17] and whose proper assembly is pivotal for the formation of uroepithelial plaques and AUM [18]. Biochemical experiments using purified proteins have

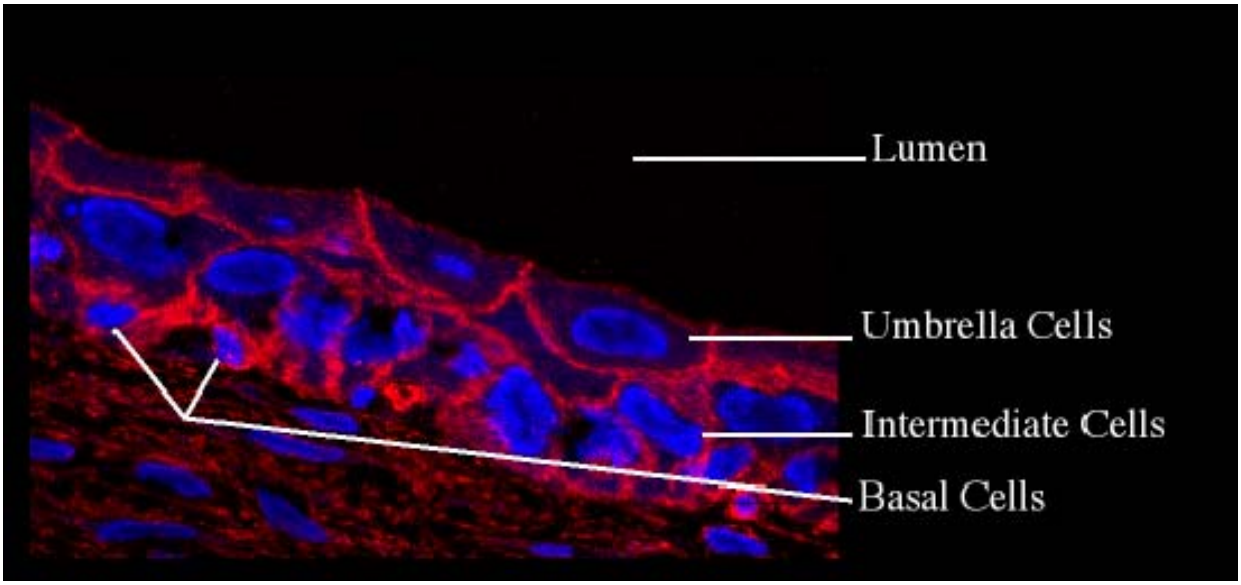

Figure 1.2: Bladder uroepithelium.

A 5 μm cryosection of rabbit uroepithelium was stained with rhodamine phalloidin to label actin (red) and Topro-3 to label nuclei (blue).

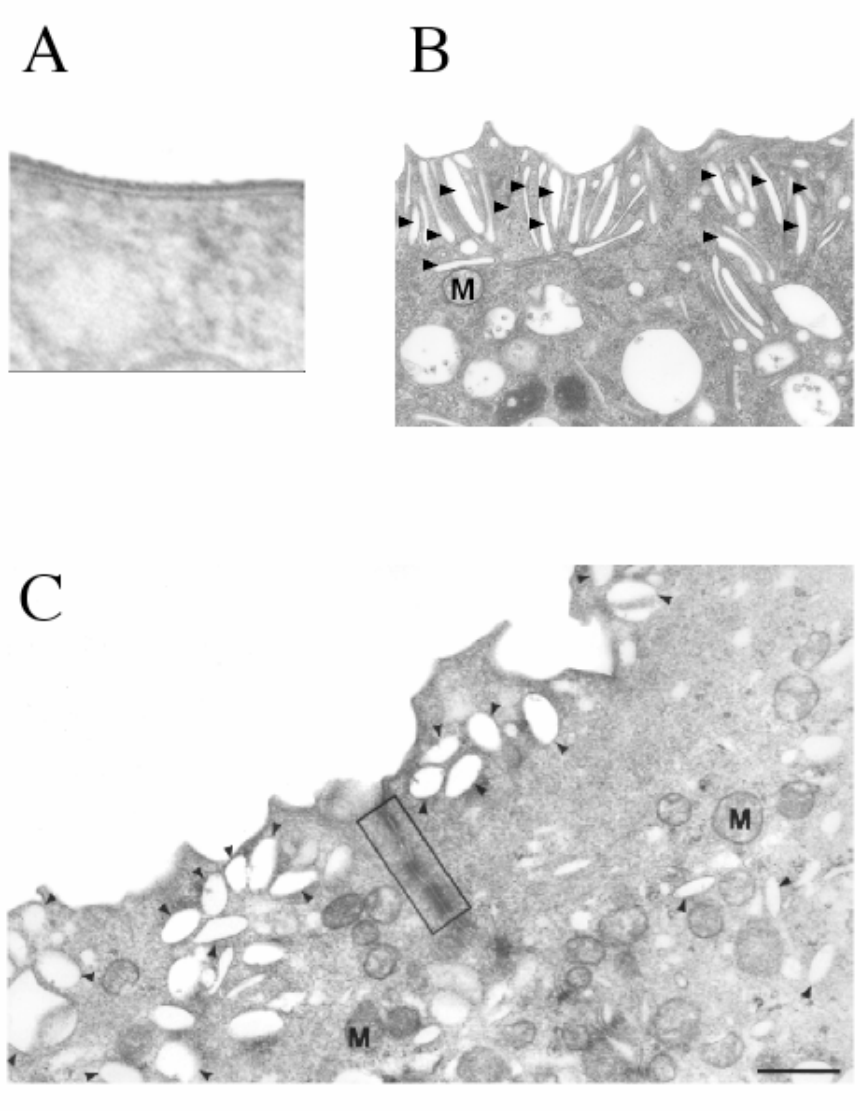

Figure 1.3: AUM and discoidal vesicles.

(A) Asymmetric unit membrane of mouse uroepithelium. Notice the membrane asymmetry in which the outer leaflet is thicker than the inner leaflet. (B) Fusiform vesicles of mouse uroepithelium underlyie the apical surface. (C) Discoidal vesicles of rabbit uroepithelium underlie the apical surface. Discoidal and fusiform vesicles are labeled with arrowheads. A tight junction between two umbrella cells is enclosed in a box, and umbrella cell mitochondria are labeled with "M." Images in A and B were prepared by Max von Bodungen, and C was imaged by Giovanni Ruiz.

revealed that UPIa pairs with UPII and that UPIb pairs with UPIIIa or UPIIIb [15], and this has been confirmed by recent structural studies [19].

1.1.5.2 Discoidal vesicles

The same UP plaques found in the apical membrane of umbrella cells are also the major components of a pool of discoidal or fusiform-shaped vesicles that resides beneath the apical surface of umbrella cells [20]. These vesicles contain plaques identical to the AUM of the umbrella cell apical surface [14] (Figure 1.3B), and their integrity is essential for the bladder's apical permeability barrier [21]. The shape of the vesicles varies among species: In humans and rabbits, the vesicles appear discoidal in shape, while they take a flatter, elongated, "fusiform" orientation in mouse and rat bladders [12]. The term discoidal vesicles will be used to designate the discoidal/fusiform-shaped subapical membrane vesicles throughout this dissertation.

Discoidal vesicles are vital to the dynamic maintenance of the apical barrier, as they are inserted and removed to regulate the surface area and content of the apical plasma membrane, as described below. However, aside from the presence of AUM, the contents of these vesicles (both their membrane constituents and their potential contents enclosed within the vesicles) are not known. Although not the focus of my dissertation, the identification of discoidal vesicle contents would enable a better understanding of their function and the mechanism for their insertion and removal from the surface.

1.1.5.3 Uroplakin IIIa

UPs themselves may perform functions beyond the formation of impermeable crystalline plaques. UPIIIa is the only major umbrella cell vesicle constituent with a substantial cytosolic tail (52 amino acids), and UPIIIa is the major (>90%) isoform of UPIII. Potential

phosphorylation sites within the tail were previously noted [22], which suggest that the functions of the tail may be regulated. Immunofluorescence experiments and imaging analysis indicate that UPIIIa colocalizes at the light microscopy level with membrane fusion/trafficking machinery, specifically synaptobrevin, SNAP23, and Rab27b [23, 24], but the functional implications of these morphological studies have not been demonstrated. Additionally, interactions of the UPIIIa tail with cytoskeleton have been proposed [21, 22], as discoidal vesicles are known to associate tightly with intermediate filaments and AUM interacts with keratin filaments [14, 25]. However, it is also possible that interactions with the cytoskeleton may be important to form a complex that provides AUM stability for normal plasma membrane function.

The UPIIIa gene-ablation mouse model demonstrates defects in membrane integrity and a phenotype of vesicoureteral reflux (VUR) [21]. The umbrella cells of UPIIIa knockout mice are abnormally small and exhibit an accumulation of immature vesicles beneath their apical surface [21]. Because of these attributes, it is tempting to speculate that the insertion of discoidal vesicles into the apical membrane is defective in these animals such that their bladders are unable to respond to and accommodate increased urine volumes, causing increased intralumenal pressures that yield the VUR phenotype.

Despite the growing list of potential interactions and the speculation about the role of UPIIIa, not much is known about these interactions. Therefore, I have explored the protein interactions of the UPIIIa cytoplasmic tail. In Appendix A, I present the results of a yeast two-hybrid screen to identify proteins that interact with the cytoplasmic domain of UPIIIa, as well as functional studies that assess the role of UPIII and UPII in the uroepithelial response to stretch.

1.1.5.4 High transepithelial resistance

In addition to the high permeability barrier offered by the uroepithelial plaques and AUM, the umbrella cells' tight junctions efficiently regulate the paracellular transport of ions and solutes. These tight junctions contain claudins-2, -4, -8, and -12 [26], which establish the paracellular barrier to the flow of molecules. The bladder uroepithelium maintains one of the tightest barriers in the body [27], as evidenced by its extremely high trans-epithelial resistance and extremely low permeability to water, protons, and small non-electrolytes, such as urea and ammonia [28, 29]. The entire surface of the uroepithelium is coated by heparin proteoglycans and mucins [13, 30]. This may serve as an additional protective layer to separate the filtered urine from underlying tissues.

1.2 BLADDER SIGNALING

The various tissues that comprise the bladder described above act in a coordinated manner to enable normal bladder function. These tissues must communicate with each other as well as receive and utilize signals from the urine, which also transmits information about the bladder's state (via hydrostatic pressure, stretch and tension, etc.). In addition to these external signals, there exists a host of internal factors and signaling mechanisms that are produced in response to the external signals, which allow the coordinated function of the tissues that make up the bladder. The signaling mechanisms employed by the urinary bladder are detailed in the following subsections.

1.2.1 Urinary Signals

The bladder may be affected by signals that originate in the urine. In normal uroepithelium, urine has been shown to induce cellular hyperplasia [31]. Various components in urine have been implicated as growth-promoting bioactive substances, including epidermal growth factor (EGF), heparin-binding EGF-like protein (HB-EGF), fibroblast growth factor, and transferrin [32-35]. EGF is produced in considerable quantities by the kidney, but its role as a bladder ligand is not well-defined [36]. These urinary growth factors must bind to the uroepithelium via apical surface receptors in order to induce effects in bladder tissue.

In addition to growth factors, the urine contains a number of other signaling factors that may impart effects on the uroepithelium and underlying bladder tissues. Many of these, such as ATP, adenosine, acetylcholine, NO, prostaglandins, and substance P [37-42], are synthesized by the uroepithelium and released into the urine, though many of which are rapidly degraded. These will be addressed in further detail below.

Beyond the presence of signaling molecules in the urine, the urine itself is able to impart mechanical signals upon the bladder as increased urine volumes transmit an increase in hydrostatic pressure and physical stretch on the uroepithelium. Mechanotransduction is the process by which cells recognize and convert mechanical stimuli into biochemical stimuli; the signals generated by bladder stretch will be discussed in detail in Section 1.3.

1.2.2 Uroepithelial receptors

While the presence of various signaling factors in urine is well established, the localization of their receptors in the bladder is a matter of discrepancy in the literature [43]. Many reports

suggest that growth factor receptors such as the EGF receptor (EGFR) are localized to the basolateral surface and only become activated upon a breach of the apical barrier, while some have localized the EGFR to the apical surface [43]. The localization of the EGFR and its regulation is particularly important, considering the availability of its ligands in the urine and its potential role in cancer; this will be explored in Chapter 2.

In addition to growth factor receptors, the uroepithelium also contains other receptors and channels that receive various signals that may originate in the urine or in uroepithelial and underling tissues, as discussed below. There are mechanosensitive ion channels that are activated in response to stretch, such as amiloride-sensitive sodium channels. Purinergic (P2X and P2Y) receptors receive ATP signals, and adenosine receptors respond to adenosine. Additionally, receptors for bradykinin (B1 and B2 receptors), nerve growth factors (p75/trkA), norepinephrine (α and β subtypes), acetylchonine (nicotinic and muscarinic receptors), and several transient receptor potential channels (TRPV1, TRPV2, TRPV4, TRPV8, which can transmit information about heat, cold, acidity, osmolarity, and/or capsaicin signals) are present with various distributions in the uroepithelium [2]. These receptors allow the uroepithelium to behave as a sensory tissue, receiving and transmiting various signals that originate in the urine or from neighboring bladder tissues.

1.2.3 Regulation of receptors and signaling from the apical surface

The ability of signaling proteins to function as receptors, signaling molecules, or transporters at the apical surface of umbrella cells depends upon their availability and presence at this cell surface. The quantity of transporters in a membrane can be controlled by protein synthesis (which takes hours) or through membrane trafficking (which can impart effects immediately).

This dynamic mechanism allows for the recruitment of preexisting transporters, their insertion for activity in the membrane, or the removal of transporters from the membrane to quickly decrease flux. Removed transporters can be recycled back to the surface or degraded. A number of different channels and transport proteins are regulated by exocytic insertion and endocytic retrieval in various cell types [44], and these membrane trafficking events may be able to regulate signaling by making signaling components available (or unavailable) for function at the apical surface of the bladder. The precise composition of receptors and channels at the apical surface is not known; it would be very important to study the proteins that are regulated by turnover at the bladder's surface.

1.2.4 Signals from bladder tissues

In addition to signals originating in the urine, various signaling molecules and neurotransmitters are generated by the uroepithelium or neighboring tissues and received by uroepithelium. The uroepithelium itself is known to secrete ATP, adenosine, acetylcholine, NO, prostaglandins, and substance P [37-42]. In autocrine signaling, the source of the signal is the uroepithelium, and its purpose is to modify uroepithelial function. In paracrine signaling, the source of the signal is another cell or tissue type, which modifies the uroepithelium.

The stimulus of stretch causes the generation of bladder signals that function in autocrine and paracrine signaling pathways. ATP and adenosine are both released by the uroepithelium in response to stretch [40-42] and have been shown to act on P2X2, P2X3, and adenosine receptors on the uroepithelium to stimulate membrane trafficking events within the umbrella cells in an autocrine manner, as discussed in greater detail below. P2X3 receptors are also present on sensory afferent nerve processes and allow for paracrine signaling of ATP released by the

uroepithelium. Prostaglandins are another example of a paracrine signal that is released by the uroepithelium in response to stretch and can modulate nerve and detrusor functions in the bladder [9].

Transmural signaling is a third type of signaling that functions in the bladder, in which signals are transmitted from the urinary space to modify tissues that underlie the uroepithelium. For example, the mere presence of ATP in the bladder lumen is able to stimulate nerve discharge by sensory afferents beneath the uroepithelium and detrusor overactivity [45]. In transmural signaling, the mucosal surface of the umbrella cells receives the signal that is somehow transmitted to underlying tissues; the mechanism is not understood, but it is proposed that the uroepithelium may release a soluble factor to modulate muscle contraction [46].

1.2.5 Intracellular Signaling

While many signals are generated by and/or act upon the uroepithelium itself, there exists a host of signaling pathways activated within the uroepithelium that have diverse cellular consequences. Intracellular signaling pathways, such as those involving calcium, cAMP, and protein kinase A (PKA) signaling, appear to be activated by signals such as mechanical stretch [47], as described in detail below.

In addition to signaling molecules, post-translational modification of proteins also serves as an intracellular signaling mechanism in many cell types. Tyrosine kinase/phosphatase signaling, which involves the addition or removal of phosphate groups by kinases and phosphatases, is a common signaling mechanism in the cell. The bladder-specific uroplakin proteins have consensus sequences for phosphorylation, and UPIII is phosphorylated in *Xenopus* oocytes [48]; however, its phosphorylation in the bladder has not been examined. Tyrosine

kinase signaling is an important component of mechanotransduction pathways in various cells, for example the response of vascular endothelial cells to shear stress [49] and the sensation of flow rate by kidney proximal tubule cells [50]. The role of tyrosine kinase signaling in bladder mechanotransduction has not been studied, and it is further explored in Chapter 2.

1.2.6 Integration of bladder signaling pathways

Clearly, there are many diverse signaling pathways that function in the urinary bladder. The outcomes of these signaling pathways, whether they are members of the same overall pathway or signaling mechanism, what their downstream signals are, and whether they regulate each other are all intriguing questions that remain to be explored. In Chapter 2, I propose a signaling model in which a single integrated pathway may regulate the several of the stretch-evoked signaling participants described below.

1.3 BLADDER MECHANOTRANSDUCTION & MEMBRANE TRAFFICKING EVENTS

One important signal that is generated in the bladder lumen is the mechanical stimulus of stretch. Mechanotransduction provides information about the bladder's capacity: Increased hydrostatic pressure causes stretch during filling, and these stimuli are released upon voiding. Mechanotransduction pathways are crucial for appropriate cellular responses to the extracellular environment and provide a means for external stimuli to influence diverse cellular functions including growth, development, cell division, death, and intracellular signaling and trafficking

events [51, 52]. The mechanisms cells use to sense and transduce mechanical signals into downstream effects are only now being explored, despite the fact that these pathways are present in many cell types. The bladder is an excellent model system to study the signal transduction pathways in mechanotransduction [51]. An important effect of bladder mechanotransduction is membrane trafficking, and in this dissertation, the signals evoked by bladder stretch and their effects on discoidal vesicle exocytosis are examined.

1.3.1 Membrane trafficking in the bladder

The bladder is capable of modulating its surface area in response to increased pressure to accommodate a wide range of urine volumes. At the tissue level, the mucosal surface unfolds to increase bladder capacity; while at the cellular level, the superficial umbrella cells change shape, from cuboidal in an empty bladder to flat and squamous in a filled bladder [20, 53], as depicted in Figure 1.4. Furthermore, it is postulated that discoidal vesicles that underlie the umbrella cell mucosal surface are dynamically inserted and retrieved from the surface, through the processes of endocytosis and exocytosis, to mediate changes in apical surface area [54-57]. During stretch, the process of exocytosis outbalances endocytosis, and there is a net increase in surface area. Various studies have contributed to our knowledge about discoidal vesicle trafficking, and the regulation of the exocytic response is a major focus of this dissertation.

1.3.2 Endocytosis

Endocytosis in the uroepithelium is a process that is not fully understood at this time. Recent studies suggest that endocytosis is stimulated during stretch, which may function to modulate the

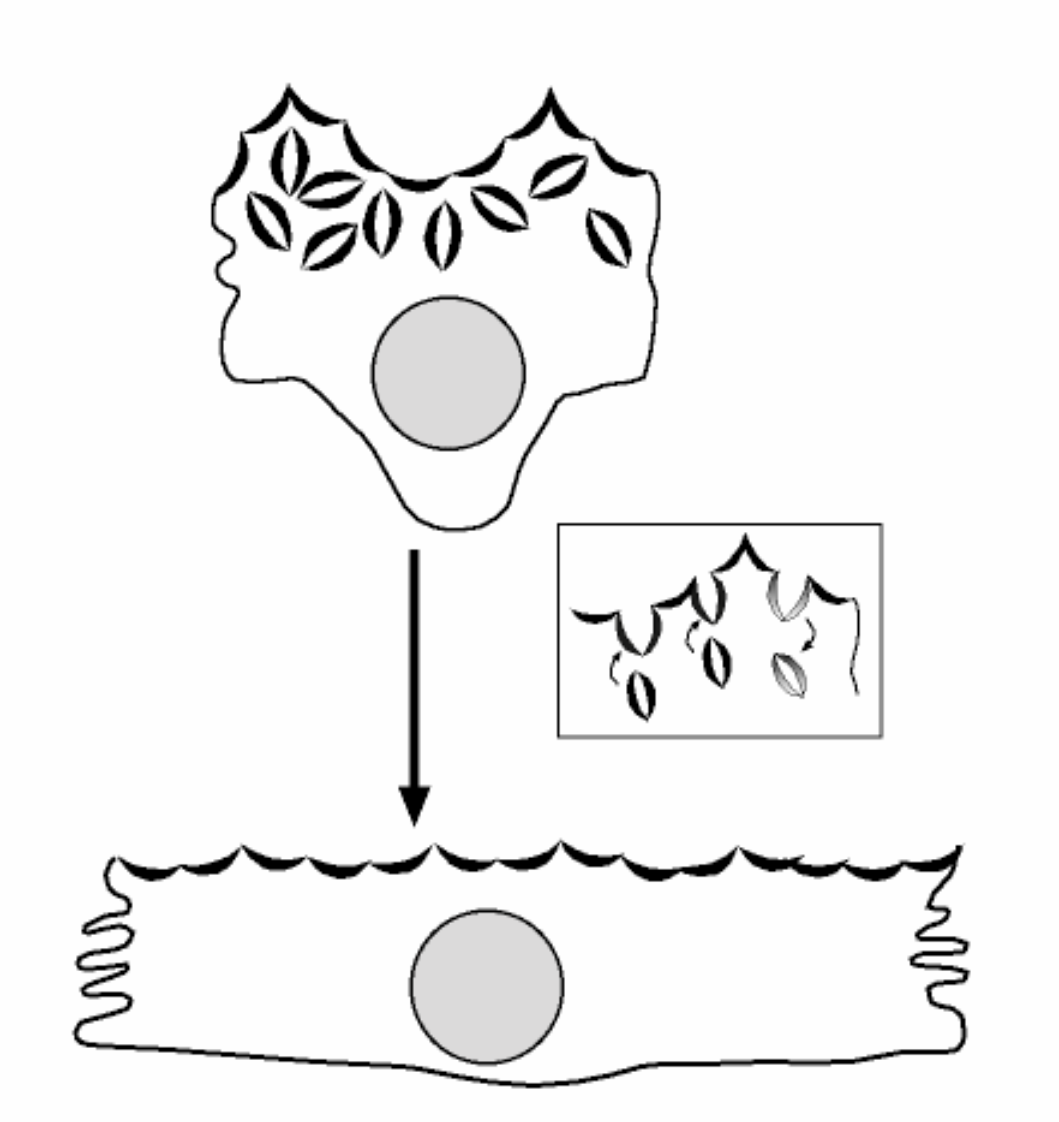

Figure 1.4: Umbrella cell changes upon stretch.

Unstretched umbrella cells have a cuboidal shape with a pool of discoidal vesicles residing beneath the apical surface. Upon stretch, the umbrella cells elongate and flatten in shape, and trafficking of discoidal vesicles occurs to mediate an increase in apical surface area. Adapted from [12].

surface area increase in response to bladder filling [47]. Endocytosis may also be required to remove membrane constituents, such as active or inactive signaling molecules at the apical surface, for degradation or recycling to modulate signaling events. The signaling pathways involved in umbrella cell regulation of endocytosis have not been explored. It is possible that the same or overlapping signals regulate both exocytic and endocytic events, but this remains to be formally tested.

1.3.2.1 Stretch-induced endocytosis

Endocytosis upon stretch was confirmed by labeling the surface, stretching to internalize the labeled surface proteins, removing all remaining surface label, and probing for internalized label. There was a large increase in internalized proteins in the lysates of stretched tissue compared to control [47], and many protein bands were observed in these studies, the identities of which are unknown. However, the major protein species (~ 67 kDa) was identified as albumin, a protein in abundance in urine. My preliminary studies suggested that albumin may be internalized through its binding of gp60 receptor. This raises the interesting possibility that the bladder is able to modulate the content of the urine.

1.3.2.2 Endocytosis upon voiding

In addition to modulating surface area, the process of endocytosis is likely vital to the recovery of surface membrane upon bladder voiding. Minsky and Chlapowski introduced this concept by visualizing the reduction of apical surface area by vesicle formation upon release of stretch [57]. Additionally, studies of endocytosis utilized the capacitance measurement approach described above. When hydrostatic pressure was increased (for either 5 min or 5 h durations) and released, capacitance measurements returned to baseline [56], suggesting that compensatory endocytosis is

a rapid process. Studies using an inhibitor of lysosome activity suggested that the endocytosed membrane components, including UPs, were delivered to lysosomes for degradation [47]. It is not known whether any of the internalized proteins are recycled to new discoidal vesicles or back to the surface.

Interestingly, endocytosis studies that utilized fluorescent-labeled lectins to monitor uptake after the release of stretch revealed punctate fluorescence uptake in the apical cytoplasm of the umbrella cell layer that concentrated around cell junctions [47] (Figure 1.5). It is curious that endocytosis occurred preferentially in these areas while the subapical pool of discoidal vesicles is spread evenly below the apical surface because the purpose of this localization is unknown. Although not the focus of this dissertation, the pathways and signaling involved in discoidal vesicle enodytosis are important topics for future study.

1.3.3 Exocytosis

Exocytosis allows for secretion of proteins such as neurotransmitters into the urine [37-42], addition of membrane to the apical surface, and insertion of integral membrane proteins into the apical surface. Over the years, it has been accepted that during bladder filling, mechanical stretch induces a net increase in surface area via exocytosis of subapical discoidal vesicles to add surface membrane [54-57]. Several lines of evidence support this model, and various components of the signaling pathway activated by mechanotransduction have been recognized, as summarized below. As more data are produced regarding the stretch-induced signaling pathways, there is an appreciation for its complexity and tight regulation for proper bladder function.

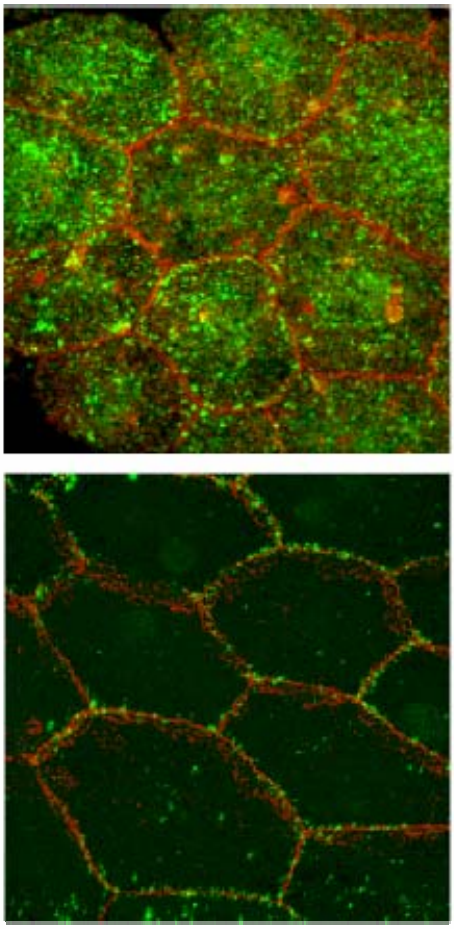

Figure 1.5: Endocytosis upon release of stretch stimulus

Rabbit uroepithelium was mounted in an Ussing stretch experiment. Prior to release of pressure, WGA-FITC was placed in the apical hemichamber. In the top figure, the tissue surface was not washed prior to fixation, showing that the marker bound to the apical surface uniformly. In the bottom image, the tissue was washed to remove surface bound WGA-FITC, such that the remaining staining reveals the endocytosed marker. The actin cytoskeleton was stained with rhodamine phalloidin (red). This study was performed by Dr. Puneet Khandelwal.

1.3.3.1 Increases in surface area

The earliest studies of bladder accommodation on the cellular level included visualization of the changes that occurred during cell stretch, and they revealed movements of discoidal vesicles that were consistent with the exocytosis model [54-57]. In general, microscopy techniques were used to visualize and compare the appearance of discoidal vesicles in stretched versus control tissues, demonstrating a reduction in the number of vesicles with stretch. Consistent with these observations, stereological measurements allowed the quantification of the apical, basolateral, and discoidal vesicle surface areas in stretched versus control tissue [47, 57]. This approach confirmed that the apical surface area of stretched uroepithelium increased by 50%, that there was no significant change in basolateral surface area, and that the discoidal vesicle membrane surface area pool decreased substantially during the 5 h stretch duration [47]. Interestingly, the magnitude of discoidal vesicle membrane loss was much greater than the increase in apical surface area; however, it has been suggested that at least some of this difference may be attributed to stretch-induced apical surface endocytosis, as described above.

Membrane capacitance measurement techniques were used to quantify changes in the apical surface area [58], and these types of studies are used throughout my dissertation work. Electrical capacitance is a measure that is directly proportional to surface area such that in the bladder: 1 μF of capacitance E 1 cm^2 of surface area [58]. Uroepithelial capacitance showed no change in the absence of stretch; however, when hydrostatic pressure was raised to ~ 1 cm H_2O for 5 h to simulate the filling and storage phases of the micturition cycle, a stretch stimulus caused a 50% increase in capacitance (Figure 1.6). This pressure stimulus is slightly less than that normally observed during the extended phase of bladder filling in rabbits [59]. The

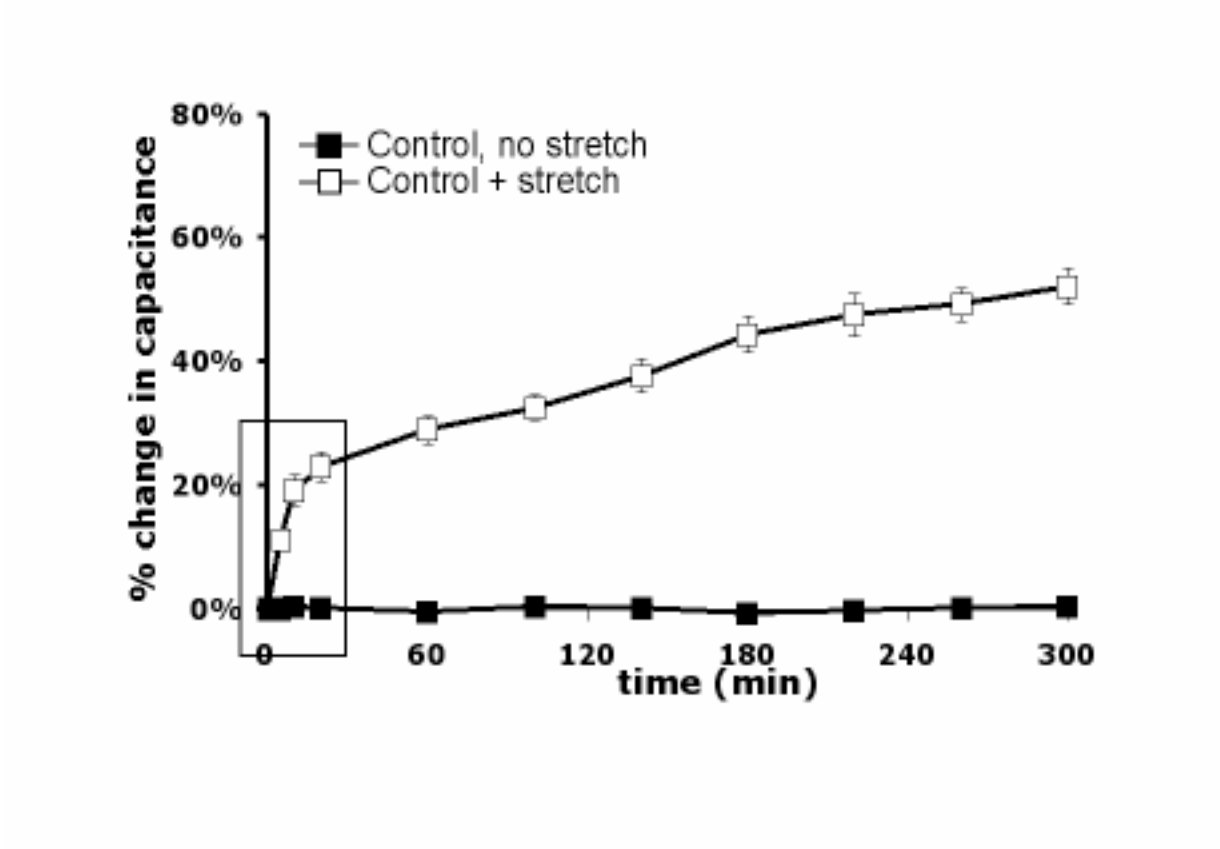

Figure 1.6: Capacitance changes in response to stretch.

Isolated rabbit uroepithelium was left unstretched or exposed to ~ 1 cm H_2O pressure (+ stretch) in an Ussing stretch chamber, and changes in membrane capacitance were measured. The box indicates the "early phase" increase in surface area upon stretch.

capacitance increase is biphasic with an early, rapid ~ 25% increase in capacitance within the first 30 min (designated by the box in Figure 1.6), followed by a prolonged increase over the following 4.5 h to a total increase of 50% over control [58]. The early phase is not inhibited by blocking secretion or protein synthesis with brefeldin A (BFA) or cycloheximide, and it may represent the fusion of a pre-formed, ready-release pool of discoidal vesicles. The late, slow-phase increase is sensitive to both cycloheximide and BFA and may involve distinct signaling components compared to the rapid early phase. This late phase is particularly interesting, as nothing is known regarding the signals or mechanisms that initiate protein synthesis; this will be further explored in Chapter 2. Also, it is not known which proteins are upregulated by stretch and how these proteins function to increase the apical surface area.

1.3.3.2 Membrane insertion and secretion of proteins

Additional approaches to confirm discoidal vesicle exocytosis monitored the insertion of UPIIIa into the apical surface and secretion of newly synthesized proteins upon stretch. While only < 5% of the total UPIIIa pool is present at the surface in control and early stretching time points, the total amount of UPIIIa increases by ~ 67% in a 5-h stretched sample, indicating an increased delivery of UPIIIa to the surface [47]. To study protein secretion, [^{35}S]-methionine/cysteine was used to label newly synthesized proteins, and their secretion into the apical hemichamber was measured upon stretch. This study indicated that little radiolabeled proteins were secreted by control tissue, while stretch induced the rapid secretion of labeled proteins, even within 5 min of stretch stimulus. An ~ 26-fold increase in secreted radiolabeled proteins was observed after 5 h of stretch relative to unstretched bladder, which can be completely blocked by incubation of the tissue with BFA [47]. Interestingly, it is not known which proteins are secreted upon stretch. A transgenic mouse expressing human growth hormone secreted this protein into the urine [60],

and bovine uroepithelium has been shown to secrete tissue plasminogen activator and urokinase [61]. The identification of additional physiologically secreted proteins would provide useful markers for study of bladder secretion and exocytosis.

1.3.3.3 Exocytosis in the absence of stretch

Together these experiments support a model in which stretch induces an increase in exocytosis, which mediates an increase in apical surface area. Of note is the lack of information specifically examining the exocytic trafficking of discoidal vesicles in the absence of stretch or during states in which the bladder is not at tension. While unstretched tissue shows no change in capacitance over time, it is important to note that this is a steady-state measure, meaning that it is possible that exocytosis occurs at a rate that is matched by endocytosis, resulting in a non-appreciable change in surface area. Discoidal vesicle exocytosis may serve as an important mechanism for the delivery of new receptors/channels/transporters to the apical surface, in addition to providing a means for secretion of proteins; however, the identities of proteins that might require replenishment at the surface or secretion into the urine have not been explored.

1.3.4 Regulation of mechanotransduction & exocytosis in the bladder

As described above, there is strong evidence supporting a model of mechanically stimulated membrane trafficking events in the uroepithelium. Mechanotransduction pathways in various cell types require a number of common components, including the cytoskeleton, ion channels, integrins, tyrosine kinases and phospholipases, cAMP, and other signaling molecules [51]. Over the past few years, a number of these components have been implicated in the regulation and signaling of stretch-induced exocytosis in umbrella cells, as described below.

1.3.4.1 Cytoskeleton

One might imagine that an intact cytoskeleton would be necessary and might participate in the insertion and removal of apical surface area without compromising the bladder's barrier. In other epithelial tissues, elements of the cytoskeleton have been established as pertinent players in both endocytic and exocytic trafficking pathways [62-64]. In the bladder, there is morphological evidence that discoidal vesicles interact with intermediate filaments [14, 65], and studies using pharmacological inhibitors support a role of the actin cytoskeleton in osmotic-induced trafficking in the umbrella cell [56]. However, a functional role for the cytoskeleton in discoidal vesicle trafficking has not been tested in a system that mimics *in vivo* bladder mechanical stretch. Also, while interfering with any of these cytoskeletal components will cause defects in trafficking events, how the cytoskeleton interacts with discoidal vesicles is not known.

1.3.4.2 Ca^{2+} signaling

In addition to cellular structural requirements, many signaling requirements are common in mechanotransduction pathways among cell types, such as Ca^{2+} signaling [51]. Ca^{2+} also appears to be important in the regulation of discoidal vesicle exocytosis: Increased cytoplasmic calcium stimulates exocytosis in the absence of stretch, while blocking calcium release attenuates the response to stretch [58]. Studies suggest that both extracellular and intracellular Ca^{2+} are required in stretch-induced exocytosis, as the use of Ca^{2+}-free buffer and an inhibitor to block intracellular inositol 1,4,5-triphosphate (IP3)-induced Ca^{2+} release from the ER both inhibited the increase of capacitance observed upon stretch [58]. The mechanism for Ca^{2+} entry into cells upon stretch is unknown, and the pathways that lead to activation of IP3-induced Ca^{2+} release from the ER remain to be explored. In addition, the downstream effectors of Ca^{2+} signaling in the uroepithelium are unknown.

1.3.4.3 cAMP signaling

Another important signal in stretch-induced exocytosis in umbrella cells is cAMP, whose concentration is increased upon stretch [47]. When concentrations of cAMP are experimentally raised in the absence of stretch, there is a tremendous increase in exocytosis in umbrella cells (~ 120%) [47]. It appears that PKA functions downstream of cAMP, as inhibition of PKA with H-89 inhibited stretch-induced increases in surface area. Both cAMP and Ca^{2+} are versatile signaling molecules, and both can be regulated by G-protein coupled receptor (GPCR) signaling. How these signals interact within umbrella cell signaling pathways is unknown.

1.3.4.4 ATP and its metabolites

It was also observed that ATP is released by uroepithelium in response to stretch [40]. This ATP release occurs on both surfaces of the uroepithelium, although to a much greater extent on its serosal surface [41, 66]. Like cAMP, addition of exogenous ATP can induce an increase in surface area in the absence of stretch, and the ATP-induced exocytosis is dependent upon Ca^{2+} and PKA signaling [41], suggesting that these signaling factors may in fact act in concert. Stretch-induced exocytosis can be blocked in studies in which apyrase (an enzyme that hydrolyzes ATP) or PPADS (a general purinergic receptor antagonist) are added to the mucosal surface of the uroepithelium, and experiments with pharmacological inhibitors and knockout mice further support a role for purinergic signaling in bladder mechanotransduction [41].

ATP activates P2 purinergic receptors, a family comprised of P2X ion channels and P2Y GPCRs. P2X activation allows cation ion influxes such as Ca^{2+}, while P2Y signaling can be coupled via G-protein activation to various downstream signaling molecules including cAMP Ca^{2+} signaling [67]. It is entirely possible that both P2X and P2Y pathways function in this response. Another unknown question regards the role of ATP as a diverse signal in the bladder.

ATP is also involved in bladder neurotransmission and pain signaling pathways [2, 68, 69], but it is unclear how the same signal interacts with both pathways simultaneously, or if this signal somehow provides integration between trafficking and pain signaling in the bladder.

Adenosine, which can be formed from the hydrolysis of ATP or conversion of cAMP, is a metabolite that also appears to regulate stretch-induced discoidal vesicle trafficking in the uroepithelium. Adenosine is generated upon stretch, and its addition to unstretched uroepithelium induced an increase in surface area through its activation of adenosine receptors [42]. Adenosine receptors are also GPCRs, which suggests that they may also be able to transactivate the EGFR. They may interact with above signals by upregulating cAMP or Ca^{2+} signaling through the action of G-proteins, although this relationship has not been tested.

1.3.4.5 Other signaling components

While a number of components are involved in discoidal membrane exocytosis, it appears that many of these signaling pathways may be integrated, and their signaling may impact one another. In addition to these signaling requirements, signaling modifications required for mechanotransduction in other cell types, such as tyrosine phosphorylation, remain to be explored. Additionally, the urine provides an abundance of growth factors and urinary ligands that may play some role in the regulation of stretch-induced discoidal vesicle exocytosis. The signaling components above may be interconnected through G-protein activation of cAMP and Ca^{2+} influxes, or integrated with other signaling pathways in a manner that remains to be formally tested. The roles of these additional potential signaling components and the integration of these signaling pathways in discoidal vesicle exocytosis are addressed in Chapter 2.

1.4 DISRUPTION OF NORMAL UROEPITHELIAL TRAFFICKING IN BLADDER PATHOLOGY

The signaling pathways that function to maintain normal bladder function are tightly regulated, and membrane trafficking plays an important role not only as a response to bladder signals (such as stretch, ATP, and cAMP), but also by modulating the available signaling receptors/transporters/channels that are delivered to the cell surface. Bladder pain and infections are examples of bladder disease states that can be affected by the dysregulation of bladder membrane trafficking, as described below.

1.4.1 Bladder Pain

Although typically not considered a result of defects in bladder membrane trafficking, umbrella cell exocytosis and relevant signaling pathways may contribute to the pathophysiology of bladder pain. Bladder pain is associated with several pathological conditions, including infection, cancer or stricture, and interstitial cystitis [2]. Interstitial cystitis is a chronic bladder disease that presents with symptoms of bladder pain, a sensation of urgency to void, and frequent voiding [3, 69, 70].

It has been shown that ATP is released from the uroepithelium in response to stretch, to stimulate discoidal vesicle exocytosis. ATP release is also a common response of cells to inflammation or injury. This release can be translated into painful sensations through its action on purinergic receptors or by lowering the threshold for sensory neurons that sense noxious stimuli, such as those activated by capsaicin [71]. It is possible that dysregulation of ATP

signaling or its downstream effects, potentially by increased ATP secretion or altered availability of relevant receptors, contributes to the pathology of bladder pain.

Furthermore, bladder trafficking events must occur while maintaining the impermeable barrier to urine. Uroepithelial damage or defects in these pathways compromises the uroepithelial barrier, which leads to pain, the sensation of urgency to void, and inflammation [1, 3]. A defect in the permeability barrier during exocytosis may also lead to bladder pain in this manner.

1.4.2 Urinary tract infections

The most common cause of urinary tract infections, one of the most common infectious diseases, is uropathogenic *Escherichia coli* (UPEC) bacteria. During infection, UPEC bacteria are able to bind to the uroplakin Ia (UPIa) proteins located in the plaques of surface AUM, specifically at mannosyl moieties [72, 73]. One can imagine how altering the availability or turnover of UPIa on the apical surface on umbrella cells can impact the ability of the bacteria to attach to the bladder surface or initiate a host response to the infection.

It was recently shown that UPEC invasion is mediated by the bacteria's attachment to AUM that is internalized; Bishop *et al.* suggest that UPEC bacteria are able to reside in internalized fusiform canals formed by the coalescence of fusiform vesicles in infected mice [72]. Treatment of these mice with forskolin increased the concentration of intracellular cAMP and induced the exocytosis of the vesicles, effectively reducing the number of *E. coli* in the uroepithelium [72]. In this manner, infections such as UPEC can utilize the trafficking of discoidal vesicles to gain access to the body, and our understanding of these mechanisms can enable the development of therapies to treat these infections.

1.5 GOALS OF THIS DISSERTATION

Exocytosis and endocytosis of discoidal vesicles are important processes to regulate the size and membrane content of the apical surface of the uroepithelium. A large number of cell signals have been implicated in this process. My dissertation hypothesis is that tyrosine kinase signaling is required for stretch-induced exocytosis in umbrella cells, which may serve as a signaling pathway that integrates many of the other known signaling factors. In Chapter 2, I characterize the requirement for EGFR signaling from the apical surface of uroepithelium during stretch, which demonstrates the relevance of both tyrosine kinase and growth factor signaling pathways in the bladder. My work describes the mechanical activation of metalloproteinases to liberate HB-EGF ligand, which subsequently activates the EGFR to stimulate downstream MAPK signaling and protein synthesis, ultimately enabling a prolonged increase in surface area. It also suggests a model that may account for the integration of several signaling pathways that are known to function in stretch-induced exocytosis, including ATP and adenosine, GPCRs, calcium influxes, growth factor signaling, and protein synthesis.

It is critical to understand the signaling pathways that are activated by physiological bladder conditions such as stretch in order to better understand how these signaling pathways may malfunction in pathological states. EGFR signaling is known to be involved in a wide variety of cellular processes that is likely relevant in the bladder including growth, healing, differentiation, and mechanotransduction. The association of EGFR with bladder carcinoma suggests that there are devastating consequences for dysregulation of these physiological pathways, and our better understanding of the role of EGFR in bladder physiology is significant because this information may be exploited in diagnostic and therapeutic approaches.

2.0 APICAL EGF RECEPTOR SIGNALING: REGULATION OF STRETCH-DEPENDENT EXOCYTOSIS IN BLADDER UMBRELLA CELLS*

*Reprinted from *Molecular Biology of the Cell,* (2007, volume 18, issue 4, pp. 1312-1323), with permission from the American Society for Cell Biology [74].

2.1 INTRODUCTION

The apical plasma membrane of epithelial cells is a dynamic sensory organelle that receives and responds to extracellular stimuli such as ATP, hormones, growth factors, and mechanical stimuli such as hydrostatic pressure and shear stress [75]. These stimuli act through apically-expressed receptors, channels, and transporters to modulate the growth, protein synthesis, division, differentiation, and apoptosis of the subjacent epithelial tissues [67]. In addition, these stimuli can increase membrane turnover (i.e. exocytosis/endocytosis) at the apical surface of the epithelial cells, thereby modulating the surface area of the apical plasma membrane, the receptor/channel/transporter content of this membrane domain, and the ability of the cell to respond to extracellular signals. At present the association between extracellular mediators, mechanical stimuli, and apical membrane dynamics is poorly understood.

The epidermal growth factor receptor (EGFR), a member of the ErbB family of receptor tyrosine kinases (including EGFR/ErbB1, ErbB2, ErbB3, and ErbB4), is an important regulator

of mechanotransduction, cell signaling, and membrane traffic [76-78]. The ErbB family of receptors can be activated upon binding of one of ten ligands, which differentially interact with ErbB1, ErbB3, and ErbB4 receptors (ErbB2 has no known ligands)[77]. The ligands are synthesized as transmembrane precursors that are released upon cleavage by metalloproteinases [79]. Ligands activate ErbB receptors in an autocrine, paracrine, or juxtacrine manner [80], and receptor activation can be initiated downstream of mechanical stimuli. Ligand binding induces the hetero- and/or homodimerization of receptors and subsequent autophosphorylation of tyrosine residues within their cytoplasmic tails. In turn the phosphorylated tyrosine residues act as docking sites for signaling proteins, which dictate activation of downstream signaling pathways including the MAPK cascades [81]. MAPKs include ERK1/2, p38 kinase, JNK, and ERK5, and are known to cause changes in protein expression through regulation of transcription [82].

Although EGFR is generally thought to be a basolateral receptor, EGFR is found at the apical surface of mouse 8-cell stage embryos, enterocytes lining the suckling rat ileum, and gastric mucosal oxyntic cells [83-85]. In many cases the function of apical EGFR is unknown, but in oxyntic cells, epidermal growth factor (EGF), acting through the EGFR, has a long-term effect of decreasing paracellular permeability and increasing the barrier to mucosal acid production [85]. Intriguingly, when EGFR is overexpressed in LLC-PK1 cells, a fraction of the receptor is mistargeted to the apical cell surface where it can stimulate downstream signaling cascades [86], indicating that EGFRs may generally have the ability to signal via apical epithelial surfaces. Several studies have described the expression of EGFR and ErbB family members (with various localization patterns) in normal human uroepithelium, the stratified transitional epithelium that lines the renal pelvis and mucosal surface of the ureters and bladder, and their

increased mucosal surface expression during cancerous states [43, 87, 88]. However, the function of EGFR in normal uroepithelial physiology is not well understood.

Extracellular signaling events modulate membrane traffic in umbrella cells, the outermost cell layer of the uroepithelium. The apical surface area of umbrella cells is highly dynamic, and it is postulated that discoidal/fusiform-shaped vesicles that underlie the apical surface are inserted and retrieved during bladder filling and voiding [47, 56]. Apical exocytosis in these cells is governed by Ca^{2+}, cAMP, the cytoskeleton [47, 53, 58], and extracellular stimuli including mechanical stretch [41, 53], ATP [41], and adenosine [42]. Intriguingly, in addition to ErbB1-4, multiple ErbB receptor ligands are also expressed in the uroepithelium [89, 90]. Although tyrosine kinases are known to be important in mechanotransduction in other cell types such as vascular endothelial cells, keratinocytes, and osteoblasts [49, 91, 92], the role that tyrosine phosphorylation in general, and the ErbB receptors in particular, play in umbrella cell exocytosis is unknown.

In this report, we provide evidence that stretch-induced exocytosis in umbrella cells is dependent on EGFR signaling initiated at the apical pole of the cells. Stretch of isolated uroepithelium resulted in the rapid activation of EGFR, and stretch-induced exocytosis was blocked by treatment with an EGFR-selective inhibitor or function-blocking antibodies when added to the mucosal, but not serosal surfaces of the tissue. EGFR activation was mediated by an autocrine mechanism that was prevented by addition of antibodies to heparin-binding EGF-like growth factor (HB-EGF) or treatment with a broad-spectrum metalloproteinase inhibitor. Stretch and EGFR ligand-induced increases in surface area were sensitive to cycloheximide and inhibitors of MAPK signaling pathways. Our data indicate a novel physiological role for the EGFR that links mechanotransduction, EGFR activation at the apical pole of the umbrella cell,

and protein synthesis downstream of MAPK activation to stimulate exocytosis at the apical pole of polarized umbrella cells.

2.2 RESULTS

2.2.1 Tyrosine phosphorylation is required for stretch-induced increases in umbrella cell surface area

In our experiments, isolated uroepithelium was mounted in a specialized Ussing stretch chamber and bladder filling was mimicked by increasing the hydrostatic pressure across the mucosal surface of the tissue [58] to a final pressure of ~ 1 cm H_2O (Figure 2.1B). Changes in mucosal surface area were monitored by calculating the transepithelial capacitance (where 1 $\mu F \cong 1\ cm^2$ of surface area), which primarily reflects changes in the apical surface area of umbrella cells and correlates well with other measures of apical exocytosis [58]. In the absence of stretch or stimulation by pharmacological agents, there was no change in capacitance after 5 h (Figure 1.6). However, when filling was performed over a period of 2 min the capacitance increased by ~ 50% after 5 h (Figure 1.6).

The kinetics of the capacitance increase occurred in two phases: an "early phase," characterized by a rapid ~ 25% increase in surface area over the first 30 min; and a "late phase," in which the capacitance increased over a prolonged period of time that resulted in an additional ~ 25% increase during the next 4.5 h (Figure 1.6). The late-phase increase in capacitance was

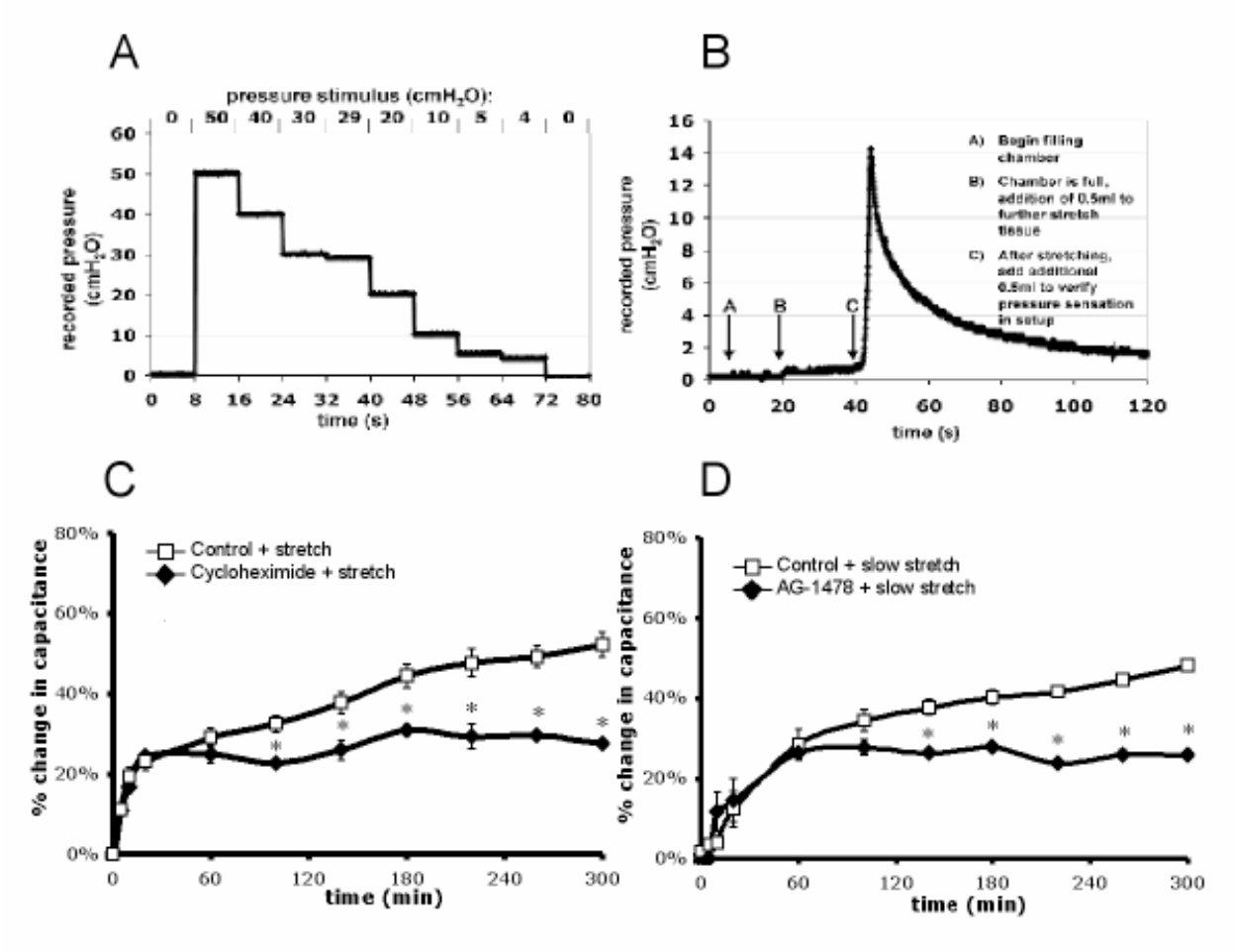

Figure 2.1: Characterization of the modified Ussing stretch model.

(A) Use of a water column to calibrate the TBM4 Transbridge Pressure Transducer. The nominal height of the water column is shown above the panel, and the measured pressure is shown along the calibrated Y-axis. (B) Isolated uroepithelium was equilibrated in the Ussing stretch chamber and the pressure was recorded in the mucosal hemichamber at the start of filling (arrow A), and after the mucosal chamber was further filled by an additional 0.5 ml (arrow B). This was the pressure used in our experiments. To confirm the ability of the system to measure higher pressures, an additional 0.5 ml of Krebs buffer was added (arrow C) and the subsequent pressure increase was recorded. (C) Protein synthesis is required for the late phase surface area increase. Tissue was pre-treated with 100 μg/ml cycloheximide for 60 min prior to stretching the tissue. Mean changes in capacitance ± SEM ($n \geq 3$) are shown. The * symbol indicates a statistically significant difference ($p < 0.05$) relative to stretched samples. (D) Slow stretching also induces an EGFR-dependent increase in surface area. Isolated rabbit uroepithelium was equilibrated in Ussing stretch chambers. The chamber was filled at a rate of 0.1 ml/min using a NE-1600 pump. Tissue was treated with 25 nM AG-1478 for 30 min prior to slow stretch. Mean changes in capacitance ± SEM ($n \geq 3$) are shown. The * symbol indicates a statistically significant difference ($p < 0.05$) relative to slow-stretched samples.

eliminated by incubating the tissue for 60 min in cycloheximide prior to stretch, indicating that the late phase is dependent upon protein synthesis (Figure 2.1C). We previously showed that the secretory inhibitor brefeldin A (BFA) impaired release of newly synthesized secretory proteins from the apical pole of umbrella cells [47]. In this study, BFA treatment eliminated the late-phase increase but had no effect on the early-phase response to stretch (Figure 2.2A). This suggests that the early-phase response may depend on exocytosis of a pre-existing pool of discoidal vesicles while the late-phase response may be more dependent on the exocytosis of newly synthesized proteins. The increases in capacitance observed in response to stretch were rapidly reversed when pressure in the mucosal hemichamber was released after 30 min or 5 h of stretch (Figure 2.2B), and increased endocytosis was detected when FITC-labeled lectins were included in the mucosal chamber during release (Figure 1.5). The data in Figure 2.2B demonstrate that extended exposure to stretch does not affect the ability of the mucosal surface to recover from stretch. The stretch-induced changes in capacitance were largely independent of the rate of chamber filling, as confirmed by studies in which filling was performed at a rate of 0.1 ml/min, which raised the pressure to ~ 1 cm H_20 over 30 min (Figure 2.1D). Under these conditions the initial kinetics of capacitance change were somewhat slower, but the absolute change in capacitance was ~ 50% after 5 h. Because there was no discernible difference in the late-phase response, we used the rapid filling technique in subsequent studies to simplify our experiments.

Our studies focused on characterizing the signaling pathways involved in the late-phase, protein-synthesis dependent response to stretch. To examine whether tyrosine kinase signaling pathways were required for this response, the uroepithelium was stretched in the presence of 100 μM genistein, a broad range inhibitor of tyrosine kinases and their signaling. Genistein treatment

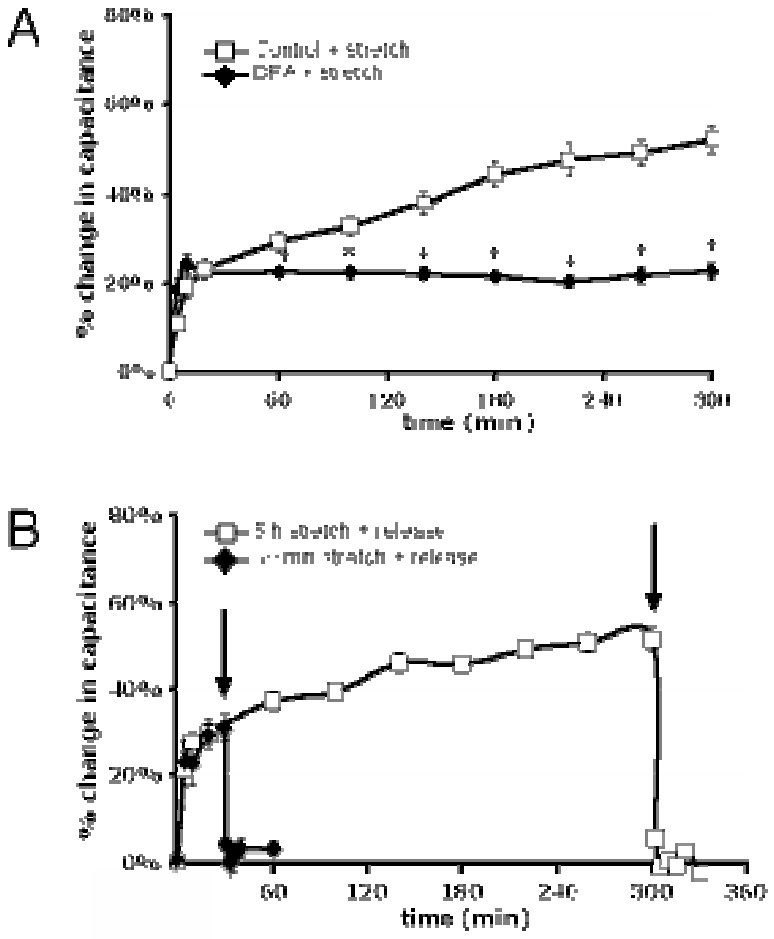

Figure 2.2: Characterization of the response to uroepithelial stretch.

(A) Tissue was pre-treated with 5 μg/ml BFA for 10 min prior to stretching the tissue in the continued presence of BFA. The * symbol indicates a statistically significant difference ($p < 0.05$) relative to stretched samples. (B) Tissue was stretched for 30 min or 5 h, and then the added Krebs buffer was removed (indicated by arrows), releasing the stretch stimulus. Mean changes in capacitance ± SEM ($n \geq 3$) are shown.

eliminated the late-phase increase in capacitance (Figure 2.3A). To further establish a role for tyrosine kinase signaling in regulating exocytosis in umbrella cells, non-stretched tissue was treated with hydrogen peroxide, which indirectly increases tyrosine phosphorylation by oxidizing a critical SH-group in the catalytic site of protein tyrosine phosphatases [93]. Hydrogen peroxide treatment induced an ~ 27% increase in surface area over 5 h. This response was significantly inhibited by pre-treatment of the tissue with genistein (Figure 2.3B), indicating that the hydrogen peroxide-stimulated increase in capacitance was a likely consequence of increased tyrosine phosphorylation and not other non-specific effects of hydrogen peroxide.

To explore which tyrosine kinase signaling pathways might be involved in modulating stretch-induced exocytosis, inhibitors were used that targeted tyrosine kinases implicated in mechanotransduction in other cell types, including the EGFR selective antagonist tyrophostin AG-1478, the PDGFR inhibitor AG-1296, the src-family selective inhibitor PP2, and the JAK-2 inhibitor AG-490. Only treatment with AG-1478 significantly decreased the stretch-induced changes in the late-phase response (Figure 2.3C). The inactive tyrophostin AG-9 control had no significant effect on the stretch response (Figure 2.3C), and AG-1478 caused no changes in surface area in the absence of stretch (Figure 2.3D). AG-1478 similarly attenuated the stretch-induced capacitance changes in slowly stretched tissue (Figure 2.1D). Overall, the data indicated that stretch-induced changes in capacitance were dependent on tyrosine phosphorylation, most likely downstream of EGFR signaling.

2.2.2 ErbB family members and their ligands are expressed in the uroepithelium

To determine the ErbB family receptor and ligand expression profile in the uroepithelium, total RNA from isolated rabbit uroepithelium was prepared and message for rabbit ErbB family

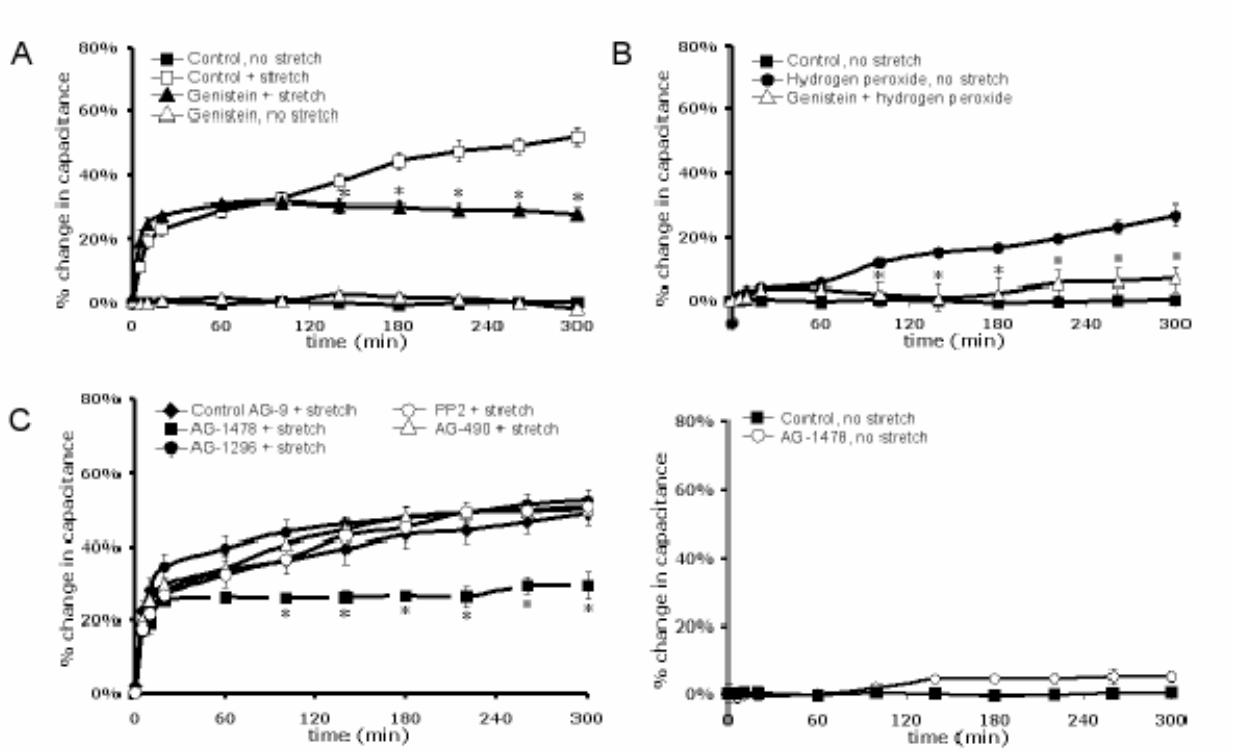

Figure 2.3: Tyrosine kinase signaling is required for the late-phase increase in capacitance.

Rabbit uroepithelium was dissected and mounted in Ussing stretch chambers, equilibrated in the absence of pressure, and stretched at t = 0. (A) Genistein, 100 μM, was added to both serosal and mucosal hemichambers for 30 min prior to stretch (Genistein + stretch). As a control, the tissue received genistein treatment in the absence of stretch (Genistein, no stretch). The * symbol designates a statistically significant difference ($p < 0.05$) between genistein-treated and control stretched samples. (B) H_2O_2 was added to the mucosal chamber at t = 0 to a final concentration of 1 mM in the absence of stretch. Genistein treatment (as above) was performed 30 min prior to H_2O_2 addition (genistein + hydrogen peroxide) and changes in capacitance were monitored. The * symbol indicates a statistically significant difference ($p < 0.05$) between treatment with H_2O_2 alone or treatment with H_2O_2 and genistein. (C) Both tissue surfaces were pretreated for 30 min with 25 nM AG-1478, 25 μM AG-1296, or 25 nM AG-9; or for 60 min with 30 μM AG-490 or 25 nM PP2; and then stretched in the continued presence of the drug. (D) Both tissue surfaces were pretreated for 30 min with AG-1478. The * symbol indicates a statistically significant difference ($p < 0.05$) between AG-1478 treated and control stretch samples. Mean changes in capacitance ± SEM ($n \geq 3$) are shown.

receptor and ligands was confirmed by RT-PCR. Rabbit nucleotide sequences for ErbB1-4, EGF, HB-EGF, and TGFα were obtained from the NCBI DNA sequence databases (http://www.ncbi.nlm.nih.gov/sites/entrez). Transcripts for EGFR, ErbB2, and ErbB3 were detected in all samples tested (n=6), consistent with previous reports that showed ErbB1-3 expression in human uroepithelium [88]. In contrast, ErbB4 transcript was not detected in 5 of 6 samples tested (Figure 2.4A), indicating that expression of ErbB4 was generally low or undetectable in this tissue. ErbB4 transcript was robustly detected in total RNA prepared from rabbit spinal cord, which was used as a positive control (Figure 2.4A). The mRNA for ErbB family ligands EGF, HB-EGF, and TGFα was present in all rabbit uroepithelial RNA preparations tested (Figure 2.4B), consistent with previous reports of these ligands being expressed in the uroepithelium [89, 90]. Negative-control RT-PCR reactions using either scrambled primer pairs or no polymerase resulted in no PCR products (Figure 2.4B). The identities of the PCR products were verified by nucleotide sequencing.

Immunofluorescence staining was performed to confirm the expression of EGFR, ErbB2, and ErbB3 in the uroepithelium and determine their distribution within this tissue. Bladder tissue was fixed, cryo-sectioned, and stained using ErbB receptor specific antibodies, along with Topro-3 to label nuclei and rhodamine phalloidin to visualize the actin cytoskeleton. In mouse tissue, EGFR staining was observed in the cytoplasm of the underlying intermediate and basal cell layers as well as in the umbrella cell layer. In addition, EGFR was prominently localized near the apical surface of ~ 70% of umbrella cells (Figure 2.4C, left panel), while no staining was observed in the remaining 30% of umbrella cells. The reason for this disparity is unknown but may reflect differences in the state of umbrella cell differentiation or their state of response to bladder filling/voiding. A similar EGFR staining pattern was observed in rabbit bladder tissue,

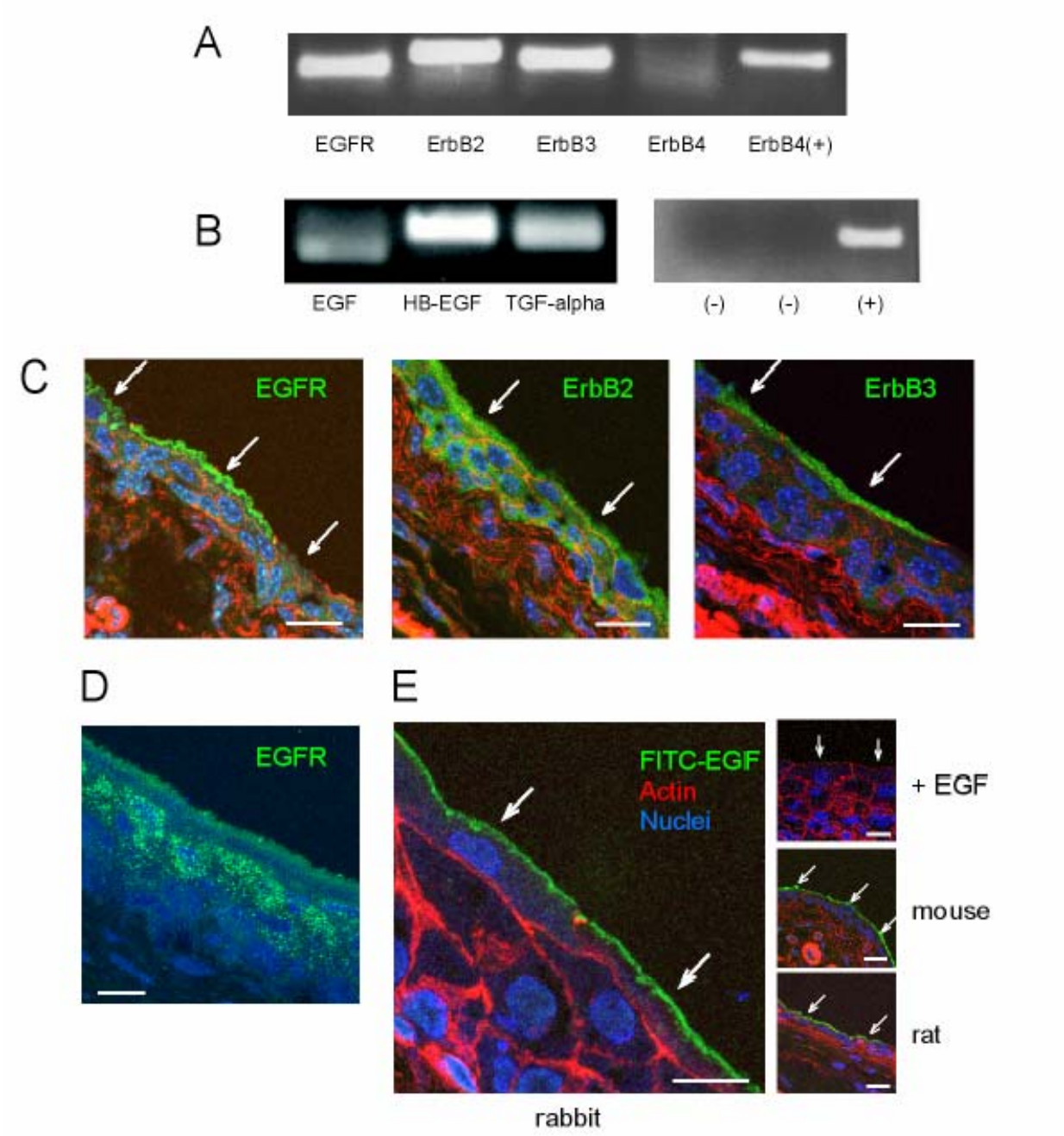

Figure 2.4: Expression and distribution of ErbB family receptors in the uroepithelium.

(A-B) Total RNA was prepared from rabbit uroepithelium and RT-PCR was used to assess expression of (A) ErbB1-4, or (B) EGFR ligands EGF, HB-EGF, and TGFα. The RNA sample in the lane designated ErbB4(+) was prepared from rabbit spinal cord tissue. In B, the first (-) control lane shows a reaction using scrambled primer pairs, the second (-) lane reaction included no polymerase, and the (+) control lane included a set of control primers provided by the manufacturer. (C) Localization of ErbB family receptors in cryosections of mouse uroepithelium, labeled with antibodies to visualize the receptors (green), rhodamine-phalloidin to label the actin cytoskeleton (red), and Topro-3 to label nuclei (blue). Scale bar = 20 μm. (D) Localization of

EGFR in rabbit uroepithelium, with Topro-3 staining to label nuclei (blue). Scale bar = 15 μm. (E) Binding of FITC-EGF to rabbit uroepithelium (left-most panel), in which tissue was bathed in 40 ng/ml FITC-EGF at 4˚ C for 1 h, washed, fixed, and sectioned. In the control study (right top-most panel), FITC-EGF binding to rabbit tissue was competed with excess unlabeled EGF (400 ng/ml). FITC-EGF binding to the apical surface of mouse and rat umbrella cells is shown in the right middle and right bottom panel, respectively. Scale bar = 15 μm for rabbit tissues and 20 μm for mouse and rat tissues. Individual umbrella cells are indicated by arrows.

with some surface staining but increased underlying cytoplasmic staining (Figure 2.4D). Immunofluorescence studies of mouse bladder tissue revealed ErbB2 staining throughout all layers of the uroepithelium (Figure 2.4C, middle panel), and ErbB3 staining within the umbrella cell layer of the uroepithelium (Figure 2.4C, right panel).

To confirm that EGFR was present at the apical surface of umbrella cells, rabbit bladder tissue was incubated with FITC-EGF (40 ng/ml) for 1 h at 4^{o}C, washed, fixed, and sectioned. Although FITC-EGF was added to both the serosal and mucosal surfaces of the tissue, appreciable binding was observed only at the apical surface of rabbit umbrella cells (Figure 2.4E, left-most panel). As a control, the tissue was incubated with competing unlabeled EGF (400 ng/ml), which effectively eliminated FITC-EGF staining (Figure 2.4E, right top panel). Binding of FITC-EGF to the apical surface of umbrella cells was also observed in mouse and rat uroepithelium (Figure 2.4E, right middle and bottom panels, respectively), further establishing that EGF receptors are present on the mucosal surface of umbrella cells. In summary, the above data confirmed expression of ErbB family receptors and ligands including EGFR, EGF, HB-EGF, and TGFα in the uroepithelium. Furthermore, the data indicated that EGF binds to the apical surface of the umbrella cell layer, where it may stimulate EGFR-dependent signaling.

2.2.3 EGF stimulates exocytosis in the uroepithelium

To determine if EGFR signaling induced membrane turnover in the uroepithelium, we explored the effects of adding EGF to either the mucosal or serosal surface of the tissue. The addition of 100 ng/ml EGF to the apical surface of the uroepithelium caused an ~ 31% increase in surface area over 5 h (Figure 2.5A). A similar increase (~ 34%) was observed upon addition of 100 ng/ml EGF to the serosal surface (Figure 2.5A). Interestingly, the kinetics of the response to EGF

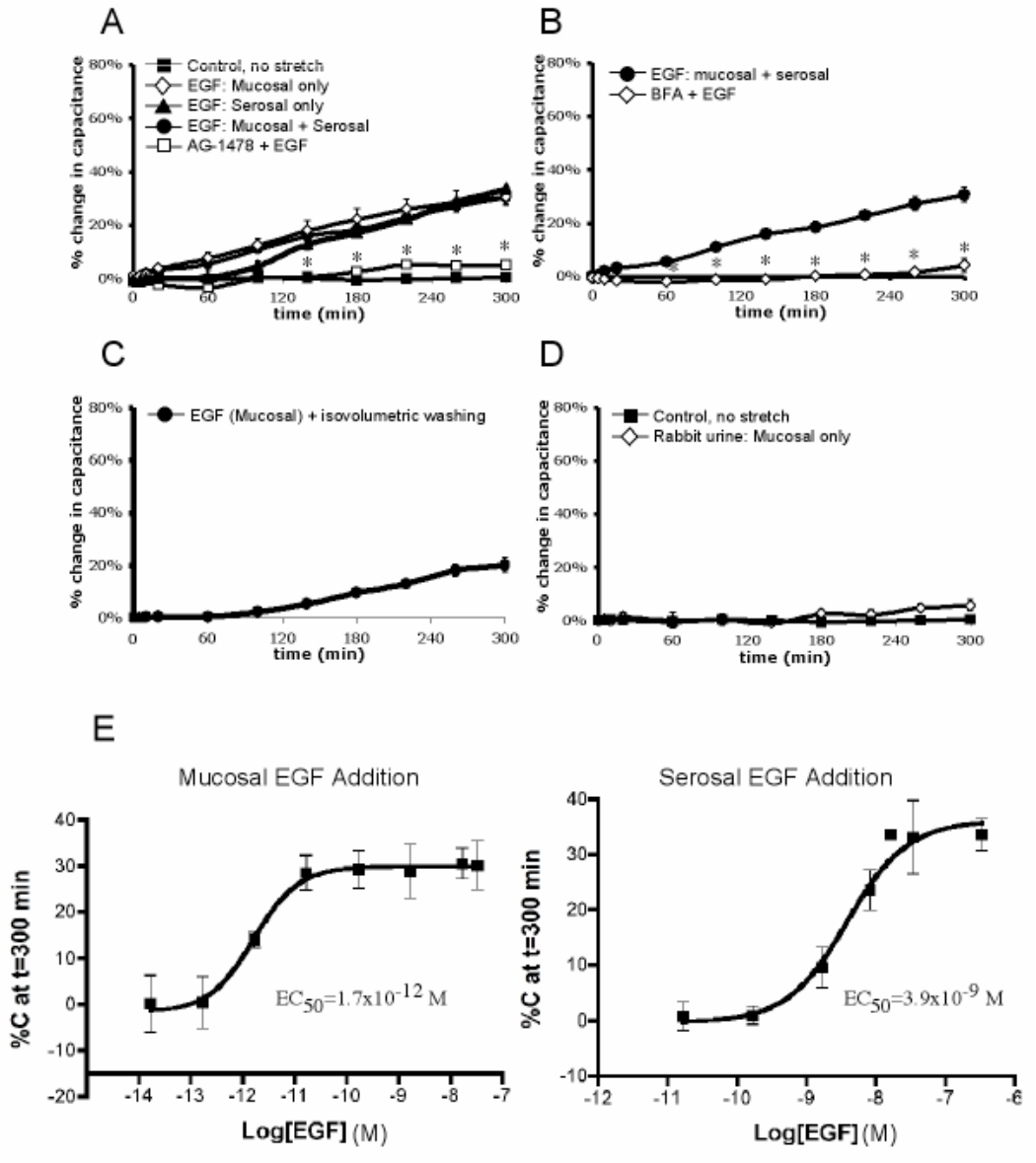

Figure 2.5: Exogenous EGF stimulates capacitance increases in the absence of stretch.

Rabbit uroepithelium was mounted in Ussing stretch chambers and incubated in the absence of pressure. (A) Changes in capacitance were recorded upon addition of 100 ng/ml EGF (± 30-min pretreatment with AG-1478) to the serosal, mucosal, or both surfaces. (B) Tissue was pre-treated with 5 μg/ml BFA prior to addition of 100 ng/ml EGF to both surfaces of the uroepithelium (BFA + EGF). (C) EGF was added to the mucosal hemichamber and after 5 min the buffer in the mucosal hemichamber was replaced with buffer lacking EGF. The change in capacitance was recorded. (D) Effect of undiluted rabbit urine on capacitance changes. (E) Dose-response curves for the change in capacitance recorded 5 h after addition of EGF to mucosal or serosal surface of the uroepithelium. In each panel the mean changes in capacitance ± SEM ($n \geq$

3) are shown. The * symbol in A & B designates a statistically significant difference ($p < 0.05$) relative to addition of EGF to both surfaces.

addition were reminiscent of the late-phase increase in response to stretch; a gradual increase of ~ 30% over 5 h. A similar response (~ 30% increase) was observed upon addition of other ErbB family ligands in the absence of stretch, including 100 ng/ml HB-EGF, 25 ng/ml TGFα, and 100 ng/ml heregulin-β (Figure 2.6A). The effect of simultaneous addition of EGF to both surfaces was not additive, indicating that the signaling mechanisms from either surface were likely to be similar, if not identical. When EGF (at 100 ng/ml) was added at the same time as stretch, the overall increase was not significantly different than stretch alone (Figure 2.6B), demonstrating that the signaling pathways for these two stimuli were not additive. The specificity of the EGF response was confirmed by pre-incubation of the tissue with AG-1478 (Figure 2.5A) or treatment with BFA (Figure 2.5B), both of which significantly inhibited EGF-dependent responses. We also examined whether the EGF-stimulated increases in capacitance required chronic treatment with ligand or whether a short pulse of EGF was sufficient to stimulate exocytosis. A 5-min treatment of EGF, followed by washes to remove the added EGF, was sufficient to stimulate an ~ 20% increase in capacitance (Figure 2.5C).

There is an appreciable amount of EGF and other EGFR ligands present in urine [36, 70]. To determine whether these urinary ligands were able to stimulate discoidal vesicle exocytosis, we added undiluted urine to the mucosal chamber of unstretched tissue and monitored capacitance. However, we found that addition of urine caused no significant change in capacitance over 5 h (Figure 2.5D).

Dose response studies were performed to determine the EC_{50} for EGF-induced changes in capacitance. The EC_{50} for mucosally added EGF was 1.7×10^{-12} M, which was ~ 2000 fold more potent than the EC_{50} for serosally added EGF (3.9×10^{-9} M)(Figure 2.5E). In subsequent studies we used the minimum effective concentration of EGF that induced a ~ 30% increase in stretch:

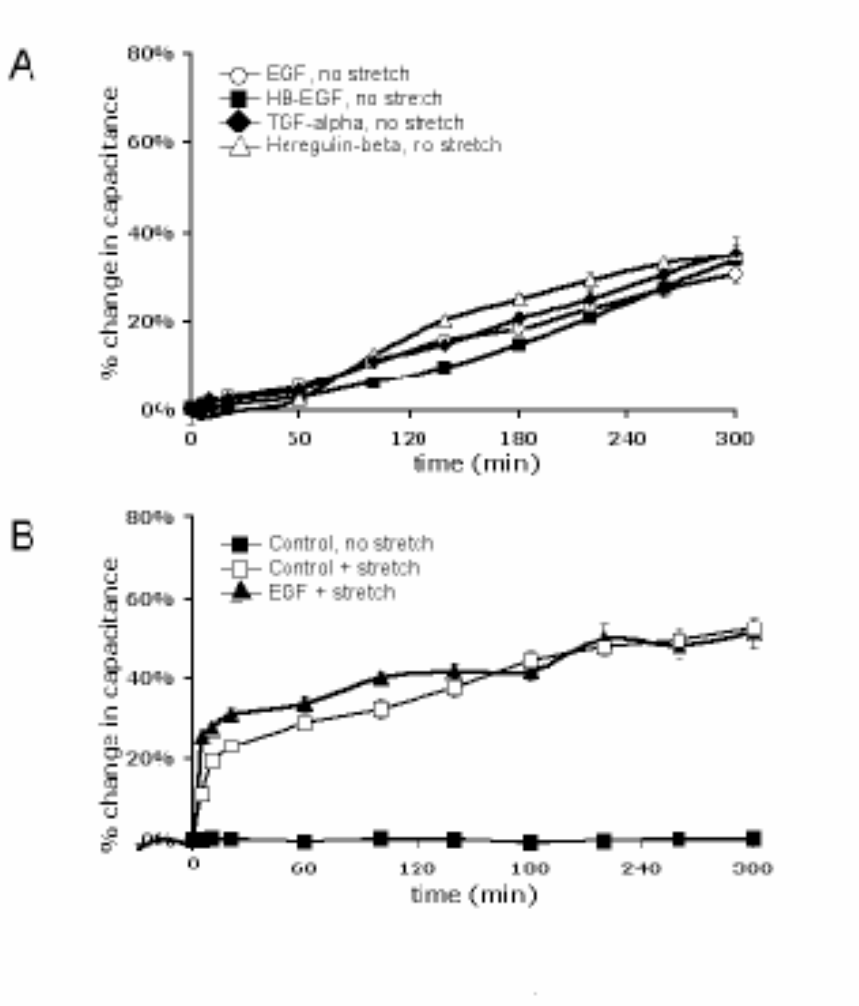

Figure 2.6: EGFR ligands induce a capacitance increase which is not additive with stretch.

Rabbit uroepithelium was mounted in Ussing stretch chambers treated as indicated. (A) Changes in capacitance were recorded upon addition of 25 ng/ml EGF, 100 ng/ml HB-EGF, 25 ng/ml TGFα, or 100 ng/ml heregulin-β to the serosal and mucosal surfaces in the absence of stretch. (B) 100 ng/ml EGF was added to both surfaces of the tissue, which was immediately stretched.

0.1 ng/ml EGF mucosally and 100 ng/ml EGF serosally. In summary, addition of EGF (as well as other ErbB-family ligands) to either surface of the bladder tissue stimulated an increase in mucosal surface area in the absence of stretch, although EGF treatment was significantly more potent when added to the mucosal surface of the tissue.

2.2.4 Stretch stimulates autocrine activation of EGFR by HB-EGF

Because EGFR signaling appeared to be necessary for late-phase, stretch-induced changes in capacitance, EGFR activation was assessed by examining the phosphorylation state of Y_{1068} and Y_{1173}, residues that are autophosphorylated in response to receptor activation [e.g. upon ligand binding, 94]. In our experiments, the uroepithelium was stretched in Ussing stretch chambers for up to 5 h, and then the tissue was rapidly removed from the chamber, placed on ice, and lysed (the isolation of tissue and preparation of lysate took approximately 5 min to complete). Total and phosphorylated EGFR were detected in lysates by western blot. Stretch was accompanied by a significant increase in Y_{1173}-EGFR phosphorylation that was apparent in as little as 2 min, and EGFR phosphorylation remained elevated for at least 10 min after stretch, but returned to baseline over time (Figure 2.7, A-B). Similar results were observed using an antibody specific for Y_{1068} phosphorylation (Figure 2.7A). As predicted, treatment with AG-1478 attenuated receptor phosphorylation (Figure 2.7C).

To ascertain the side of the tissue from which EGFR signaling occurred during stretch, a function-blocking EGFR antibody (LA1) was added to the mucosal or serosal surface of stretched tissue. Addition of the antibody to the mucosal surface blocked the late-phase

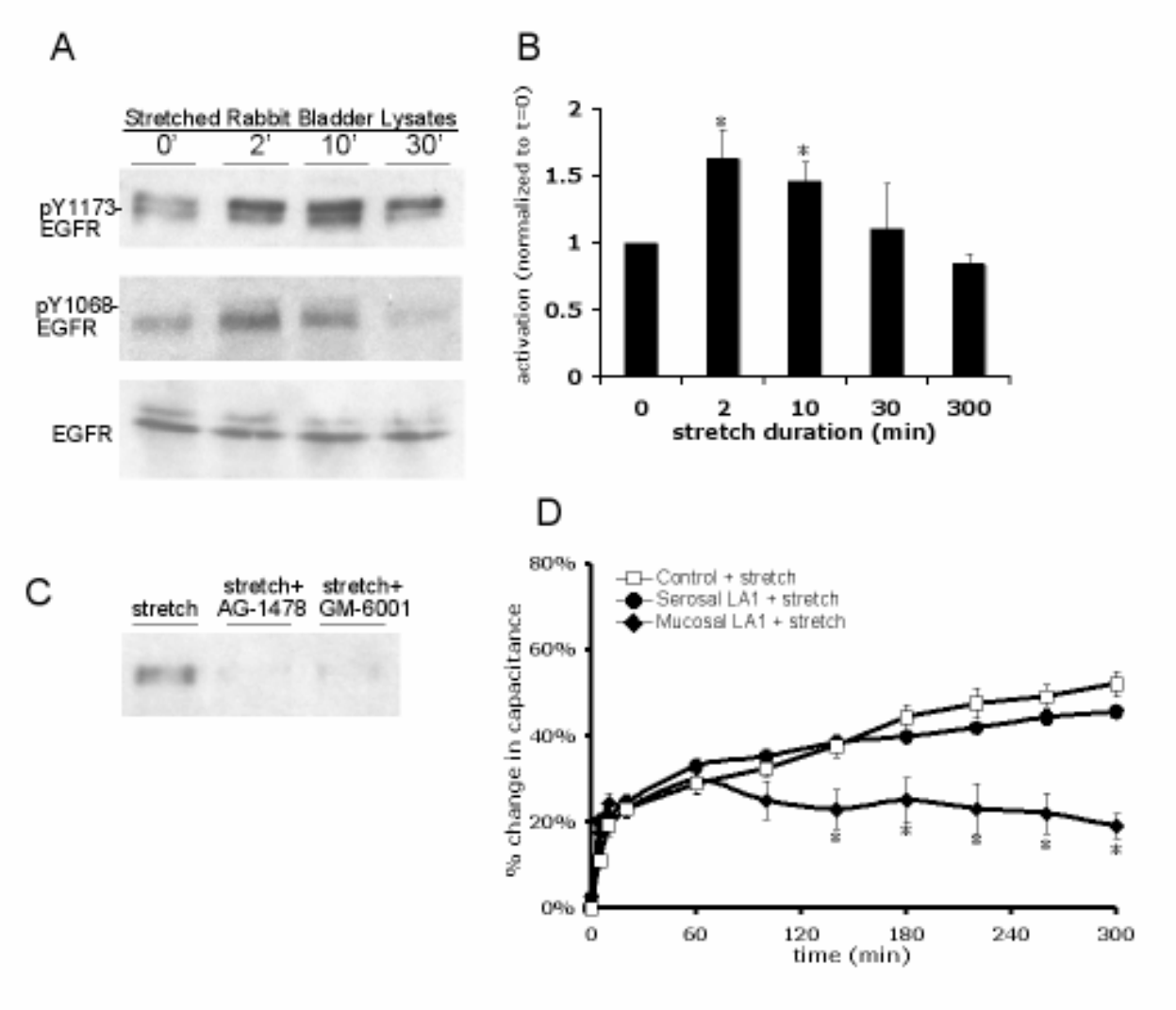

Figure 2.7: Stretch activates the EGFR.

(A) Tissue was stretched for the indicated time, lysates of rabbit uroepithelium were prepared and resolved by SDS-PAGE, and Western blots were probed with antibodies specific for Y_{1173}–EGFR, Y_{1068}–EGFR, or total EGFR. (B) Quantification of Y_{1173} phosphorylation in response to stretch, relative to unstretched (t = 0') tissue samples. The mean changes in capacitance ± SEM are shown (n=4). The * symbol indicates a statistically significant difference ($p < 0.05$) relative to unstretched tissue. (C) Tissue was stretched for 2 min in the absence of additional treatment, or pre-treated for 30 min with 25 nM AG-1478 or 10 μM GM-6001 prior to stretch, followed by lysate preparation. (D) Rabbit uroepithelium was placed on tissue rings and the mucosal or serosal surfaces were pretreated with 1 μg/ml LA1 EGFR function-blocking antibody for 1 hour prior to mounting, equilibrating, and stretching the tissue in Ussing stretch chambers. The mean changes in capacitance ± SEM ($n \geq 3$) are shown. The * symbol indicates a statistically significant difference ($p < 0.05$) relative to control stretch samples.

capacitance change (Figure 2.7D). Conversely, addition of the antibody to the serosal surface of the tissue had no significant effect on capacitance changes (Figure 2.7D). Because the serosal surface of our epithelial preparation contains residual connective, nervous, and muscle tissue that may impair access of large molecules like antibodies, we cannot rule out a role for basolateral EGFR in this process. However, the ability of mucosal LA1 and ligand-specific antibodies (see below) to completely block the late-phase increase in capacitance indicates that events at the apical surface of the umbrella cell are those most likely to be physiologically relevant to changes in mucosal surface area.

EGFR can be activated in an autocrine, paracrine, or juxtacrine manner [80]. Autocrine activation is modulated by metalloproteinases, which proteolytically cleave the transmembrane precursors of the ligands, releasing soluble ligands that can then bind and initiate receptor activation [80]. To explore the mechanism of ligand production in our system, uroepithelial tissue was treated with GM-6001, a broad-spectrum metalloproteinase inhibitor. Treatment with GM-6001 blocked stretch-activated EGFR phosphorylation (Figure 2.7C) and reduced the late-phase tissue response to stretch (Figure 2.8A). In contrast, the catalytically inactive GM-6001 (negative control) treatment had no effect on the response (Figure 2.8A). To define which ligand may be responsible for receptor activation, function-blocking antibodies to EGF, HB-EGF, or TGFα were added to the mucosal surface of the tissue for 1 h prior to tissue equilibration in the Ussing chamber. Mucosal addition of HB-EGF neutralizing antibody attenuated the late-phase capacitance response, while addition of antibodies to TGFα or EGF had no significant effect on the response (Figure 2.8B).

As further evidence that autocrine activation of EGFR was due to HB-EGF binding, the mucosal surface of the tissue was incubated with 5 μg/ml CRM-197, a non-toxic variant of

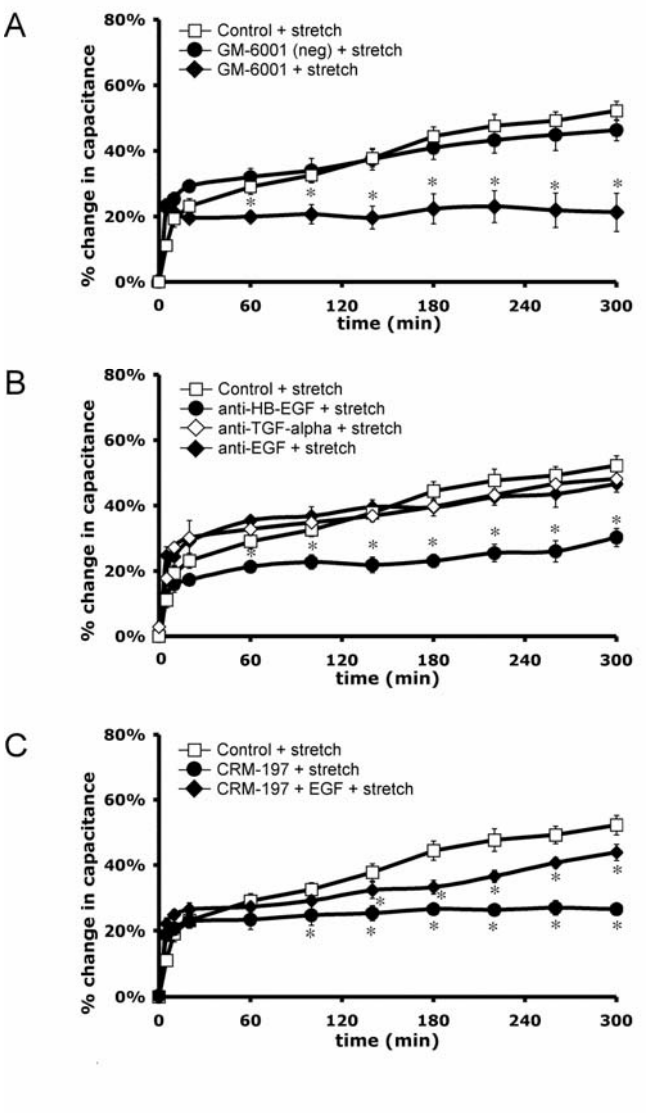

Figure 2.8: Metalloproteinase activity and HB-EGF ligand are required for the stretch-induced response.

Rabbit uroepithelium was isolated and mounted in Ussing stretch chambers. (A) Tissue was pretreated with 10 μM GM-6001 or inactive GM-6001 analog for 30 min prior to stretch. (B) Tissue was incubated with the specified ligand-neutralizing antibodies (20 μg/ml) added to the mucosal surface for 1 h prior to equilibration of the tissue and stretch. (C) Tissue was pretreated 30 min with 5 μg/ml CRM-197 toxin and then stretched in the presence or absence of 100 ng/ml mucosal EGF. In each panel, mean changes in capacitance ± SEM ($n \geq 3$) are shown. The * symbol indicates a statistically significant difference ($P < 0.05$) relative to control stretch samples.

Corynebacterium diphtheria toxin that strongly binds to membrane associated and soluble HB-EGF, preventing HB-EGF from activating EGFR [95]. CRM-197 binding does not affect the activity of other ErbB ligands. CRM-197 treatment significantly inhibited the late-phase, stretch-induced changes in capacitance, and this effect was partially rescued by the simultaneous addition of EGF (100 ng/ml) to the mucosal hemichamber (Figure 2.8C). Taken together, the above studies indicate that EGFR is activated by stretch and that stretch-induced capacitance changes are initiated at the mucosal surface of the tissue as a result of autocrine activation of receptor upon HB-EGF binding.

2.2.5 EGFR-stimulated exocytosis depends on protein synthesis and acts via a MAPK signaling pathway

The late-phase changes in capacitance are dependent on protein synthesis (Figure 2.1C). However, the upstream mechanism that initiates this synthesis is unknown. The EGFR can regulate protein synthesis through several mechanisms including downstream stimulation of MAPK cascades. In the classical MAPK pathway, extracellular stimuli lead to the activation of MAPKs through the serial phosphorylation of a cascade of serine/threonine-specific protein kinases including a MAPK kinase kinase (e.g. Raf), a MAPK kinase (e.g. MEK1/2), and finally a target MAPK, such as p38, JNK, or ERK1/2. The phosphorylated MAPK, in turn, phosphorylates transcription factors that alter gene expression [82]. While EGFR signaling activates many downstream signaling pathways including phosphoinositide-3-kinase, JAK-STAT, and protein kinase C, we chose to focus on MAPK signaling because of its known interface with protein synthesis regulation machinery and our interest in the late-phase response to stretch.

To further dissect the pathway by which EGFR signaling induces the late-phase increase in surface area, we examined whether the EGF-dependent increase in capacitance required protein synthesis. Indeed, when uroepithelial tissue was pretreated with 100 μg/ml cycloheximide for 1 h, the response to EGF was eliminated (Figure 2.9A). Next, we examined whether MEK 1/2, the upstream kinase that activates ERK1/2, was involved in the response to stretch. The MEK1 inhibitor PD-098059 (10 μM) and dual MEK1/2 inhibitor U0126 (10 μM) both caused a significant attenuation of the stretch-induced capacitance response, effectively eliminating the late-phase rise in capacitance (Figure 2.9B). These inhibitors were also effective in eliminating EGF-induced increases in surface area (Figure 2.9C). Treatment with SB-203580 (10 μM), a p38 MAPK selective inhibitor, also attenuated the late-phase, stretch-induced increase in surface area (Figure 2.9B), and eliminated the capacitance increase in response to EGF (Figure 2.9C). In contrast, the JNK Inhibitor II (500 nM) had no significant effect on stretch- or EGF-induced capacitance changes (Figure 2.9, B-C).

Finally, we examined whether ERK1/2 was phosphorylated as a result of stretch and whether its activation occurred downstream of EGFR activation. When western blots of lysates (obtained from tissue ± stretch) were probed with antibodies that detect phosphorylated forms of ERK1/2, stretch stimulated the phosphorylation of ERK1/2 (Figure 2.9D). Stretch-stimulated phosphorylation of ERK1/2 was attenuated by treatment with either AG-1478 or GM-6001 (Figure 2.9E), indicating that the ERK1/2 phosphorylation was dependent on upstream EGFR activation. Collectively, these studies implicate MAPK signaling cascades as acting downstream of EGFR activation to stimulate stretch-induced changes in capacitance, possibly by regulating changes in protein synthesis.

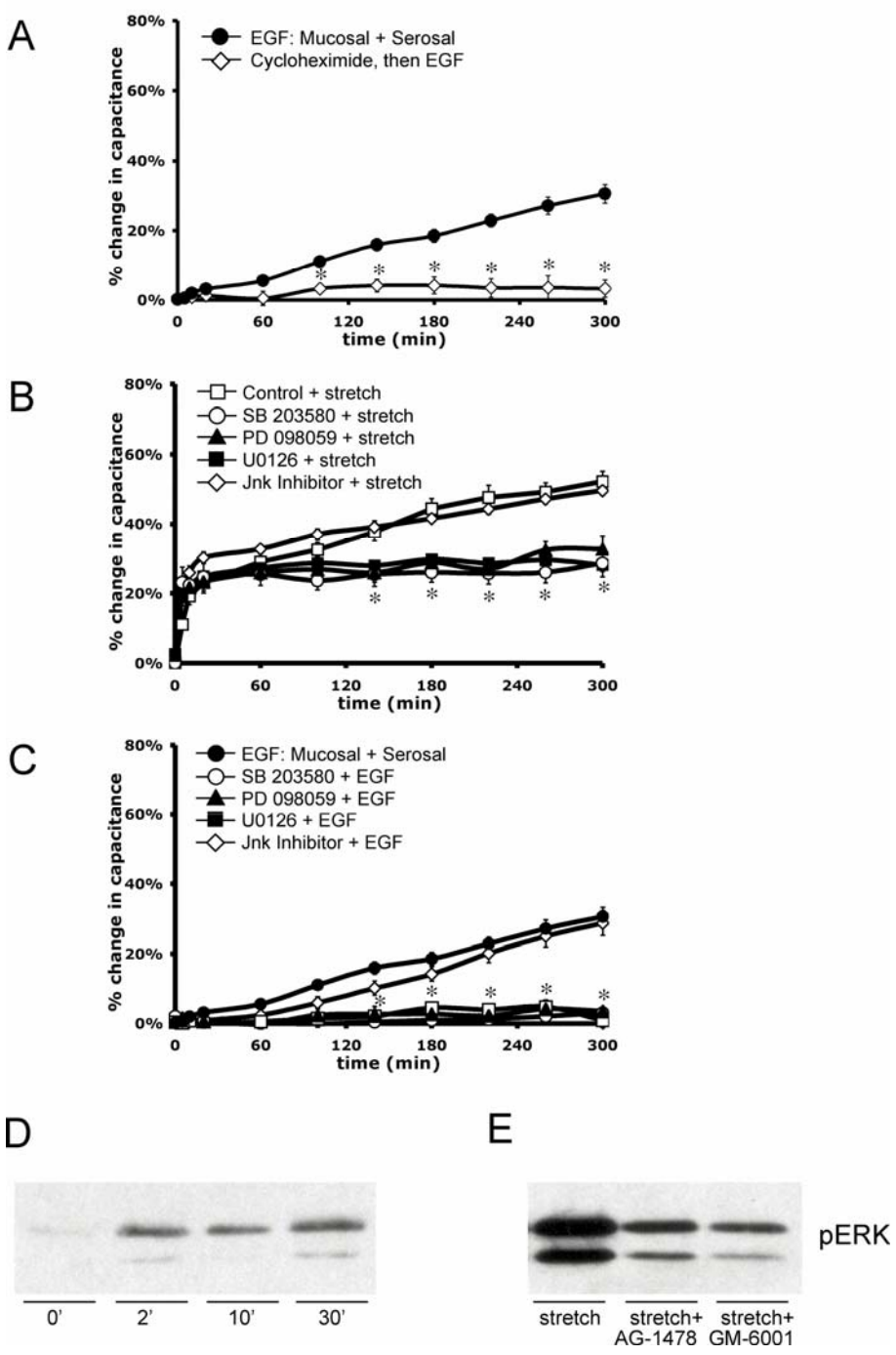

Figure 2.9: Protein synthesis and MAPK signaling pathways are required.

Rabbit uroepithelium was isolated and mounted in Ussing stretch chambers. (A) Tissue was incubated with 100 ng/ml EGF (± 60 min pretreatment with 100 μg/ml cycloheximide). The * symbol indicates a statistically significant difference ($p < 0.05$) relative to EGF-treated samples. (B) Prior to stretch, tissue was pretreated with p38 inhibitor SB-203580 (10 μM for 1 h), MEK1 inhibitor PD-098059 (10 μM for 30 min), MEK1/2 inhibitor U0126 (10 μM for 30 min), or JNK Inhibitor II (500 nM for 30 min) as indicated. The * symbol indicates a statistically significant

differences ($p < 0.05$) relative to control samples were observed for tissue treated with SB-203580, PD-098059, or U0126 at t ≥ 140 min. (C) Prior to treatment with 100 ng/ml EGF, tissue was incubated with SB-203580, PD-098059, U0126, or JNK Inhibitor II as above. The * symbol indicates a statistically significant differences ($p < 0.05$) relative to control samples were observed for tissue treated with SB-203580, PD-098059, or U0126 at t ≥ 100 min. In each panel, the mean changes in capacitance ± SEM ($n \geq 3$) are shown. (D) Tissue was stretched for the indicated time prior to lysate preparation. Western blots were probed with antibodies specific for pERK1/2. (E) Tissue was left untreated (stretch) or pretreated for 30 min with 25 nM AG-1478 (AG) or 10 μM GM-6001 (GM) as indicated. Tissue was then stretched for 2 min prior to lysate preparation and blotting with phospho-specific antibodies to ERK1/2.

2.3 DISCUSSION

Mechanotransduction is a complex process that converts physical stimuli to biological responses. While stretch-activated channels, integrins, and intracellular signaling pathways such as tyrosine kinase signaling cascades have been implicated in these responses, we still lack a precise understanding about how mechanical inputs are sensed and deciphered by the cell [51, 52]. Previous analysis has pointed to roles for the EGFR and ErbB family members in bladder development, hypertrophy of bladder smooth muscle in response to mechanical stress, and pathogenesis of transitional cell carcinoma [96-98]. Other than studies showing potential roles for ErbB signaling in the regulation of uroepithelial growth and proliferation [96, 99], significantly less information is available about the physiological function of EGFR in the uroepithelium. Our data provide a novel link between mechanical stimuli, apical EGFR signaling, and changes in apical membrane turnover in the umbrella cell layer of the uroepithelium.

2.3.1 Distribution of ErbB family receptors in epithelia including the uroepithelium

In the mammalian bladder, the EGFR and other ErbB family members have been variably localized in the uroepithelium [43, 87, 88], with the majority of studies reporting that the EGFR is found in the basal cell layers. EGFR is typically localized to the basolateral surface of polarized cells. In contrast, our data indicate that the EGFR is localized, in part, to the apical surface of the umbrella cell layer where, as discussed below, it regulates apical membrane

turnover. Data in support of the apical localization of EGFR included: (i) our immunofluorescence studies showing that the EGFR in both mice and rabbits was localized at or near the apical surface of the umbrella cell layer; (ii) demonstration that FITC-labeled EGF bound to the apical surface of umbrella cells at 4˚C in rabbit, rat, and mouse tissue; (iii) the ability of small amounts of apically administered EGF to stimulate exocytosis (with an EC_{50} of ~ 2 pM); and (iv) the finding that neutralizing anti-EGFR specific antibodies or anti-HB-EGF antibodies impaired stretch-induced exocytosis when added to the mucosal surface of the isolated uroepithelium.

2.3.2 Activation of EGFR by uroepithelial stretch: a possible autocrine loop

The EGFR is activated by mechanical stimuli in a number of cell types including mesangial cells, keratinocytes, vascular smooth muscle cells, type II alveolar cells, bronchial epithelial cells, cardiac myocytes, and proximal tubule cells [50, 76, 92, 100-103]. However, the link between mechanical stimuli, EGFR activation, and changes in membrane traffic has not been described. We observed that stretching the uroepithelium stimulated a rapid increase in EGFR receptor phosphorylation, and treatments that blocked EGFR activation (e.g. treatment with AG1478 or apical addition of LA1 anti-EGFR antibody) inhibited late-phase changes in exocytosis.

While these data indicate that EGFR signaling initiated at the apical surface of the umbrella cells is primarily responsible for the late-phase stretch-induced changes in surface area, we cannot rule out a role for EGFR at the serosal surface of the tissue. In fact, EGF (in the absence of stretch) stimulated similar changes in capacitance when added to either surface of the tissue; however, mucosal EGF was ~ 2000-fold more potent at stimulating exocytosis than serosal EGF.

The EC_{50} for EGF-stimulated changes in apical membrane capacitance (~ 2.0 pM) was similar to the reported 10-100 pM K_D associated with the high-affinity type EGFR [104], indicating that subnanomolar amounts of ligand are sufficient to give the maximal response. The EGFR can form homodimers or heterodimers with ErbB2-4, and because ErbB2 and ErbB3 were expressed in the uroepithelium, it is possible that other ErbB family receptors are activated during stretch-induced changes in exocytosis by formation of heterodimers with EGFR. The higher EC_{50} we measured upon serosal EGF addition may suggest the presence of lower-affinity receptors present at the basolateral surface of the umbrella cells. However, this interpretation is likely to be simplistic as there are multiple cell types present on the serosal side of the tissue, and we cannot rule out that EGF is binding to underlying cell types that release secretagogues that stimulate exocytosis in the umbrella cell layer. As such, the higher EC_{50} could reflect mixed populations of low and high affinity EGFRs present on different cell types, decreased receptor density, or increased turnover of ligand or receptors at this surface of the tissue.

EGFR activation in our system is likely via an autocrine mechanism. Consistent with previous studies [89, 90], we observed that rabbit uroepithelium expressed the ErbB ligands EGF, HB-EGF, and TGFα. Importantly, we observed that addition of function-blocking antibodies directed against HB-EGF, but not EGF or TGFα, inhibited late-phase changes in exocytosis when added to the mucosal surface of the tissue. Furthermore, we observed that the general metalloproteinase inhibitor GM-6001 inhibited stretch-induced EGFR activation and blocked late-phase changes in exocytosis, consistent with blocking the generation of HB-EGF. However, we cannot rule out that GM-6001 blocked exocytosis by preventing metalloproteinase-dependent cleavage of an unknown substrate required for stretch-regulated exocytosis.

Autocrine activation of EGFR by mechanical stimuli such as stretch may occur as a result of receptor transactivation, where an upstream stimulus such as elevated intracellular Ca^{2+}, exposure to radiation, or activation of G-protein coupled receptors promotes proteolytic processing and release of ErbB family ligands, typically HB-EGF, that rapidly bind to and activate the EGFR [105]. We previously reported that stretch stimulates rapid release of ATP from the uroepithelium, and that serosal ATP acts through a Ca^{2+}-dependent pathway to stimulate umbrella cell discoidal vesicle trafficking [41]. However, our previous studies could not rule out a role for G-protein coupled P2Y receptors in this process.

One plausible model is that ATP binds to P2Y receptors, which in turn stimulates a heterotrimeric G-protein to activate proteolytic cleavage and release of ligand(s) such as HB-EGF. Transactivation of EGFR downstream of ATP has previously been shown to occur in Muller glial cells [106]. Alternatively, the increased Ca^{2+} stimulated by ATP binding to P2X receptors could result in EGFR transactivation. The extremely low EC_{50} we measured for EGF-stimulated increases in exocytosis indicates that even small amounts of local ligand production would be sufficient to stimulate exocytosis. It is equally plausible that many of the mediators we have previously found to stimulate exocytosis, such as adenosine and agents that increase intracellular Ca^{2+} and cAMP [41, 42, 47, 58], may act, in part, by EGFR transactivation.

We examined the possibility that EGFR ligands present in urine may activate the EGFR in a paracrine manner. However, we found that urine added to the mucosal surface of the isolated uroepithelium did not stimulate exocytosis. This may indicate that urinary EGFR ligands may not be functional, e.g. urinary exopeptidases and endopeptidases could decrease the fraction of active EGF [36, 107], or they may have limited access to EGFR present on the apical surface of the umbrella cells. However, we cannot rule out a paracrine role for EGF at the serosal surface of

the tissue as EGF addition at this surface of the tissue stimulated exocytosis in the umbrella cell layer.

We also observed that exogenous stimulation of the EGFR by EGF addition caused a slow rise in capacitance, similar to the late-phase increase in response to stretch; however, this response was not reversible upon EGF washout. On the other hand, stretch-induced changes in capacitance were fully reversible, indicating that "unstretching" the tissue activated its own set of responses that effectively turned off the pathway(s) that stimulated exocytosis. These "unstretching" responses are likely to include increased compensatory endocytosis of apical membrane in a pathway independent of EGFR signaling. Future studies will explore the uroepithelial response to removal of a stretch stimulus and the endocytic pathways associated with bladder voiding.

2.3.3 Requirement for MAPK signaling and protein synthesis

The early phase of the stretch-induced capacitance increase is inhibited by the P2 receptor antagonist PPADS and agents that deplete extracellular ATP [41], and is insensitive to cycloheximide treatment [47](Figure 2.1C). In contrast, the late-phase capacitance response is dependent on protein synthesis (Figure 2.1C). While we do not know the nature or identity of the proteins whose synthesis is altered in response to stretch, our data indicate that their expression may be altered downstream of MEK1/2 and possibly p38 MAPK signaling pathways. In contrast, a JNK-selective inhibitor had no effect on the stretch- or EGF-induced response. The likely requirement for both MEK/ERK and p38 indicates that they may regulate distinct classes of gene products, both of which are required for late-phase increases in capacitance. The activation of other ErbB downstream pathways (such as phosphoinositide-3-kinase, JAK-STAT, and protein

kinase C) and their roles in stretch-induced trafficking in the bladder have not been explored, but they may also have significance in uroepithelial biology.

2.3.4 Concluding Remarks

The apical plasma membrane of epithelial cells serves as a signaling platform that receives input from the extracellular milieu. Through surface receptors and channels and their associated signaling cascades, extracellular stimuli are transduced into changes in cell function. In the case of the umbrella cell, exocytosis/endocytosis at the apical surface of the cell is particularly important as it allows for surface area expansion during bladder filling (and recovery of membrane upon voiding), and modulation of the sensory input/ouput pathways by regulating the release of transmitters and the density of receptors at the surface of the umbrella cell. This regulation is likely to be clinically important, as increased ErbB family receptor expression is observed in bladder cancers [43, 87, 88], and painful bladder conditions are associated with increased ATP release and expression of increased levels of nociceptive $P2X_2$ and $P2X_3$ receptor subunits [68, 108]. In this report we provide evidence that bladder filling may stimulate autocrine activation of EGFR at the apical pole of the umbrella cell layer, initiating a signaling cascade that regulates the extended late phase of exocytosis in the umbrella cell layer in a MAPK- and protein synthesis-dependent manner (Figure 2.10). The uroepithelium is thus an excellent model system to explore the interface between the apical membrane of epithelial cells, mechanical stimuli, growth factor signaling, and apical membrane dynamics. Further, these data offer a novel function for apical EGFR in the regulation of surface area changes in the uroepithelium during physiological stretch.

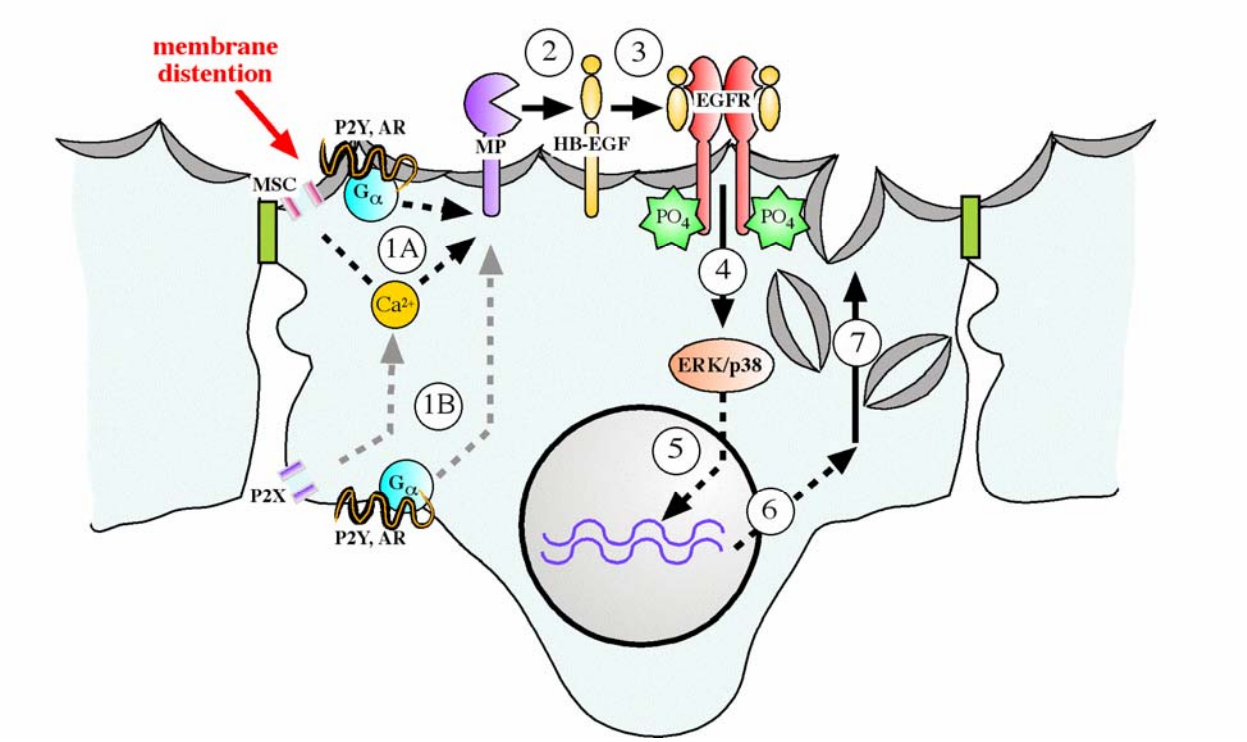

Figure 2.10: Model for regulation of late-phase exocytosis by transactivation of EGFR.

The mechanical distention caused by bladder filling may stimulate release of mediators such as ATP and adenosine (not shown)[41, 42], which bind to P2X, P2Y, or adenosine receptors (AR). Alternatively, filling may directly activate other signaling pathways such as those initiated by putative mechanosensitive channels (MSC). The increased intracellular Ca^{2+} or activation of heterotrimeric G proteins that initiates at the mucosal (step 1A) or possibly serosal (step 1B) surfaces of the cell activates metalloproteinase activity through an uncharacterized mechanism. The metalloproteinase (possibly a member of the a disintegrin and metalloproteinase family or matrix-associated metalloproteinase family) cleaves apical pro-HB-EGF (step 2) to liberate soluble HB-EGF, which stimulates EGFR dimerization and cytoplasmic auto-phosphorylation (step 3), allowing recruitment of signaling molecules including those that may activate p38 and ERK1/2 MAPK signaling pathways (step 4). MAPK signaling pathways may regulate the transcription of gene products (step 5), which encode unknown proteins (step 6) that facilitate exocytosis of discoidal vesicles that mediate the late-phase expansion of apical surface area (step 7).

3.0 CONCLUSIONS

The urinary bladder serves an important function in the human body: the storage and excretion of waste filtered into the urine by the kidney. The advancements of recent studies have enabled our appreciation of the dynamic nature of this organ during mechanotransduction and of its sensory components, which allow communication among various tissue types that comprise the bladder. Discoidal vesicle trafficking may serve as not only a response to, but also a means for regulation of signaling. Understanding these signaling pathways and their physiological functions provides insights into how these pathways are dysregulated in disease states, which offer hope for future diagnostic and therapeutic advancements.

The major theme of my work is to further understand the bladder's signaling mechanisms during mechanotransduction. This dissertation provides evidence that bladder filling stimulates EGFR signaling at the apical pole of the umbrella cell layer and that EGFR signaling is required for the prolonged phase of surface area increase during sustained increased pressure. This type of prolonged pressure stimulus is representative of the storage phase of the micturition cycle, when urine is contained in the bladder until voiding. The upstream and downstream signals in this pathway remain to be explored.

In addition to the EGFR signaling pathway described in Chapter 2, a variety of other internal and external factors are required for the bladder's exocytic response to stretch, and it is plausible that some of these mediators may act, in part, by stimulating EGFR transactivation. In

fact, there exists evidence that relates some of these signaling elements to EGFR transactivation in other cell types, as detailed in the sections below. It is possible that the EGFR signaling pathway acts as a common pathway in which the other known required signaling factors feed into or regulate.

This signaling pathway is also significant not only because of the role of EGFR as a mechanotransducer, which has been shown in other cell types [102, 109, 110], but also because the EGFR is present in an unusual distribution on the apical surface of epithelial cells, where it is potentially able to bind to the abundance of ligands present in the urine. This work provides a physiological role for EGFR in bladder mechanotransduction that must be tightly regulated due to the ready availability of urinary EGFR ligands. Additionally, EGFR is known to be dysregulated in carcinoma, as described below, which further highlights the significance of tight regulation of this signaling pathway. It is important to understand the upstream and downstream signaling components and how they interact with other signaling mechanisms in this organ in order to appreciate the consequences of disrupted or dysregulated EGFR signaling in this organ.

3.1 SIGNALING UPSTREAM OF EGFR

As described in Chapter 2 and summarized in Figure 2.10, the activation of the EGFR by mechanical stimuli, such as stretch, may occur as a result of receptor transactivation, in which an upstream stimulus promotes the release of ErbB family ligands that can bind to and stimulate the EGFR. EGFR transactivation is known to occur in response to diverse signals such as integrins, cytokines, Ca^{2+}, membrane depolarization, and various GPCRs (from ligands that include lysophosphatidic acid, bradykinin, UTP, bombesin, carbachol, endothelin, thrombin, and

angiotensin II (ANGII)) [111]. Transactivation can occur through a pathway involving metalloproteinase cleavage of an EGFR ligand, although the molecular activation of metalloproteinases by these diverse stimuli is not well understood in any cell type. Alternatively, transactivation of the EGFR can occur in the absence of ligand release, through strictly intracellular signaling pathways that lead to phosphorylation of the cytoplasmic tail of the EGFR. While the mechanism for EGFR transactivation in umbrella cells is unknown, work in other systems may give us clues to the upstream signaling components that are activated upon stretch. These possibilities are diagrammed in Figure 3-1 and described below.

3.1.1 Ion Influxes and EGFR transactivation

Intracellular pathways such as EGFR transactivation may be activated by ion fluxes enabled by "mechanosensitive" channels, which are physically activated by mechanical stretch. Mechanical stimuli can cause increased sodium transport in bladder tissue via the epithelial sodium channel [40, 56]. Additionally, previous work from our laboratory has demonstrated stretch-induced chloride and potassium secretion from the apical surface of bladder tissue [112]. The roles of TRP family ion channels, which are activated by a variety of signals including stretch, have been a recent subject of study in the bladder. While sodium, chloride, and potassium fluxes have not been directly associated with EGFR transactivation *per se*, these ions may activate other intracellular components that stimulate the activation of EGFR. Conversely, EGFR ligands are able to stimulate potassium influxes in umbrella cells [113] in addition to activating the Na/K-ATPase pump and inhibiting the amiloride-sensitive epithelial sodium channel [114, 115], suggesting that ion fluxes may occur downstream of EGFR activation in this system. This possibility warrants further investigation in the bladder stretch model.

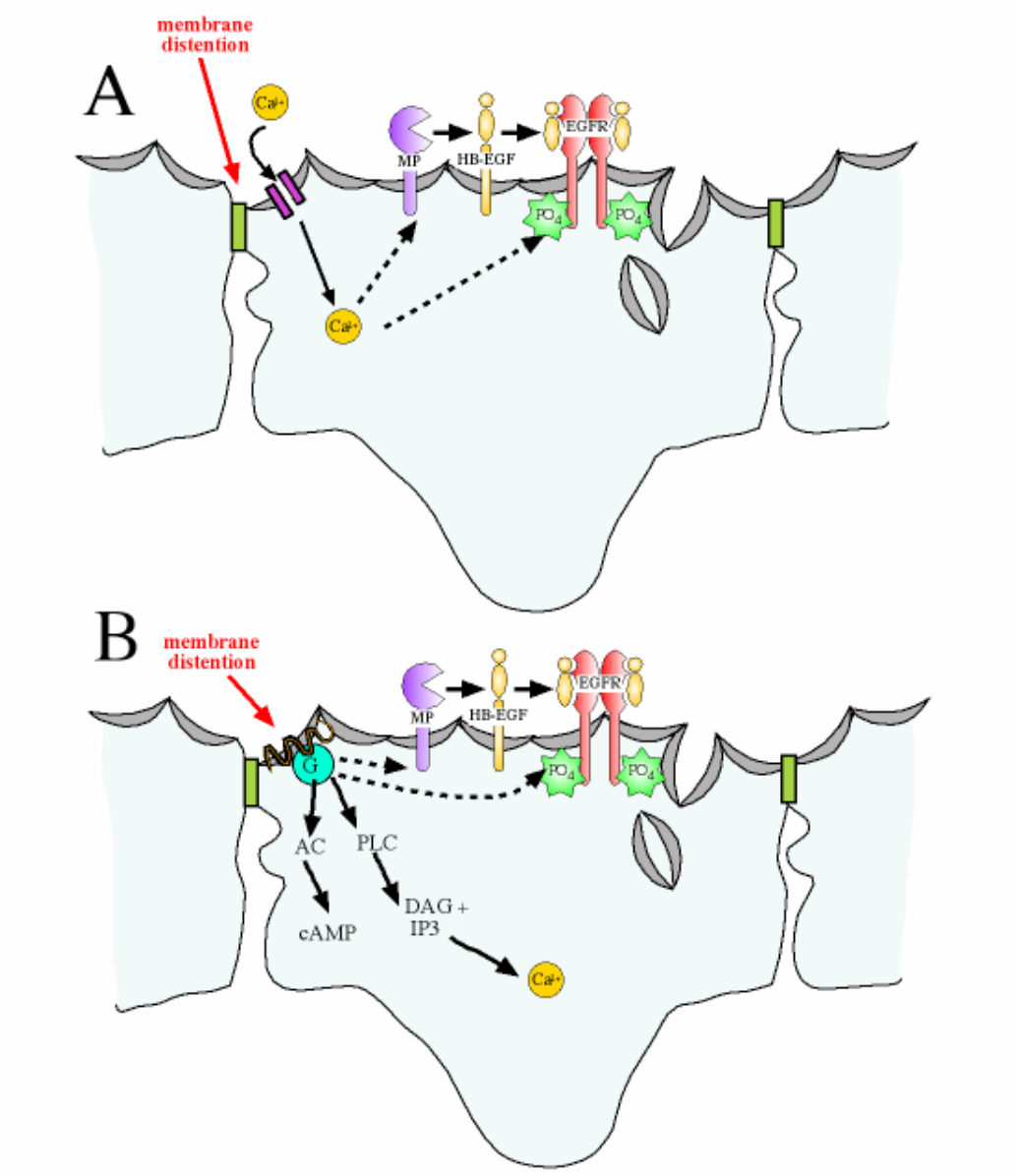

Figure 3.1: Models for upstream activation of EGFR.

(A) Calcium influx mediated by a mechanosensitive ion channel on the apical surface (the analogous pathway for calcium influx by a P2X channel on the basolateral surface is not shown). (B) Signal transduction upon activation of a GPCR, such as a P2Y or adenosine receptor, from the apical surface (the analogous pathway for a basolateral GPCR is not shown). Activation of G-proteins ("G") regulate the activity of adenylyl cyclase, which generates cAMP. Other G-proteins activate phospholipase C (PLC), which generates dialylglycerol (DAG) and inositol 1,4,5-triphosphate (IP3). IP3 stimulates increased cytoplasmic calcium, which can act on metalloproteinases or EGFR directly through unknown mechanisms. Dotted lines represent pathways that are not understood.

Mechanosensitive channels that conduct Ca^{2+} ions are particularly interesting, as Ca^{2+} influxes have previously been associated with both changes in membrane trafficking and EGFR transactivation. As described in Chapter 1, previous work in our lab has shown that stretch-induced discoidal vesicle exocytosis requires both intracellular and extracellular Ca^{2+} [58]. Additionally, P2X purinergic receptors are ligand-gated cation channels that function in the umbrella cell's response to stretch [41] and may conduct Ca^{2+} ions into the cell. Interestingly, Ca^{2+} is known to cause EGFR transactivation by activating metalloproteinases and/or by direct intracellular transactivation (Figure 3.1A).

There may also be a very complex interplay between EGFR and Ca^{2+} signaling, as explored by Bryant *et al.* [116]. Their study demonstrated that EGFR phosphorylation occurs upstream of increased intracellular Ca^{2+} in human glioma cell lines. In a separate pathway, EGFR signaling propagates ATP-induced Ca^{2+} waves. These two distinct pathways suggest a function for EGFR signaling either upstream and/or downstream of a Ca^{2+} influx, which may serve to regulate discoidal vesicle trafficking during the late phase response to stretch.

In order to directly examine the role of ion fluxes on EGFR transactivation, an important study is to ascertain which mechanosensitive ion channels are present on the apical surface of umbrella cells. Once this profile is determined, specific inhibitors can be sought to examine whether elimination of the channel's function attenuates the uroepithelial capacitance increase in response to stretch. Then, the affected channels can be stimulated and uroepithelial lysates probed for downstream EGFR phosphorylation. It is entirely possible that mechanosensitive and P2X ion channels are activated upon stretch, but their signals do not interact with the EGFR transactivation pathway. Additionally, it remains to be tested whether other non-P2X, non-mechanosensitive ion channels may also be activated during EGFR transactivation.

3.1.2 GPCR transactivation of EGFR

Another candidate for transactivation of EGFR in the bladder is the GPCR family of receptors. There are several attractive candidate GPCRs expressed in the bladder that regulate discoidal vesicle trafficking, as described below. GPCRs have seven transmembrane domains, an intracellular carboxy terminus, and an extracellular amino terminus, and they comprise the largest group of cell-surface receptors [117]. In 1996, it was shown that the EGFR became rapidly phosphorylated upon Rat-1 cell stimulation with GPCR agonists [105], elucidating the pathway by which GPCR stimulation caused metalloproteinase, EGFR, SHC/Grb2 complex, and ERK/MAP kinase activation. Upon GPCR activation, the GTP-bound α subunit and $\beta\gamma$ complex initiate intracellular signaling through effector proteins.

Two specific GPCRs have been implicated in stretch-induced discoidal vesicle trafficking in the uroepithelium: P2Y and adenosine receptors. There are eight isoforms of P2Y purinergic receptors, which may stimulate discoidal vesicle exocytosis in umbrella cells [41]. There are four types of adenosine receptors, all of which are expressed in the uroepithelium, and their activation also causes increases in uroepithelial apical exocytosis [42]. ATP could activate GPCR pathways in two ways: either directly via P2Y receptors on umbrella cells or indirectly through metabolism to adenosine, which could subsequently activate adenosine receptors in the uroepithelium. It is possible that the ATP or adenosine ligands bind to their GPCRs, which in turn stimulate heterotrimeric G-protein activity that leads to activation of the metalloproteinases (Figure 3.1B). The mechanism for G-protein activation of metalloproteinases is not understood, but it is possible that this pathway interfaces with Ca^{2+} signaling pathways. Briefly, G-protein signals can stimulate adenylyl cyclase activity (which generates cAMP) and phospholipases, which in turn generate diacylglycerol and IP3, subsequently inducing the release of Ca^{2+} (Figure 3.1B). Ca^{2+}

may then mediate EGFR transactivation directly or via metalloproteinase activation, as described above (Figure 3.1A). Transactivation of EGFR by ATP has been shown to occur in Muller glial cells through P2Y signaling [106].

To study the relationship between GPCRs and EGFR activation in the uroepithelium, one might begin by examining the phosphorylation of EGFR upon stimulation of uroepithelium by GPCR ligands, such as ATP or adenosine. Alternatively, it is possible to inhibit the EGFR using tyrophostin AG1478, followed by stimulation of the uroepithelium with GPCR activators, to determine whether elimination of EGFR signaling also eliminates the response to GPCR stimulation. These studies may implicate a model in which GPCR and EGFR signaling are integrated in the response to stretch.

In addition to the uroepithelium, GPCRs have also been implicated in EGFR transactivation in neighboring bladder smooth muscle cells. In a bladder smooth muscle stretch study, ANGII signaling causes an increase in levels of HB-EGF expression, with maximal mRNA expression at 4 h after stretch [118]. It is possible that the same ligand, HB-EGF, is able to transactivate the EGFR in two distinct tissues within the bladder during the response to stretch. It would be relevant to examine the presence of ANGII in the uroepithelium to determine whether this pathway is relevant for HB-EGF release in the uroepithelium.

3.1.3 Metalloproteinase activation & ligand generation

The transactivation of EGFR is implicated by the data presented in Chapter 2, which suggests that metalloproteinase cleavage of pro-HB-EGF is required to generate ligands for stretch-induced EGFR activation. Several metalloproteinases are known to cleave ErbB family ligands in other cell types, which may also be relevant to the bladder signaling pathway. To study the

activation of metalloproteinases upon stretch, an initial approach would be to experimentally determine the expression profile of the family of metalloproteinases in the bladder; there are over 20 metalloproteinases and it is not known which are present in the uroepithelium. It is also important to explore the localization of metalloproteinases on the apical or basolateral cell surface, which may have implications on their activity or function in EGFR transactivation or alternative effects, such as wound healing or proliferation [119].

Several metalloproteinases are associated with EGFR transactivation in other cell types. The TNF-α converting enzyme (TACE), also known as a disintegrin and metalloproteinase 17 (ADAM17), causes cleavage and release of membrane-associated pro-HB-EGF that subsequently binds and activates EGFR [120, 121]. In keratinocytes, matrix metalloprotinase (MMP) inhibitors of MMP-2/MMP-9 are able to effectively reduce amphiregulin release and EGFR activation [122]. Additional studies have reported that ADAM10, 12, 15, 17, and 19 cleave EGFR ligands, among many other substrates [123].

These above metalloproteinases are attractive candidates to begin exploring the mechanism of HB-EGF cleavage in the bladder. To test their involvement, specific inhibitors could be added to the uroepithelium prior to stretch to ascertain whether blocking their activity also eliminates the stretch-induced late phase increase in capacitance. Further, blocking the appropriate metalloproteinase should prevent phosphorylation of EGFR upon stretch, as assessed by western blot.

Consistent with the results presented in Chapter 2, it has been shown that stretch increases the urinary concentration of HB-EGF in human bladders [124]. The measurement of HB-EGF ligand liberation by metalloproteinase activity in the bladder stretch model has not been

performed, and ELISAs can be utilized to monitor HB-EGF concentrations over time in stretched bladders to assess metalloproteinase activity.

In addition to examining the activity of metalloproteinases, the surface availability of pre-cleaved pro-HB-EGF remains to be studied. Is pro-HB-EGF a normal constituent in the uroepithelium's apical surface, and what is its density at the surface? In MDCK, CHO, and HeLa cell lines, pro-TGF-α is internalized by clathrin-mediated endocytosis and recycled back to the surface to regulate EGFR activation [125]. In this manner, discoidal vesicle trafficking may regulate the delivery of transmembrane HB-EGF to the apical surface, where it is cleaved by metalloprotinases upon stretch for activation of the EGFR.

3.2 EGFR ACTIVATION

3.2.1 Binding of ligands to EGFR

In addition to EGFR ligands produced by metalloproteinase activity, one must consider the activity of urinary EGFR ligands. Previous studies have reported the presence of EGF (and other ligands) in adult human urine at a concentration of 30-60 ng/ml [36]. The majority of urinary EGF is produced by the kidney [126], and is not filtered from the plasma [36]. As such, paracrine stimulation of EGFR at the mucosal surface of the uroepithelium *in situ* cannot be ruled out.

The lack of stimulation of exocytosis by isolated rabbit urine described in Chapter 2 was a negative result that warrants further examination. It is possible that the centrifugation step removed a vital component of the urine or affected urine pH in a way that interfered with EGFR activation. In addition, the concentration of EGFR ligands in the urine and their bioactivity were

not assessed, and it is possible that urinary ligands are active *in vivo,* albeit highly regulated. It is worth noting that few studies have assessed whether these ligands are biologically active, and urinary exopeptidases and endopeptidases may limit the fraction of urinary EGF that is functional [36, 107]. Determination of their activity in rabbit urine and of ligand concentrations remain to be studied in this model system.

In addition to ligand generation, there may also be an issue of limited access to EGFR at the apical surface of the umbrella cell. The surface is coated by a glycocalyx including heparin proteoglycans and mucins, and has a unique protein and lipid composition that is characterized by cholesterol-rich and detergent-insoluble UP crystalline plaque and hinge regions [20, 28, 127]. The proteoglycan coat associated with the apical surface may assist in trapping and concentrating liberated growth factors close to surface receptors. Conversely, the lipid raft-like environment may interfere with ligand binding by altering the availability of ligand-binding domains, as occurs in other cell types [128-130]. A better understanding of EGFR localization within the apical membrane of umbrella cells, perhaps through ultrastructural localization, is required to begin to assess the potential regulation of EGFR by this unique membrane.

With respect to the unique apical surface of the uroepithelium, one particular type of glycoproteins that may impact EGFR signaling is the mucins, which are a family of secreted or membrane-associated high molecular weight glycoproteins that protect many epithelial surfaces. The predominant mucin genes expressed in the uroepithelium are Muc1 and Muc4 [131]. Recent surprising data suggests that the transmembrane subunit of Muc4 is able to activate ErbB2, which was previously thought to have no physiological ligands [132]. Additional studies implicate Muc1 in not only the apical localization of EGFR, but also signal transduction in breast

tissue [133]. Whether the mucins have a role in stretch-induced EGFR signaling remains to be explored.

EGFR itself may have binding sites that are uniquely available to certain ligands, providing a mechanism for regulation in environments containing multiple potential ligands, such as the urine. It was shown that HB-EGF cannot be fully displaced by an excess of EGF, while HB-EGF was able to fully displace bound EGF [90]; this suggests the presence of a privileged HB-EGF binding site, which remains to be explored. Perhaps the EGFR is able to respond to various ligands in different ways, such that the readily available urinary EGF and TGF-α act as a signal for responses distinct from HB-EGF-mediated mechanotransduction *in vivo*.

Not only does EGFR have high and low affinity binding sites, but it also has different configurations that regulate its activity, such as its active extended and autoinhibited monomer configurations, providing a further level of structural-based regulation of activity [134]. Extracellular cues may also impact the affinity of the EGFR for its ligands. For example, the reduction of urinary pH has no effect on apical surface density of EGFR in transitional cell carcinoma cell lines; however, lower pH reduced the affinity of EGFR for its ligands by ~ 20 fold [43]. In fact, at a pH of 7.5, the affinity of EGFR for EGF is only 75% of the binding at pH 8.0 [135]. High-affinity EGF binding is compromised at pH values lower than 7.5 and undetectable at pH less than 6.0 [136]. In this manner, the activation of EGFR may be affected by the pH of the urine, which in humans is typically ~ 5-6 (this figure ranges from pH 4.5–8 and may vary as a symptom of disease [137]). Additional work is needed to verify the affects of pH on EGFR ligand binding and activation in the stretched uroepithelium.

3.2.2 Intracellular EGFR transactivation

Activation of EGFR via ligands is only one mechanism that may be functional in the stretched bladder; in addition, there exist other known EGFR-activating mechanisms in the bladder that are not well explored. As described above and depicted in Figure 3.1A-B, both GPCRs and Ca^{2+} ion fluxes can transactivate the EGFR directly, without metalloproteinase activation and ligand generation.

Another upstream signal that could circumvent metalloproteinase activation is transduced by integrins, which are cell surface adhesive receptors that bind to extracellular matrix proteins and stimulate intracellular signaling pathways. Thogh typically activated as basolateral signals, it is quite possible that integrins are mechanically activated upon bladder stretch. Integrins are known to transactivate the EGFR in other cell types such as fibroblasts [138]. Integrin signaling pathways are known to involve Ca^{2+} influx, potassium channel activation, and tyrosine phosphorylation of intracellular proteins [139], all of which are active signaling mechanisms in the stretched bladder. To examine the role of integrins in uroepithelial mechanotransduction, it is possible to utilize a soluble peptide to compete for binding sites on the integrin [140], and thereby indicate if the peptide interferes with the control response to stretch or EGFR phosphorylation upon stretch. It is possible that integrins are required for the exocytic response in a manner that is independent of the EGFR signaling pathway, and it will be important to determine their function in bladder mechanotransduction.

3.3 DOWNSTREAM SIGNALING

As noted above, it is possible that various signaling components are activated upon stretch as part of other signaling pathways, concurrently with EGFR signaling. These alternative pathways may be entirely independent from the EGFR signaling pathway, they may feed into the EGFR pathway, or they may serve to downregulate EGFR signaling. The manner in which these signals interact and the identification of signals that are required for stretch-induced discoidal vesicle trafficking *versus* other simultaneous signaling outcomes are complex topics that require considerable research.

The EGFR is the hub of many intracellular signaling pathways, as its activation causes recruitment and stimulation of effectors including Src, Cbl, PLC, P13K, SHP2, and Grb2, and ultimately ERK/MAPK and anti-apoptotic Akt signals [141]. Though this dissertation has focused on ERK/MAPK signaling and protein synthesis, one must not forget that the EGFR is responsible for diverse outcomes in many cell types, and its activation in bladder stretch could affect outcomes including apoptosis, migration, growth, adhesion, and differentiation [141]. Particularly interesting is the role of EGFR in growth and differentiation, as it is plausible that a sustained stretch stimulus activates the insertion of new apical membrane through the growth and differentiation of underlying uroepithelial cells. The effects of stretch or EGF ligand stimuli on growth could be assessed by [^{3}H]-thymidine incorporation studies and by experiments that monitor markers of umbrella cell differentiation. Alternative downstream effectors of EGFR can be examined by observing the functional affects of inhibiting each of the pathways.

The concept of stretch-induced protein synthesis in the bladder warrants discussion, as it may seem counterintuitive that protein synthesis would occur each time the bladder fills. It is important to point out that the stretching stimulus in these studies is actually a 5 h sustained

stretch, which is more representative of physiological urine storage over hours than the filling process. This response appears to be distinct from the early phase response, which is not sensitive to cycloheximide, and it may require sustained stretching for its initiation. With this in mind, it is conceivable that the bladder senses a prolonged full state and protein synthesis is initiated to allow further accommodation of urine.

3.3.1 Protein synthesis

One can imagine that stretch-induced protein synthesis functions to increase the number of newly synthesized discoidal vesicles, providing more membrane for subsequent insertion into the apical surface. Alternatively, as the apical surface area increases, the junctional ring that surrounds the apical surface must also expand to accommodate the increased surface size, so it is possible that this pathway upregulates junctional proteins. There is evidence that EGFR, along with PPAR-γ signaling, has a role in the regulation of tight junction formation in normal human uroepithelial cells [142]. EGFR is known to stimulate the expression of claudins and has an important role for maintaining tight junctions and transepithelial resistance [143]. In addition to junctional proteins, it is possible that other types of proteins are upregulated in response to EGFR and stretch-induced signals.

Determining the proteins that are upregulated by stretch and their function in the bladder will help us better understand mechanotransduction in this organ. Candidate proteins that may be regulated were were studied by two-dimensional differential gel electrophoresis (DIGE) and identified by MALDI-MS/MS techniques; the results of these experiments are included in Appendix B. Potential relevant results include the uporegulation of phosphatases, which may be involved in regulation of tyrosine kinase signaling cascades such as EGFR and ERK/MAPK

signaling, and various annexin family members, which are proteins that bind to phospholipids in a Ca^{2+}-dependent manner. It is important to acknowledge that this study only examines steady-state levels that could also be affected by degradation. Changes in expression for these proteins of interest require further confirmation, and the functional implications of their upregulation on bladder physiology remain to be studied.

3.4 PHYSIOLOGY AND REGULATION OF EGFR IN THE BLADDER

While roles of the EGFR as a bladder mechanotransducer and regulator of membrane trafficking described in Chapter 2 were not previously reported, the EGFR was long recognized as a functioning receptor in the bladder for purposes of growth and regeneration. How mechanically-stimulated EGFR signaling interacts with this receptor's signaling towards its other functions is not known. Any of these physiological EGFR functions may be overactive or dysregulated in pathological states such bladder carcinoma.

3.4.1 EGFR in normal bladder growth

The uroepithelium, while having a generally slow growth and turnover rate, has a remarkable rate of regeneration upon injury [144]. The EGFR plays a role in the normal and abnormal growth of the uroepithelium, and EGF was able to induce proliferation and hyperplasia of rat and pig uroepithelium [145]. But while increased EGFR expression causes increased proliferation and promotes bladder tumor growth, it does not cause carcinoma *per se* [98]. It appears that urinary EGF can initiate signaling pathways that affect underlying tissue layers. Urinary EGF in

rat bladders caused increased [^{3}H]-thymidine incorporation in only the basal cell layer of the uroepithelium. As radiolabeled EGF can not cross the apical umbrella cell barrier [145], this finding is suggestive of transmural EGF signaling.

3.4.2 EGFR and cancer

The importance of the regulation of EGFR signaling in the uroepithelium is highlighted by the fact that transitional cell carcinoma is often an EGFR-correlated cancer. In 2006, an estimated 61,400 new cases of bladder cancer were diagnosed, and there were approximately 13,000 deaths due to bladder cancer [146]. EGFR and signaling by other ErbB family members is known to be dysregulated in various types of cancer, including bladder carcinoma; however, no specific EGFR mutations have been described for transitional cell carcinoma patients. EGFR mRNA and protein are overexpressed in approximately 40–60% of human bladder tumors [147-149]. At the same time, EGF ligand concentration in urine is significantly reduced compared to concentrations in urine from control patients [147, 150]. EGFR staining in bladder cancer histological samples indicates that EGFR positivity correlates with prognosis [151]. This suggests that it is very important to study and understand the mechanisms involved in regulation of EGFR signaling in the bladder.

This stretch-activated EGFR signaling pathway can be dysregulated in cancer at other steps, such as upstream at the metalloproteinase level. Ohtsu *et al.* reviewed the potential for ADAMs and the GPCR-induced EGFR transactivation mechanism in cancer cells, as well as cells associated with other inflammatory diseases [123]. For example, ADAM17 and ADAM9 expression are upregulated in breast cancer and prostate carcinoma pathophysiology, respectively, while ADAM17 expression is predictive of a poor prognosis in breast cancer [152].

Because metalloproteinase production and activation are associated with the invasive edge of a cancer and their activation correlates with aggressive behavior of tumors, it has been proposed that their activity be monitored and targeted for therapy [153].

Another potential target for regulation is the functional EGFR ligand HB-EGF, which has been shown to potently induce tumor growth and angiogenesis [154]. Curiously, not only does HB-EGF have biological activity in its cleaved/secreted form, but it also serves distinct growth/regulatory functions as a transmembrane proHB-EGF precursor and a cleaved cytoplasmic tail, as reviewed by Kim *et al.* [155]. Because pro-HB-EGF also serves as the receptor for diphtheria toxin, Freeman *et al.* have proposed that the diphtheria toxin binding site is a promising target for intralumenal treatment of bladder diseases [90].

EGF is excreted in very high quantities into the urine, so the EGFR could exploit this phenomenon to confer a growth advantage for tumor cells. In culture, EGFR ligands can induce expression of MMP-9 and cancer cell motility [156], or expression of MMP-1 via transcription factor AP-1 [157]. Perhaps overactive EGFR is simply an effect of upregulated metalloproteinase activity, generating excess cleaved ligands.

Because the EGFR has been so strongly implicated in bladder carcinoma and it can be dysregulated at so many points in its signaling pathway, it is an attractive target for cancer therapeutics. The uncoupling of EGFR from downstream MAPK signaling is targeted by Gefitinib anti-cancer treatment [158]. Anti-ErbB antibodies, such as Cetuximab, block ligand binding and stimulate the internalization of receptors residing at the surface. Tyrosine kinase inhibitors (tyrophostins) block downstream signaling of the receptor-ligand complex. Hsp90 inhibitors (geldanamycin) prevent the stabilization of ErbBs at the membrane by saturating these chaperone proteins. One could imagine that EGFR signaling in response to stretch must be

tightly regulated in order to prevent the transition of the epithelium to a cancerous state, and this regulation can be exploited in therapeutic approaches.

3.5 CLOSING COMMENTS

In this dissertation, I presented data that furthered our understanding of the signaling events that accompany mechanically stimulated membrane trafficking in the uroepithelium and provided a model for the potential integration of many signaling pathways activated upon bladder stretch. My research raised questions about the upstream activation of mechanically activated metalloproteinases in transactivation, which may reveal an interconnection between several signaling components that are required for stretch-induced exocytosis and the EGFR signaling pathway. Further studies are required to fully understand the various signaling pathways that function in the bladder and how these pathways interact and regulate each other. This work also suggests the importance of the tight regulation of EGFR signaling in the bladder, which may be required to prevent disease states with uncontrolled EGFR activity, such as bladder carcinoma.

4.0 MATERIALS AND METHODS

4.1 BLADDER STUDIES

4.1.1 Reagents and antibodies

All reagents were obtained from Sigma-Aldrich unless otherwise specified. Pharmacological agents were prepared as stock solutions in the following diluents: cycloheximide (10 mg/ml in sterile distilled water); genistein (10 mM in DMSO); AG-1478 (Calbiochem, 25 μM in DMSO); AG-1296 (Calbiochem, 25 mM in DMSO); AG-490 (Calbiochem, 30 mM in DMSO); PP2 (Calbiochem, 25 μM in DMSO); AG-9 (25 μM in DMSO); brefeldin-A (5 mg/ml in ethanol); GM-6001 (Calbiochem, 10 mM in DMSO); GM-6001 negative control (10 mM in DMSO); U0126 (Cell Signaling, 10 mM in DMSO); PD-098059 (10 mM in DMSO); SB-203580 (Calbiochem, 10 mM in DMSO); JNK Inhibitor II (Calbiochem, 500 μM in DMSO); CRM-197 (5mg/ml in dH_2O). Stock solutions of EGFR ligands were prepared as follows: EGF (100 μg/ml in PBS with 0.1% BSA); HB-EGF (100 μg/ml in PBS with 0.1% BSA); heregulin-β (100 μg/ml in PBS with 30% glycerol); TGFα (Chemicon, 25 μg/ml in sterile distilled water). The EGFR antibody #2232 (Cell Signaling) was used at 1:200 for immunofluorescence analysis. EGF-FITC (Molecular Probes, 40 μg/ml) was diluted in Krebs buffer (110 mM NaCl, 5.8 mM KCl, 25 mM $NaHCO_3$, 1.2 mM KH_2PO_4, 2.0 mM $CaCl_2$, 1.2 mM $MgSO_4$, 11.1 mM glucose, pH 7.4 at 37^{o}C,

bubbled with 5% CO_2 gas) just prior to use. Primary rabbit antibodies against EGFR and phosphorylated Y1173-EGFR (Cell Signaling) were used at 1:1000 dilution. Rabbit polyclonal antibodies against ErbB2 and ErbB3 (Santa Cruz Biotechnology, Inc) were used at 1:25 dilution. Mouse monoclonal antibodies against pERK (Santa Cruz Biotechnology, Inc) were used at 1:500 dilution. EGFR neutralizing antibody LA1 (Upstate) was used at 1 μg/ml. Ligand neutralizing antibodies against HB-EGF (R&D Systems), EGF (R&D Systems), and TGFα (Calbiochem) were used at 20 μg/ml.

4.1.2 Animals

Urinary bladders were obtained from female New Zealand White rabbits (3.5–4 kg; Myrtle's Rabbitry), female C57BL/6J mice (12-14 weeks; Jackson Laboratory, Bar Harbor, ME), and female Sprague-Dawley rats (250-300 g; Harlan, Indianapolis, IN). All animals were fed a standard diet with free access to water. Rabbits were euthanized by lethal injection of 300 mg Nembutal into the ear vein, and mice and rats were euthanized by inhalation of 100% CO_2 gas and subsequent thorocotomy. Following euthanization, the animal was placed in a supine position and the bladder was exposed by making a midline incision from the base of the pelvis toward the sternum. Next, the bladder was cut at the transition between the urethra and bladder, and the excised bladder was immediately placed in a 100 ml beaker filled with 37^{o}C Krebs solution for subsequent experiments. All animal studies were approved by the University of Pittsburgh Animal Care and Use Committee. Animals were maintained according to the standards described by the American Physiological Society's handbook on the care and use of animals.

4.1.3 Capacitance Measurements

4.1.3.1 Stretch and capacitance measurements of rabbit uroepithelium

The bladder was cut open along its superior vesical artery and opened over a custom-made Teflon rack with the mucosal side facing down. The uroepithelium was isolated by dissecting the underlying tissues and smooth muscle using scissors and forceps. The isolated uroepithelium was mounted on rings with pins that exposed 2 cm^2 of tissue, which were placed between two Ussing hemichambers as described previously [58]. The hemichambers were filled with 12.5 mL Krebs buffer, and the basolateral chamber was bubbled with 5% CO_2 gas, as shown in Figure 4.1. Tissues were only used if their initial resistance was greater than 4000 Ω and capacitance between 1.8 – 2.0 μF.

To determine the apical membrane capacitance (where 1 μF ≈1 cm^2), the epithelium was modeled as an electrical circuit composed of a resistor and capacitor [58]. The Scope application (ADInstruments Inc., Colorado Springs, CO) run on a PowerPC G5 Macintosh computer (Apple, Cupertino, CA) was used to direct the MacLab 8's A/D converter (AD Instruments, Victoria, Austrailia) to generate a 1 μA square current pulse for 10 ms, which was passed over the tissue via a VCC MC6 current/voltage clamp (Physiological Instruments, San Diego, CA) connected to silver electrodes placed within the Ussing chamber. Prior to the experiment, the VCC was calibrated to assure that an appropriate current pulse could be generated, the offset was adjusted to correct for any differences in electrodes, and the fluid resistance compensation was adjusted for the Krebs buffer. The tissue's voltage response was measured and displayed on Scope, and the data was copied to Microsoft Excel (Microsoft, Seattle, WA). In Excel, the data were used to calculate the tissue's capacitance (where 1 μF = 1 cm^2 of apical membrane surface area) as

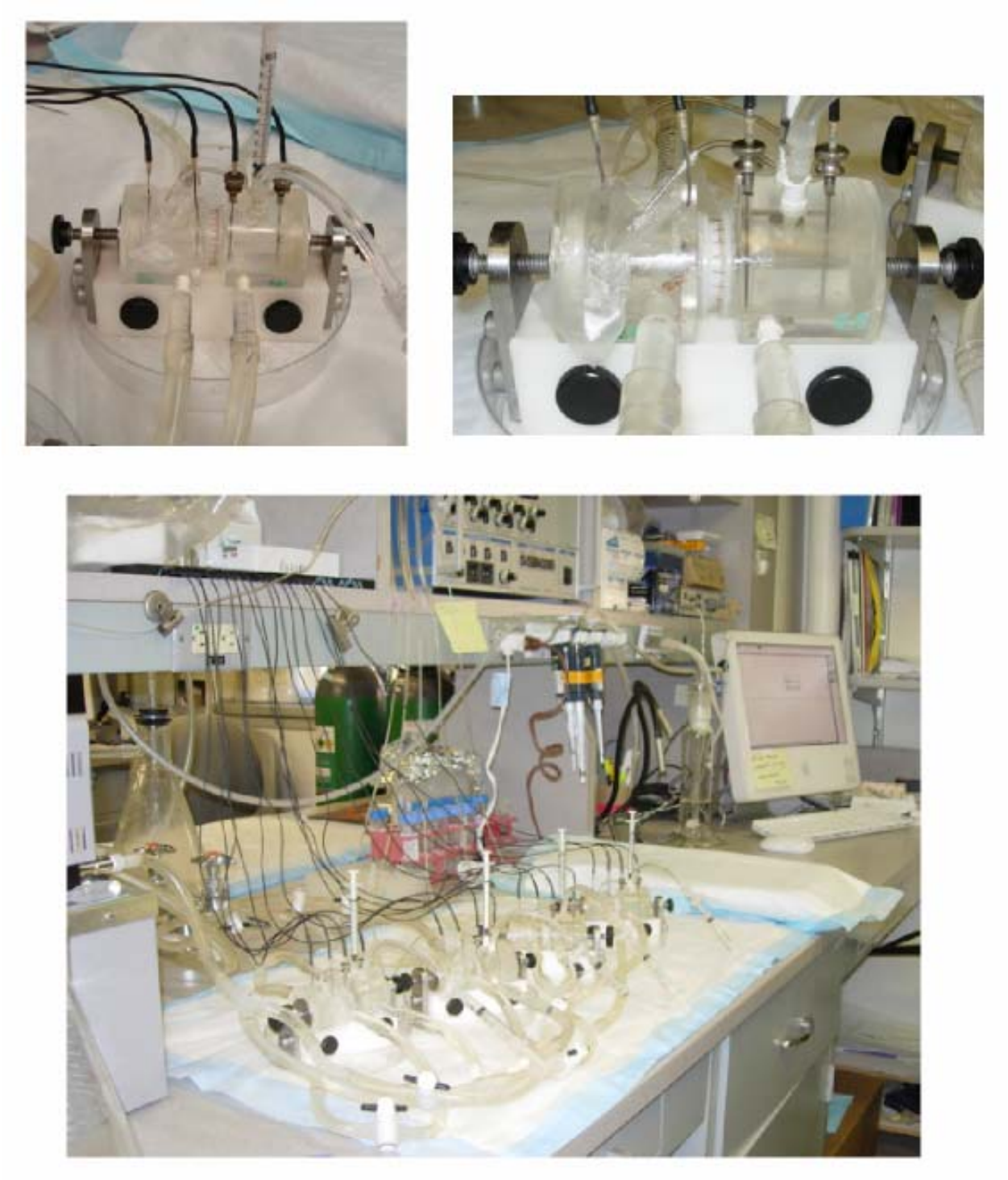

Figure 4.1: Ussing chamber setup.

The top right image depicts a single Ussing chamber setup. The water jacket running into the front of the chambers and draining from the back maintains the temperature within each chamber. Four silver electrodes are connected and run out of the top of the chambers. The left basolateral or serosal chamber is bubbled with 5% CO_2, and the right apical or mucosal chamber

is sealed for a stretch study. The top right image is a closer view of the chamber setup. The bottom image depicts the experimental area, containing four chambers that are connected to a water heater for the water jacket, the electrodes to pass a current and sense the voltage of the tissue, interfaced to the voltage current clamp on the shelf, the Mac Lab, and finally the PowerMac desktop computer.

previously described [58]. The voltage response data were calculated at time = 0, 5, 10, 20, 60, 100, 140, 180, 220, 260, and 300 min during each experiment.

To simulate bladder filling, Krebs buffer was added to the mucosal hemichamber, filling it to capacity. The chamber was sealed and additional 0.5 ml of Krebs solution was infused, over a total of 2 min. Our initial reports described the pressure change induced by filling to be ~ 8 cm H_2O; however, new measurements using a more sensitive pressure transducer (TBM4 Transbridge Pressure Transducer, World Precision Instruments, New Haven, CT) indicated that the final change in pressure was ~ 1 cm H_2O (Figure 2.1B). The pressure transducer was interfaced with a 1.8 GHz PowerPC G5 Macintosh computer (Apple, Cupertino, CA) and used Chart 5 software (AD Instruments) for measurements. For slow filling, the mucosal chamber was filled at 0.1 ml/min using a NE-1600 pump (New Era Pump Systems, Farmingdale, NY); when the chamber was full, it was sealed and an additional 0.5 ml of Krebs buffer was added at the same filling rate. To unstretch the tissue, the sealed Luer ports were opened and Krebs buffer was rapidly removed from the apical chamber to restore baseline capacitance values.

4.1.3.2 Stretch and capacitance measurements of mouse bladder tissue

The bladder was cut open and pinned open on a rubber mat with the mucosal side up. It was mounted on a ring that exposed 0.28 cm^2 of tissue, and the ring was positioned between 2 halves of a custom-made Ussing pressure chamber as described. The tissue was equilibrated for 45-60 min in Krebs buffer. Tissue preparations were used only if their total resistance was greater than 1000 Ω. At time = 0, 5, 10, 20, 60, 100, 140, 180, 220, 260, and 300 min, a square current pulse (10 μA for 20 ms) was passed through the tissue, and the resulting voltage response was recorded using the Scope program [58].

To stretch the bladder tissue, the level of Krebs buffer in the mucosal hemichamber was raised to the top of the upper Luer fitting (see Figure 1D in[58]) at a rate of 0.1 ml/min using a NE-1600 pump (New Era Pump Systems, Farmingdale, NY), over approximately 20 minutes, and sealed. Stretching began at t=0 and voltage responses were measured at the times indicated above.

To determine the apical membrane capacitance (where 1 μF ≈1 cm^2), the epithelium was modeled as an electrical circuit composed of an apical resistor and capacitor, a basolateral resistor and capacitor, and a series resistor [159]. This equation is more complex than the single-exponential equation used for rabbit uroeptihelium because the data from mouse bladder tissue, which has lower resistance and contains undissected uroepithelium with underlying tissue layers, do not adequately fit the simple model. The equivalent equation for this circuit is as follows: $V(t) = I(t)[R_0 + R_1(1-e^{-t/R_1C_1}) + R_2(1-e^{-t/R_2C_2})]$. In this equation, R_1 and C_1 represent the apical umbrella cell resistance and capacitance, R_2 and C_2 represent the values for the basolateral plasma membrane (and possibly underlying cell layers), and R_0 is the series resistance.

This voltage response data were transferred from the Scope program to Microsoft Excel, where the data points corresponding to the current pulse were isolated and normalized to zero, and total resistance values were calculated. These data were transferred to the PRISM application (GraphPad Software, Inc., San Diego, CA) and graphed with time on the independent axis and the voltage response (at time X) on the dependent variable axis. Using the double exponential equation described above, values for R_1, C_1, R_2, and C_2 were calculated by non-linear regression best-fit analysis. Rules were defined such that all variables were positive values, and values for R_1 and R_2 were constrained such that $R_1 + R_2 = R_T$ (total resistance). R_T was calculated from the voltage response of the tissue upon application of the square current pulse for each time point.

The double exponential model fit the voltage response data with R^2 values falling in the range of 0.97 - 0.99 for most time points. C_1 values were plotted over time, as percent of pre-stretched capacitance values. Data were graphed as mean ± SEM ($n \geq 3$).

4.1.4 RT-PCR analysis

Rabbit bladder tissue was isolated and pinned open on a rubber pad with the mucosal surface facing upwards. A 25-cm cell scraper (Sarstedt, Newton, NC) was used to scrape the uroepithelium, and scraped cells were collected into a 1.5-ml Eppendorf tube. The RNAqueous-4PCR kit (Ambion, Austin, TX) was used for lysis and total RNA preparation, as directed by the manufacturer. DNAse I treatment and DNAse inactivation were performed prior to reverse transcription, which was carried out according to instructions for RETROscript (Ambion, Austin, TX) using Oligo(dT) primers. Amplification of ErbB family receptors and ligands was performed using standard PCR protocols and rabbit-specific sequence primer pairs, listed in Table 4.1.

Table 4.1: Rabbit-specific sequence primer pairs for RT-PCR

Target	5' Primer	3' Primer
ErbB1	CAGCTACGAGGTGGAGGAAG	GGATGTGCAGATCACCACTG
ErbB2	AAGTCCCGAGGACTGTCAGA	GGACTCAAAGGTGTCCGTGT
ErbB3	GTCACATGGACACGATCGAC	AAAGCAGTGGCCGTTACACT
ErbB4	GAACAATGTGATGGCAGGTG	TTCGCATTGAAGTTGTGCTC
EGF	GAGGGAGGCTACACTTGCAT	GGAGAGGGCTCATCTTCCTT

HB-EGF	GAGACCCATGTCTTCGGAAA	CCACCACAGCCAGGATAGTT
TGF-α	AAGCCCTGGAGAACAGCAC	CAGAGTGGCAGACACATGCT

4.1.5 Immunofluorescence and image acquisition

4.1.5.1 Preparation and staining of bladder cryosections

Rabbit, rat, and mouse bladders were isolated as described above. They were fixed in 4% paraformaldehyde, 100 mM sodium cacodylate buffer, pH 7.4 for 1h at room temperature. Next the tissue was incubated in phosphated buffered saline (PBS) containing 30% (w/w) sucrose for 1h at 4^{o}C on a rotator for cryoprotection. Tissue was placed in OCT Compound (Tissue-Tek, Torrance CA, USA) and frozen in molds placed on dry ice blocks. Cryosection blocks were stored at -80^{o}C. Sections were cut at a 4 μm thickness using a CM 1900 cryostat machine (Leica, Bannockburn, IL). The sections were collected on Fisherbrand Superfrost/Plus slides (Fisher, Waltham, MA), and dehydrated by incubating the slides for 1 min at room temperature. The sections were washed 3 times with PBS for 5 min each. The paraformaldehyde was quenched and the cells permeabilized with quenching solution (PBS containing 20 mM glycine, pH 8.0, 75 mM ammonium chloride, and 0.1% [v/v] Triton X-100) for 10 min at room temperature. Following 3 quick washes with block solution (PBS containing 0.7% [w/v] fish skin gelatin and 0.025% [w/v] saponin), the samples were incubated in block solution containing 10% (v/v) newborn calf serum for 30 min at room temperature. Next, sections were incubated for 60 min at room temperature with primary antibody diluted in block solution. The sections were washed 3 times with block solution over a 15 min period of time. The sections were incubated with the

secondary antibody for 60 min at room temperature, and again washed 3 times with block solution over a 15-min time period. Following 3 quick washes with PBS, the tissue was post-fixed for 10 min by 4% paraformaldehyde in 100 mM sodium cacodylate, pH 7.4. After a final wash with PBS, coverslips were placed over the stained tissue using p-diaminobenzidine-containing mounting medium [160].

4.1.5.2 FITC-EGF binding studies

Freshly-isolated tissue was incubated with 40 ng/ml FITC-EGF (Molecular Probes) for 1 h at 4˚C, and the tissue was washed with Krebs buffer, three times for 5 min. In control experiments competing 400 ng/ml EGF was added 5 min prior to FITC-EGF addition. Following incubation with ligand, the tissue was fixed, sectioned, and stained as described above.

4.1.5.3 Image acquisition

Images were acquired using Leica Confocal Software interfaced with a TCS-SL confocal microscope equipped with argon and green and red helium-neon lasers (Leica, Deerfield, IL). A X100 (1.4 numerical aperture) planapochromat oil objective lens was used. OpenLab software (Improvision, Lexington, MA) was used to project the 0.5 μm sections into one image, and Adobe Photoshop software (Adobe Systems, San Jose, CA) was used to adjust the contrast level of the final images.

4.1.6 Activation of EGFR and Immunoblotting

4.1.6.1 Preparation of rabbit bladder lysates

After stretching rabbit uroepithelium in the Ussing stretch chamber for the indicated duration of

time, the tissue was rapidly removed from the chamber and pinned, mucosal side up, to a rubber pad. The tissue was washed with ice-cold Krebs solution and placed on ice. Next, 200 μl of lysis buffer (100 mM NaCl, 50 mM TEA pH 8.6, 5 mM EDTA, 0.2% NaN_3, 0.5% SDS) containing freshly-added phosphatase inhibitor cocktail set II (Calbiochem), 0.5 mM PMSF, and 1 mM protease inhibitor cocktail was added to the bladder apical surface. The uroepithelium was scraped and the cells were collected into a 1.5-ml Eppendorf tube. The scraped cells were sonicated (Fisher Scientific Sonic Dismembrator Model 100, Fair Lawn, NJ) on ice with ten 1 s pulses at a setting of 4. Following centrifugation, the protein concentration of the lysate was determined using bichinoic acid assay reagents (Pierce; Rockford, IL).

4.1.6.2 Western Immunoblotting

The samples were resolved by SDS-PAGE, transferred to nitrocellulose, and the membrane blocked overnight at 4^{o}C with 5% nonfat milk in TBS + 0.05% Tween-20. After incubation with primary antibody in 1% milk in TBS + 0.05% Tween-20, the membrane was washed three times. Next, the membrane was incubated in 1% milk in TBS + 0.05% Tween-20 containing HRP-conjugated anti-rabbit or anti-mouse antibodies, and immunoreactive bands were visualized using SuperSignal West Substrate (Pierce; Rockford, IL) and exposed to Kodak BioMax MR Film. Quantification was performed using Quantity One software (Bio-Rad, Hercules, CA).

4.1.7 Statistical analysis

For mouse capacitance data, Chauvenet's correction was used to identify outlying data for each time point [27]. To test for significant difference between two samples (stretched vs. control tissue), a student's two-tailed unpaired t-test was used, and values of $p < 0.05$ were considered

significant. To test for significant differences among all stretched or all control samples, a one-way analysis of variance test was performed with a Bonferroni post-test comparing all sets of data, using PRISM software. The 95% confidence interval was computed and values of $p < 0.05$ were considered significant.

4.2 YEAST TWO-HYBRID SCREEN

A yeast two-hybrid screen was performed according to BD Matchmaker user manuals, specifically documents # PT3183-1 and PT3247-1, and the BD Yeast Protocols Handbook, # PT3024-1 (BD Biosciences, San Jose, CA).

4.2.1 Cloning and constructs

The 52 amino acid cytoplasmic tail of UPIIIa was expressed as a fusion to the DNA binding domain (BD) of the GAL4 transcription factor by subcloning the DNA into the pGBKT7 (Clontech) cloning vector using EcoRI and BamHI restriction endonuclease sites. This vector was used to transform AH109 yeast, and expression of the bait (UPIIIa-BD fusion protein) was tested by western blot using an antibody to the cytoplasmic tail of UPIIIa [161]. The pGBKT7 vector also conferred the ability to grow in the absence of tryptophan (-Trp). A kidney cDNA library fused to the GAL4 activation domain (AD) was used to transform Y187 yeast for the two-hybrid screen. This construct was able to grow in the absence of leucine (-Leu). Successful mating enabled growth of yeast on media lacking both tryptophan and leucine (-Trp/-Leu). A protein interaction reconstituted the complete and functional GAL4 transcription factor, which

induced reporter gene expression and enabled growth in the absence of histidine (-His) and adenine (-Ade).

4.2.2 Yeast transformation

To transform yeast with the appropriate construct, 1 ml of YPDA (containing 1% yeast extract, 2% bactopeptone, 2% glucose, and 100 ug/ml adenine) was inoculated with several colonies and vortexed. This was transferred into 50 ml of YPDA in a 250 ml sterile flask, which was incubated at 30^{o}C for 18 h shaking at 250 rpm (until OD_{600} > 1.5). 30 ml of the overnight culture was transferred to a sterile 1L flask containing 300 ml of YPDA. This was incubated at 30^{o}C for 3 h with shaking (230 rpm) until the OD_{600} was 0.4-0.6. Cells were placed in six 50 ml sterile tubes and centrifuged at 1000 x *g* for 5 min at room temperature. The supernatants were discarded and cell pellets were resuspended with distilled water and combined in one tube with a final volume of ~ 30 ml. This tube was centrifuged at 1000 x *g* and the supernatant was removed. Cells were resuspended in 1.5 ml of freshly prepared, sterile 1X TE/1X LiAc, and this was the competent yeast used for subsequent transformations. For each transformation, 0.1 ug of plasmid DNA (in ~ 5 µl) and 0.1 mg of herring testes carrier DNA was added to a clean 1.5 ml tube and mixed. 0.1 ml of competent yeast cells was added to each tube and mixed, followed by addition of 0.6 ml of sterile PEG/LiAc solution to each tube. Tubes were incubated for 30 min at 30^{o}C with shaking at 200 rpm. Next, 70 µl of DMSO was added, followed by mixing by gentle inversion. The samples were shocked for 15 min in a 42^{o}C water bath and chilled on ice for 1 min. Next, samples were centrifuged at 14,000 rpm at room temperature briefly before removal of supernatant. Cells were resuspended in 0.5 ml of sterile 1X TE buffer and plated on

appropriate restrictive media for growth at 30^{o}C in serial dilutions to calculate transformation efficiency.

As a control, transformation and reporter gene assay were used to assure that the bait did not activate transcription in the absence of the GAL4 AD (auto-activation control for false positive interactions). Also, the rate of growth and colony appearance of transformed yeast were monitored to assure that the expression of the fusion protein did not affect growth or mating. Finally, the yeast were grown on plates that lacked tryptophan and histidine to test for leaky histidine expression; 3-aminotriazole titration was performed to determine the appropriate concentration to add to plates.

4.2.3 Two-hybrid mating

For the two-hybrid mating, the AH109 yeast strain expressing the UPIIIa-BD fusion was mated with the Y187 strain expressing the cDNA library-AD fusion per manufacturer's instructions (BD Matchmaker Libraries, BD Biosciences, San Jose, CA). An overnight culture of the bait strain was prepared and its concentration was determined to be greater than 1 x 10^{9} cells/ml. A 1 ml aliquot of yeast containing a human kidney cDNA library was thawed and combined with the bait culture in a 2 L sterile flask in a total volume of 50 ml 2X YPDA/kan. The culture was incubated for 24 h at 30^{o}C with gentle swirling (30 rpm). The mating mixture was centrifuged at 1000 x *g* for 10 min and resuspended in 0.5X YPDA/Kan. Dilutions of the mating mixture were plated to perform the mating efficiency controls and calculations. The mating mixture was spread on 50 large (15 cm) plates with high stringency selection (SD/-Ade/-His/-Leu/-Trp). The plates were incubated at 30^{o}C until colonies appeared. Colonies were replica plated on plates with X-α-gal substrate and grown. Approximately 600 colonies were selected for identification; this

processing consisted of yeast plasmid preparation, *E.coli* transformation, miniprep, diagnostic digestion, and sequencing by standard protocols.

The negative controls for two-hybrid interactions were empty vector and Lamin C, which does not interact with the AD-fusion proteins. Unfortunately, there are no known proteins that interact with the cytoplasmic tail of UPIIIa, so there was no established positive control. Reciprocal transfer of proteins (switching BD-fusion and AD-fusion proteins) was performed to assure that the fused proteins did not affect the interactions.

4.2.4 CPRG assay

A β-galactosidase assay was performed to assess reporter expression, using chlorophenol red-β-D-galactopyranoside (CPRG) as a substrate. Briefly, 5 ml overnight cultures were prepared in liquid SD (-Trp/-Leu/-His/-Ade) media to maintain selection on the plasmids. The culture was vortexed and 2 ml was transferred to 8 ml of YPD. The culture was incubated at 30^{o}C for 3 h with shaking at 230 rpm until the cells were in mid-log phase (OD_{600} was 0.5-0.8/ml). 1.5 ml of culture was placed into three 1.5 ml tubes, and the tubes were spun at 14,000 rpm for 30 s. The supernatant was removed and the pellet was resuspended in 1 ml of CPRG buffer (2.38 g HEPES, 0.9 g NaCl, 0.065 g L-Aspartate [hemi-Mg salt], 1 g BSA, and 50 µl Tween-20 in a total of 100 ml deionized water, pH 7.23-7.3). The sample was centrifuged at 14,000 rpm for 30 s and the supernatant removed, and cells were resuspended in 300 µl of CPRG buffer. Next, 0.1 ml of the suspension was transferred to a fresh 1.5 ml tube, frozen in liquid nitrogen, and thawed for 1 min in a 37^{o}C water bath. The freeze-thaw was repeated two more times. Next, 0.7 ml of CPRG buffer with substrate (freshly prepared, containing 27.1 mg of CPRG per 20 ml of CPRG buffer) was added to each sample and vortexed thoroughly, and the timer was started to keep

track of duration during color change. CPRG buffer with substrate (1 ml) was reserved as a blank. When the sample colors turned yellow/grey to red, 0.5 ml of 3 mM $ZnCl_2$ was added to each sample and the buffer blank to stop the reaction, and the stopping time was recorded. Samples were spun at 14,000 rpm for 1 min to pellet cell debris, and the supernatant was transferred to fresh tubes. The OD_{578} values of the samples were recorded and used to calculate β-galactosidase units (in which one unit of β-galactosidase hydrolyzes one micromole of substrate per minute per cel).

4.2.5 Mutant constructs

Site directed mutagenesis was used to generate mutants of the UPIIIa tail-BD construct in pGBKT7 vector, such that the protein's cytoplasmic tail was truncated after amino acid 35, truncated after amino acid 17, and a conserved tyrosine (Y31) was converted to an alanine residue. Briefly, primers were designed to impart the desired mutation, and mutant strand synthesis was performed by thermal cycling. The parental plasmid was digested with *Dpn I* restriction enzyme, and XL1-blue supercompetent bacterial cells were transformed. Finally, Y187 yeast were transformed by bacteria expressing the mutant construct, and construct expression was confirmed by western blot. The mutant-expressing Y187 yeast were mated with AH109 yeast expressing a protein of interest that was identified by the two-hybrid screen to determine if the mutation eliminated the protein-protein interaction.

4.3 DIFFERENTIAL GEL ELECTROPHORESIS

Two dimensional differential gel electrophoresis was performed under the instruction of Anupam Gopal in the laboratory of Dr. Jonathan Minden, 247 Mellon Institute, Carengie Mellon University. The protocol performed was adapted from Viswanathan *et al.* [162].

4.3.1 Preparation and labeling of samples

Rabbit bladder lysates were prepared by scraping as described above; however, the DIGE lysis was comprised of 7 M urea, 2 M thiourea, 4% [w/v] CHAPS, 10 mM DTT and 10 mM Na-HEPES, pH 8.0. The solution was never heated above room temperature, and all steps were performed with preparations kept on ice. After scraping the cells into the DIGE lysis buffer, the lysate was vortexed at 4^{o}C for 5 min. Next, the solution was homogenized using a PT-2100 Polytron (Kinematica AG, Switzerland) at setting 11 for 7 one-second pulses. The homogenized lysate was centrifuged at 15,000 rpm at 4^{o}C for 15 min, and supernatant was frozen in liquid nitrogen for storage at -80^{o}C until its use.

Immediately prior to running the gel, a Bradford protein assay was run on the lysate and its concentration was adjusted to 1-2 mg/ml by adding DIGE lysis buffer. For comparison of two samples (stretch and control), the lysates were labeled for 2 gels in which the first gel contained Cy3-control and Cy5-stretch labeled proteins, and the second gel contained Cy5-control and Cy3-stretch labeled proteins. For each labeling reaction, 150 μg of lysate was used. As a loading control, 1 μl of 1 mg/ml BSA was added to each tube. To label the proteins, 1 μl Cy3-NHS or Cy5-NHS stock solution (Amersham Biosciences, Piscataway, NJ) was added to each tube, vortexed briefly, and incubated in the dark on ice for 15 min. Dyes were added synchronously

for the two protein samples in each gel. Next, 1 μl quenching solution (5 M methylamine-HCL and 10 mM HEPES, pH 8.0) was added to each tube synchronously, and incubated for 30 min in the dark on ice.

4.3.2 Two-dimensional gel electrophoresis

The labeled samples for each gel were combined, IPG buffer solution was added, and the samples were loaded immediately onto rehydrated Immobiline DryStrips (pH 4-10) isoelectric focusing (IEF) strips (Amersham Biosciences). The rehydration buffer that was used to rehydrate the IEF strips contained 7 M urea, 2 M thiourea, 4% (w/v) CHAPS, 10 mM DTT, 2 mM acetic acid, 0.002% (w/v) bromophenol blue and 1% (w/v) IPG buffer (pH 4-10). The first dimension was prepared according to manufacturer's instructions using the IPGphor (Amersham Biosciences) and run with the following settings: 1 h 500 V gradient, 1 h 4000 V gradient, 2 h 8000 V gradient, followed by 8000 V step-and-hold gradient until the total amount of delivered volt hours was 40,000-50,000 Vh, which takes ~ 12 h.

The IEF strip was equilibrated twice prior to running the second dimension in equilibration buffer (50 mM Tris pH 8.8, 6 M urea, 30% (v/v) glycerol, 2% (w/v) SDS, and 0.002% (w/v) bromophenol blue). The first equilibration was performed with 1% (w/v) DTT in equilibration buffer for 15 min at room temperature. Next, the strip was briefly rinsed with water and equilibrated for 15 min in equilibration buffer containing 2.5% iodoacetamide. The strip was placed in the stack of a previously casted 24 x 18 cm, 1.5 mm thick 10-15% gradient gel for use in the SE660 vertical gel-electrophoresis apparatus (Hoefer, San Francisco, CA). The gel was run at 15 mA per gel in tank buffer consisting of 25 mM Tris, 190 mM glycine, and 0.1% (w/v) SDS.

Next the gel was soaked in fixative solution (50% [v/v] HPLC grade methanol and 1% [v/v] glacial acetic acid) for 2 h with gentle rocking.

4.3.3 Image acquisition and sample selection

Images of the gels were acquired using Dr. Minden's custom imaging system, resulting in four 1024 x 1042 pixel images with a resolution of 135 μm per pixel, stored as raw 16 bit data. IPLab (Scanalytics, BD Biosciences, Rockford, MD) was used to perform image analysis, and the BSA loading control was used to balance the image-display parameters to compare Cy3 and Cy5 samples. Visual inspection of a two-frame looping QuickTime movie of the Cy3 and Cy5 gel images was performed to detect protein differences. A subset of difference-protein spots was selected for excision using Dr. Minden's spot-cutting tool. The 1.8 mm diameter gel plugs were excised from the gel and deposited in a 96-well plate, stored in 1% (v/v) acetic acid.

4.3.4 MALDI-MS/MS analysis of samples

The samples were submitted to the University of Pittsburgh's Genomics and Proteomics Core Laboratory for MALDI-TOF/TOF MS/MS analysis.

APPENDIX A

STUDIES OF THE UROPLAKIN III CYTOPLASMIC TAIL

Several studies were performed to better understand the function of UPs in umbrella cell discoidal vesicle trafficking, with a focus on the role of the UPIIIa cytoplasmic tail. First the distribution of this protein was assessed by immunofluorescence staining, which indicated that UPIII is present at the umbrella cell apical surface, within punctate structures in the apical cytoplasm of umbrella cells, and in a similar distribution in the apical-most cells of the intermediate cell layer of the uroepithelium (Figure A.1). As described in the methods section, the UPIIIa tail sequence was used as bait in a yeast two-hybrid screen. Several interesting protein interactions were further explored with a CPRG quantitave assay.

To explore the role of UPIII and UPII in stretch-induced exocytosis, knockout mice were obtained from the laboratory of Dr. Tung-Tien Sun (New York University). Their bladders were excised and used for capacitance studies to monitor changes in surface area upon stretch (Figure A.2).

A.1 CELLULAR DISTRIBUTION OF UPIIIA

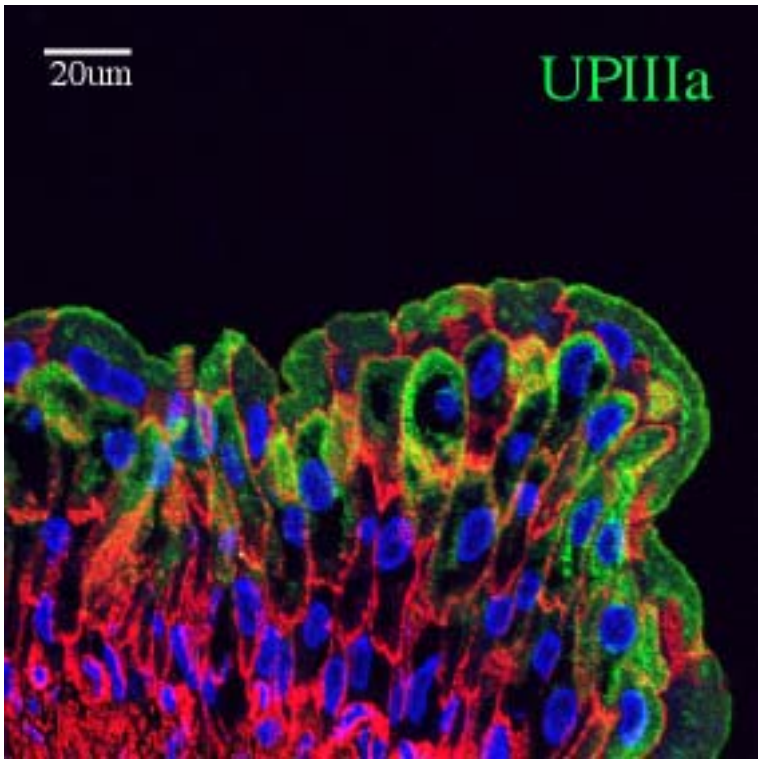

Figure A.1: Distribution of UPIIIa in rabbit uroepithelium

A 5 μm cryosection of rabbit uroepithelium was labeled with UPIIIa (green), rhodamine phalloidin to stain actin (red) and Topro-3 to stain nuclei (blue).

A.2 PROTEIN-PROTEIN INTERACTIONS

A.2.1 Two-hybrid screen

A yeast two-hybrid screen was performed to identify proteins that interact with the 53 amino acid cytoplasmic tail of uroplakin III, as described in the Methods section. The following proteins were identified as members of a human kidney cDNA library that had positive interaction multiple times with the uroplakin III cytoplasmic tail (Table A.1) and had strong matches to proteins in the NCBI database (Table A.2). The complete table of all identified proteins is also included (Table A.3).

Table A.1: Yeast two-hybrid screen with UPIIIa tail: protein interactions that occurred multiple times.
In this table, n indicates the number of samples returning this protein identity. The E-value is the "expect value," which describes the number of hits one can expect by chance when searching the database, or the random background noise for the data. A lower E-value suggests a more significant sequence match.

n	**protein**	**E-value**
6	NADH dehydrogenase 1	8.00E-18
5	Alu contamination	0
5	similar to mucin 11/gp80	0.54
5	LOC90806 protein from breast	0.45
4	rab11-family interacting protein 4-like	2.5
4	cytochrome c oxidase subunit I	1.00E-20
3	Na/K ATPase beta subunit	1.00E-118
3	BAC11041 unnamed	0.003
2	PEG10	3.4
2	KIAA1973	1.5
2	fibrillin 15	12
2	KIAA0553	0.77
2	CAC85341	0.43
2	DAAT9248	1.9
2	Titin	1.4
2	pregnancy zone protein	1.4
2	cerebroside sulfate activator protein	1.00E-124
2	choline dehydrogenase	1E-146

2	TRIM26: tripartate motif-containing 26	0.15

Table A.2: Yeast two-hybrid screen with UPIIIa tail: protein interactions with high confidence.
The ID number specifies the clone as numbered during the experiment. The E-value is the "expect value," which describes the number of hits one can expect by chance when searching the database, or the random background noise for the data. A lower E-value suggests a more significant sequence match.

ID	protein	E-value
2	KIAA1973	1.5
3	NADH dehydrogenase 1	8.00E-18
4	similar to mucin 11	0.54
6	lipin 1	0
9	Bestrophin	7.00E-14
10	pregnancy zone protein	1.4
13	toll-like receptor 4-like protein	1.00E-171
21	G protein beta subunit-like protein	1.00E-179
48	K-voltage gated channel	1
22	PI-binding clathrin assembly protein isoform 1	0.22
25	Alu contamination	0
26	Alu contamination warning	3.00E-16
28	sperm Na/H exchanger	1.4
29	LOC90806 protein from breast	0.45
30	unnamed protein product	1.4
34	LOC90806 protein from breast	0.45
37	melastatin 1	1.3
40	BAC87172 hyp protein	0.013
44	MEF2-monocyte enhancer binding factor 2	1.2
46	pregnancy-zone protein	1.4
51	myosin heavy chain 12	0.6
52	laminin alpha 5 chain	e-148
57	koyt binding protein 1,2,3 (interacts with PKA)	0
58	KI110515	5.00E-09
59	NADH dehydrogenase 1	9.00E-18
60	cytochrome c oxidase subunit I	1.00E-20
63	unnamed protein from cerebellum	1.4
67	unnamed from placenta	0.01
71	KIAA0553	0.77
72	KIAA0853	7.00E-15
74	CAC85341	0.43
77	LOC90806, from breast CA	0.45
78	LOC90806, from breast CA	0.45
79	Na/K ATPase beta subunit 1	1.00E-155
80	FLJ11273 from brain	9.00E-31

85	guanidinoacetate N-methyltransferase isoform B	5.00E-27
522	unnamed form whole 10wk embryo	0.01
523	phosphatidylinositol-4-phosphate 5 kinase, regulates focal adhesions	0.43
524	predicted Rho GEF	4.00E-02
525	unnamed prot from thymus	0.14
527	predicted hyp protein, from Chr 5	0
528	DNA polymerase gamma subunit 2	0.63
529	FLJ31846 - unnamed/hyp	0.005
532	C20-orf6	0.8
537	OTTHUMP40406	1
539	similar to GP80	0.5
94	cytochrome c oxidase subunit 2	6.00E-18
204	BAC11041 unnamed	0.003
205	ARPKC polycystin 1	4.00E-93
208	XP-374191 pred hyp protein	1.4
212	SH3BP1 - SH3 domain binding protein	0.85
213	Chr 14 ORF 45	0.68
515	BAC03893 unnamed protein	1.00E-12
517	scavenger receptor hlg	0.004
518	seq similarity family 13, member A1 Chr 4	0.55
209	dihydrolipamide dehydrogenase	0
217	NADH dehydrogenase 1	5.00E-29
218	KIAA0553	0.77
220	aspartoacylclase 3	0
503	Niemann Pick Dz type 2 precursor	2.00E-62
504	Uromodulin, zymogen granule membrane glycoprotein, alpha tectorin	5.00E-30
505	cytochrome c oxidase subunit I	2.00E-27
506	synaptotagmin XI, XII	0.67
507	Niemann Pick Dz type 2 precursor	2.00E-62
510	LOC90806 protein from breast	0.032
511	putative acyl CoA dehydrogenase	2.00E-39
513	STAT3	0.21
514	hyp prot from skeletal muscle	0.55
238	unnamed from testis	0.025
242	ZnT3 solute carrier family 30	0.89
244	interleukin 3 precursor	1.2
247	NADH dehydrogenase 1	2.00E-21
292	SGT1, suppressor of GT allele of SKP1	0.6
499	FT0 protein & many unnamed proteins	8.00E-25
500	cytochrome c oxidase subunit 2	2.00E-59
555	solute carrier family 35	1.4
224	NADH dehydrogenase 1	6.00E-14
225	BAC11041, unnamed from 10d whole embryo	0.004
228	LOC64864	0.48
229	type 1 hair keratin 5, int. filament	1
231	mitogen-activated protein KKK11, protein tyrosine kinase 1	1.00E-05
232	NADH dehydrogenase 1	6.00E-14

233	LOC389199	0.05
234	BAC85184 from prostate	0.65
236	Na/K ATPase beta subunit 3	1.00E-118
123	BAC87611 from thalamus	4.00E-05
124	KIAA0664 from brain/PNS	1
127	cerebroside sulfate activator protein	1.00E-124
128	CAI146268 from endometrium	0.15
130	ornithine decarboxylase antiqyme 3	0.51
134	neuronal apoptosis inhibitory protein	8.00E-94
136	NFASC protein, neurofascin	1.00E-89
138	Titin	1.4
139	Titin	1.4
102	guanidinoacetate N-methyltransforase isoform b	5.00E-27
103	TRIM26: tripartate motif-containing 26	0.15
105	TRIM26: tripartate motif-containing 26	0.15
108	rho GDI alpha	6.00E-35
109	FCH domain only 1	0.34
111	Na/K ATPase beta subunit 1	1.00E-50
113	MSTP078 from aorta	4.00E-82
117	BAC87120, unnamed protein product	1.00E-05
121	BAC11041 from 10wk embryo	0.001
265	pred similar to gp80, mucin11	0.57
266	cubilin-1, intrinsic factor	1.00E-131
267	PRO0113 from fetal liver	0.21
269	XP_379200	0.35
271	mitochondrial ribosome protein L15	1.5
274	KIAA0423 from brain	0.2
276	BAC11041 from whole embryo	0.001
278	IgE variable region	1.1
280	Alu family contamination	2.00E-38
281	choline dehydrogenase	1E-146
282	choline dehydrogenase	1E-146
284	PDZ-domain containing protein AIPC	0.11
285	MGC2226 - hyp protein from lung, SMA3	1.00E-111
302	PRO664 from fetal liver, unnamed from trachea	5.00E-09
303	XP_496740	0.015
141	Parkin, PARK2	1.00E-127
147	unknown protein Chr 2	0.66
149	BAB14918 unnamed prot product	0.13
152	prosaposin, cerebroside sulfate activator prot	1.00E-124
155	BAC83720 from testis	2.00E-07
156	NADH dehydrogenase	5.00E-29
157	R-PTP-delta - receptor-type turosine protein phosphatase delta precursor	2.00E-82
158	AP1 gamma 1 subunit	1.00E-52
160	FLJ22875 pred. Protein	1.00E-05
161	fibronectin 1	0
162	synaptotagmin VII	10

163	NADH dehydrogenase	6.00E-14
165	AAL55777 unknown	0.003
166	NYD-SP29 testis development protein	1.4
167	unnamed from thalamus	0.1
168	MLCK: myosin light chain kinase	1.3
174	alpha 3 type IV collagen isoform 3	0
177	CAC85341 from skeletal muscle	0.52
178	NADH dehydrogenase	2.00E-21
180	BAC87169	0.66
181	MutS homolog	1.5
182	cytochrome c oxidase subunit I	1.00E-16
185	BAC86823	0.2
186	adenosine receptor 1	0.82
187	pred similar to gp80	0.49
191	aldehyde oxidase	1.00E-108
196	AAH57836	0.19
197	pred similar to gp80, mucin11	0.57
198	Alu family contamination	6.00E-06
236	hyp protein, unnamed, with fumarylacetoacetate domain	1.00E-129
238	otoferlin	0.19
251	Alu family contamination	6.00E-11
252	enolase 1	0
257	lysine hydroxylase	0.13
258	Na/K ATPase beta subunit 1	0
259	NADH dehydrogenase	8.00E-20
260	AAL55847	2.00E-23
263	pred similar to paraneoplastic antigen like 6A	0.016
465	Chorea acanthocytosis	1.5
466	FLJ35834 from Chr 7	0
415	XP_496425 - predicted hyp	9.00E-26
417	ENO1 - enolase 1	0
418	ENO1 - enolase 1	0
419	Unnamed - BAD18527	0.004
421	Rab11-family interacting protein 4	1.5
425	RAB18, member RAS oncogene family	1.2
426	Unnamed, BAC11041	0.001
427	Hyp protein LOC55172 Chr 14	0
429	PAPSS1 - paps sunthetase	3.00E-94
431	Na,K-ATPase beta subunit	2.00E-55
432	Pred similar to mucin11, GP80	0.58
336	A Kinase PRKA anchor protein	9.00E-102
340	Ub-conjugating enzyme E2G	4.00E-104
341	NECAP1 protein	4.00E-172
343	XP_373772 - Pred. hyp. protein	1.2
344	LOC51647 - hyp protein	4.00E-116
401	Glucosamine-fructose-6-phosphate aminotransferase	0.55
404	Solute carrier family 19 member 2	0.08

405	Neighbor of COX4	2.00E-150
411	Cubilin = intrinsic factor vit B12 R	6.00E-114
281	Choline dehydrogenase	3.00E-146
304	ATPase, Na/K transporting, beta1	5.00E-78
314	AAL55847 - unknown	2.00E-23
320	Acetyl-CoA carboxylase alpha	1.00E-28
322	Cytidine 5'-monophosphate N-acetylneuraminic acid synthetase variant	2.00E-104
329	OTTHUMP00000028903	2.00E-04
332	G-protein coupled receptor	0.11
334	Doublesex and mab-3 related TF1c	0.002
335	BAC11041 - unnamed	0.004
435	BAC86879 - unnamed and others	1.00E-10
436	cubilin	2.00E-71
437	NADH dehydrogenase subunit 1	1.00E-09
438	NADH dehydrogenase subunit 1	1.00E-09
439	NADH dehydrogenase subunit 1	6.00E-13
448	BAC86958 - unnamed	0.002
449	Ribulose-5-phosphate-3-epimerase	7.00E-165
461	Interleukin 3 precursor	1.2
463	Rab11 family interacting protein 4	1.5
116	BAC87120 - unnamed	9.00E-06
120	CGI-128 protein = LOC51647 -hyp	4.00E-116
241	NADH dehydrogenase subunit I	9.00E-16
245	T1 protein, NIK and IKKbeta-binding protein	8.00E-90
247	Pred similar to mucin 11	1
249	NADH dehydrogenase subunit 1	2.00E-21
305	Niemann-Pick ds, type C2 precursor	2.00E-62
308	Cubilin, intrinsic factor vit B12 R	6.00E-68
350	BAC86300 - unnamed	0.061
481	Heat shock protein	6.00E+116
482	Scavenger receptor hlg	0.004
483	Ig heavy chain variable region	0.63
484	Cytochrome C oxidase subunit I	9.00E-26
485	Lutheran blood group glycoprotein	0.43
487	BAB71696 -unnamed	2.00E-52
490	PLCG1 variant	0.33
491	NADH dehydrogenase subunit 1	5.00E-29
492	SGT1	0.62
494	Phospholipase A2 activating protein	1.5
499	FTO protein	8.00E-25
500	Cytochrome oxidase subunit 2	2.00E-39
541	Neuronal PAS domain protein 2	1.6
543.2	CAC21648 - hyp protein	0.39
543	CAC21648 - hyp protein	0.39
545	PI glycan, class M	0.5
547	TM7SF2	1.1
550	Na/K ATPase beta 3 subunit	3.00E-44

118	CUB and sushi multiple domains	0.86
226	MCM3	7.00E-04
254	Doublesex and mab-3 related TF 1c	0.48
272	KIAA1409	0.042
273	PSAP prosaposin, cerebroside sulfate activator protein	2.00E-70
283	2'-phosphodiesterase	1.00E-54
289	Scavenger receptor hlg	0.005
309	Tumor endothelial marker 5 precursor, G protein-coupled receptor 124	0.12
311	Cubilin	6.00E-101
313	Niemann-Pick dz, type C2 precursor	4.00E-75
316	BAC85863 unnamed	1.00E-08
346	Immunoglobulin heavy chain variable region	0.83
347	KIAA1127	0.35
348	Putative endothelin receptor type B-like protein	0.42
349	ATP1B1	0
403	RAN binding protein 9 (RANBP9)	0
414	ATP1B1	5.00E-95
553	Uromodulin (UMOD)	1.00E-24
556	Similar to mucin11, gp80	0.58
559	Similar to TAR DNA binding protein	0.18
560	LOC55172 Hyp protein, C14orf104	0
352	Similar to mucin11, gp80	0.58
354	ABT1-associated protein	0.85
355	Immunoglobulin heavy chain variable region	1.5
356	EEF1A1 protein – elongation factor	0
357	PSAP prosaposin	2.00E-70
360	Haptoglobin-related protein	0.006
361	NADH dehyrdogenase subunit 2	2.00E-04
363	HLA-A*0204	5.00E-45
364	Putative p150	1.00E-07
365	Cytochrome c oxidase subunit I	1.00E-35
368	BTB and CNC homology 1 isoform A	1.3
369	ATP-binding cassette, sub-family A, member 6, isoform a	0.25
371	Poly(rC)-binding protein 2 isoform a	5.00E-127
373	Melastatin 1, transient receptor potential cation channel	1.5
374	Peptidylglycine alpha-amidating monooxygenase isoform a	0.35
378	Doublesex and mab-3 related TF 1c	0.48
379	BAB13911	2.00E-12
381	BAC86209	0.98
382	Cytochrome c oxidase subunit 1	1.00E-19
384	ANGEL2 protein	5.00E-05
387	ANGEL2 protein	0.033
390	BAC86912	7.00E-04
391	LOC65996	2.00E-25

392	CAD62601	1.00E-09
394	Amyloid lambda light chain variable region	0.5
395	Similar to mucin11 and gp80	0.58
396	LOC23131	0.82
397	ATP1B1	0
398	BAC85647	0.86
399	CAC85341	0.58
400	BAC86849	0.081

Table A.3: Yeast two hybrid screen with UPIIIa tail: complete list of identified proteins.
The ID number specifies the clone as numbered during the experiment. The E-value is the "expect value," which describes the number of hits one can expect by chance when searching the database, or the random background noise for the data. A lower E-value suggests a more significant sequence match.

ID	protein	E-value
1	PEG10	3.4
2	KIAA1973	1.5
3	NADH dehydrogenase 1	8.00E-18
4	similar to mucin 11	0.54
6	lipin 1	0
7	dedicator to cytokinesis 8	2.5
8	ENaC	4.5
9	Bestrophin	7.00E-14
10	pregnancy zone protein	1.4
12	unnamed protein form lung	3.5
13	toll-like receptor 4-like protein	1.00E-171
17	rab11-family interacting protein 4-like	2.5
18	ameloblastin	4.3
19	proton/aa Xporter	6.2
21	G protein beta subunit-like protein	1.00E-179
27	XP_378453 - hypothetical	2.1
33	olfactomedin-like protein	3.5
47	fibrillin 15	12
48	K-voltage gated channel	1
53	immunoglobulin epison chain, membrane bound form	7.2
22	PI-binding clathrin assembly protein isoform 1	0.22
23	DKFZp586P2221 hyp protein	3
24	OTTHUMP00000021539, toll-like R4	17
25	Alu contamination	0
26	Alu contamination warning	3.00E-16
28	sperm Na/H exchanger	1.4
29	LOC90806 protein from breast	0.45
30	unnamed protein product	1.4
32	V-gated Na channel type III alpha	11
34	LOC90806 protein from breast	0.45
35	aldehyde dehydrogenase 9A1	1.9
36	Laminin AH, A3	15

37	melastatin 1	1.3
38	Ca channel, V-gated beta2 subunit	15
39	RhoGEF 19	6.3
40	BAC87172 hyp protein	0.013
41	pred. Similar to succinate CoA ligase	3.5
42	hyp protein from spinal cord	5
43	--	
44	MEF2-monocyte enhancer binding factor 2	1.2
45	RASAL1 - Ras GAP activating like prote	1.9
46	pregnancy-zone protein	1.4
49	fibrillin 15	12
50	polo-like kinase 4	33
51	myosin heavy chain 12	0.6
52	laminin alpha 5 chain	e-148
55	OTTHUMP00000059419 from Chr 10	16
56	ZNF554, zinc finger domains	1.7
57	koyt binding protein 1,2,3 (interacts with PKA)	0
58	KI110515	5.00E-09
59	NADH dehydrogenase 1	9.00E-18
60	cytochrome c oxidase subunit I	1.00E-20
61	advillin	20
62	rheumatoid factor D5 light chain	2.6
63	unnamed protein from cerebellum	1.4
64	natriuretic peptide receptor A	33
65	GARP: glycoprotein A repetitions	21
66	URB - steroid sensitive protein 1	1.7
67	unnamed from placenta	0.01
68	MGC15396, from Chr 17	11
69	KIaa0232	2
70	TPA:MICL2 - MT-associated monooxygenase, calponin, and LIM domain containing	6.2
71	KIAA0553	0.77
72	KIAA0853	7.00E-15
73	extracellular matrix protein 2	11
74	CAC85341	0.43
75	--	
76	Cub domain containing protein 1 = gp140	6.1
77	LOC90806, from breast CA	0.45
78	LOC90806, from breast CA	0.45
79	Na/K ATPase beta subunit 1	1.00E-155
80	FLJ11273 from brain	9.00E-31
85	guanidinoacetate N-methyltransferase isoform B	5.00E-27
521	casein alpha s1, titin	15
522	unnamed form whole 10wk embryo	0.01
523	phosphatidylinositol-4-phosphate 5 kinase	0.43
524	predicted Rho GEF	4.00E-02
525	unnamed prot from thymus	0.14
526	crumbs homolog 1	12
527	predicted hyp protein, from Chr 5	0
528	DNA polymerase gamma subunit 2	0.63
529	FLJ31846 - unnamed/hyp	0.005
530	PEG10 = MEF3	3.4

531	MADD - map kinase activating death domain	90
532	C20-orf6	0.8
533	--	
534	rictor: rapamycin-insensitive companion of MTOR, regulates cytoskeleton	1.9
535	BRCA2	8.5
536	desmin	2.5
537	OTTHUMP40406	1
538	MSTP159	2
539	similar to GP80	0.5
540	acid ceramidase 1b	5.6
92	PRKDC: prot kinase DNA-dependant catalytic subunit	28
93	--	
94	cytochrome c oxidase subunit 2	6.00E-18
201	pred Similar to V-SNARE	8.4
203	MLEL1, putative DEXH/RNA helicase	1.8
204	BAC11041 unnamed	0.003
205	ARPKC polycystin 1	4.00E-93
206	V-gated Na channel type IV, alpha	20
207	p21/Cdc42/Rac1-activated kinases 1,3	8.3
208	XP-374191 pred hyp protein	1.4
210	unnamed from hippocampus	2.9
211	C-type lectin receptor 1	2.1
212	SH3BP1 - SH3 domain binding protein	0.85
213	Chr 14 ORF 45	0.68
214	--	
215	IL-kappa chain variable region	8.4
515	BAC03893 unnamed protein	1.00E-12
516	ACATE2, acyl coA thioesterase	6.1
517	scavenger receptor hlg	0.004
518	seq similarity family 13, member A1 Chr 4	0.55
520	AIRE isoform 1: autoimmune regulator	8.5
209	dihydrolipamide dehydrogenase	0
216	solute carrier family 2 protein	4.6
217	NADH dehydrogenase 1	5.00E-29
218	KIAA0553	0.77
219	--	
220	aspartoacylclase 3	0
501	--	
502	KIAA1173	2.9
503	Niemann Pick Dz type 2 precursor	2.00E-62
504	Uromodulin, zymogen granule membrane glycoprotein, alpha tectorin	5.00E-30
505	cytochrome c oxidase subunit I	2.00E-27
506	synaptotagmin XI, XII	0.67
507	Niemann Pick Dz type 2 precursor	2.00E-62
508	--	
509	unnamed from caudate nucleus	6.2
510	LOC90806 protein from breast	0.032
511	putative acyl CoA dehydrogenase	2.00E-39
512	smoothelin	2.6
513	STAT3	0.21
514	hyp prot from skeletal muscle	0.55

238	unnamed from testis	0.025
239	KIAA0586	6.2
240	utrophin anchors cytoskel to PM	1.9
241	--	
242	ZnT3 solute carrier family 30	0.89
243	rab11-family interacting protein 4- class 2	1.8
244	interleukin 3 precursor	1.2
245	--	
246	--	
247	NADH dehydrogenase 1	2.00E-21
292	SGT1, suppressor of GT allele of SKP1	0.6
495	Zinc finger & BTB domain containing 16	3.5
499	FT0 protein & many unnamed proteins	8.00E-25
500	cytochrome c oxidase subunit 2	2.00E-59
543	--	
555	solute carrier family 35	1.4
221	DAAT9248	1.9
222	DAAT9248	1.9
223	Rough Deal homolog	8.4
224	NADH dehydrogenase 1	6.00E-14
225	BAC11041, unnamed from 10d whole embryo	0.004
227	Ig heavy chain variable region	3.5
228	LOC64864	0.48
229	type 1 hair keratin 5, int. filament	1
230	LOC285889, hyp protein	5.5
231	mitogen-activated protein KKK11, protein tyrosine kinase 1	1.00E-05
232	NADH dehydrogenase 1	6.00E-14
233	LOC389199	0.05
234	BAC85184 from prostate	0.65
235	--	
236	Na/K ATPase beta subunit 3	1.00E-118
237	LOC55783 hyp protein	8.5
122	solute carrier family 40, iron regulated	59
123	BAC87611 from thalamus	4.00E-05
124	KIAA0664 from brain/PNS	1
125	ERG-1 uterus/ovary putative Tm protein	2.6
126	neural precursor cell expressed developmentally downregulated 1	2.6
127	cerebroside sulfate activator protein	1.00E-124
128	CAI146268 from endometrium	0.15
129	A430083B18 hyp protein	2.7
130	ornithine decarboxylase antiqyme 3	0.51
131	Rab-related GAP binding protein Rab-39A	4.1
132	--	
134	neuronal apoptosis inhibitory protein	8.00E-94
135	--	
136	NFASC protein, neurofascin	1.00E-89
137	magic roundabout	16
138	Titin	1.4
139	Titin	1.4
140	--	
101	ankyrin repeat and BTB/POZ domain prot 1	4.1

102	guanidinoacetate N-methyltransforase isoform b	5.00E-27
103	TRIM26: tripartate motif-containing 26	0.15
104	solute carrier organic anion transporter family member 4A1	4.9
105	TRIM26: tripartate motif-containing 26	0.15
106	TRIM protein, t-cell receptor interacting molecule, fibrillin15	6.9
108	rho GDI alpha	6.00E-35
109	FCH domain only 1	0.34
110	splicing factor, R/S-rich 14	3.6
111	Na/K ATPase beta subunit 1	1.00E-50
112	pred, similar to CAT-3 cationic aa transporter 3	1.6
113	MSTP078 from aorta	4.00E-82
114	G-protein coupled receptor 8	3.5
115	--	
117	BAC87120, unnamed protein product	1.00E-05
119	--	
120	--	
121	BAC11041 from 10wk embryo	0.001
264	melanostatin-1	38
265	pred similar to gp80, mucin11	0.57
266	cubilin-1, intrinsic factor	1.00E-131
267	PRO0113 from fetal liver	0.21
268	ankyrin 3	5.2
269	XP_379200	0.35
270	MSTP140 from aorta	2.1
271	mitochondrial ribosome protein L15	1.5
274	KIAA0423 from brain	0.2
275	rab11 family interacting protein 4	2.6
276	BAC11041 from whole embryo	0.001
278	IgE variable region	1.1
279	pred similar to tripartite motif containing 51	4.8
280	Alu family contamination	2.00E-38
281	choline dehydrogenase	1E-146
282	choline dehydrogenase	1E-146
284	PDZ-domain containing protein AIPC	0.11
285	MGC2226 - hyp protein from lung, SMA3	1.00E-111
296	rab11 family interacting protein 4	1.8
298	centaurin delta 1	3.5
301	MOB1 - sphingomyosin synthase	8.6
302	PRO664 from fetal liver, unnamed from trachea	5.00E-09
303	XP_496740	0.015
141	Parkin, PARK2	1.00E-127
142	similar to Hkr1p	16
143	39S mitochondrial ribo protein L19	29
144	TGIF-interacting Ub ligase 1	6.5
145	Chr 1 ORF 22	3.6
146	kallikrien 1	6.6
147	unknown protein Chr 2	0.66
148	Leucine rich repeat containing G-protein coupled receptor 6	2.6
149	BAB14918 unnamed prot product	0.13
150	piccolo, aczonin	4.7
151	plasma hyaluronidase	6.5

152	prosaposin, cerebroside sulfate activator prot	1.00E-124
154	KIAA1973	1.7
155	BAC83720 from testis	2.00E-07
156	NADH dehydrogenase	5.00E-29
157	R-PTP-delta - receptor-type turosine protein phosphatase delta precursor	2.00E-82
158	AP1 gamma 1 subunit	1.00E-52
159	RP1-95L4, CGI-103 protein, androgen induced	2.2
160	FLJ22875 pred. Protein	1.00E-05
161	fibronectin 1	0
162	synaptotagmin VII	10
163	NADH dehydrogenase	6.00E-14
164	FLJ21394, similar to hyp	6.4
165	AAL55777 unknown	0.003
166	NYD-SP29 testis development protein	1.4
167	unnamed from thalamus	0.1
168	MLCK: myosin light chain kinase	1.3
169	spastin protein	3.1
170	BAC86815	1.6
171	WWP2 E3 ligase	6.5
172	RAP1A, Ras family, small GTP binding	3
173	--	
174	alpha 3 type IV collagen isoform 3	0
175	PRKAA1 protein - kinase domain from brain	2.7
176	KLHL10: kelch-like protein 10	12
177	CAC85341 from skeletal muscle	0.52
178	NADH dehydrogenase	2.00E-21
179	KLHL10: kelch-like protein 10	12
180	BAC87169	0.66
181	MutS homolog	1.5
182	cytochrome c oxidase subunit I	1.00E-16
183	URB	1.7
184	T-cell receptor interacting molecule	6.9
185	BAC86823	0.2
186	adenosine receptor 1	0.82
187	pred similar to gp80	0.49
189	H+ ATPase B subunit	16
190	carboxypeptidase B	2
191	aldehyde oxidase	1.00E-108
192	methly-CpG binding domain protein 2, isoform 1	6.3
193	Sp4 transcription factor	202
194	transmembrane 7 superfamioly member 1	8.6
195	WBSCR14: williams beuren syndrome chr region 14	4.8
196	AAH57836	0.19
197	pred similar to gp80, mucin11	0.57
198	Alu family contamination	6.00E-06
199	mannosidase, endo-alpha	4.9
200	aristaless-like 4	4.8
236	hyp protein, unnamed, with fumarylacetoacetate domain	1.00E-129
237	XP_490539	5.2
238	otoferlin	0.19
251	Alu family contamination	6.00E-11

252	enolase 1	0
253	SH120: putative G-protein coupled receptor	4.8
256	AAL55779, unknown	4.8
257	lysine hydroxylase	0.13
258	Na/K ATPase beta subunit 1	0
259	NADH dehydrogenase	8.00E-20
260	AAL55847	2.00E-23
261	pred similar to pepsinogen B	3.5
262	secretory pathway Ca ATPase 2	14
263	pred similar to paraneoplastic antigen like 6A	0.016
465	Chorea acanthocytosis	1.5
466	FLJ35834 from Chr 7	0
468	--	
469	POU 5 domain protein	21
470	--	
415	XP_496425 - predicted hyp	9.00E-26
416	KIAA1973 protein from brain	1.6
417	ENO1 - enolase 1	0
418	ENO1 - enolase 1	0
419	Unnamed - BAD18527	0.004
420	Unnamed - BAC11127	22
421	Rab11-family interacting protein 4	1.5
422	--	
423	--	
424	Polycystic kidney and hepatic disease 1	16
425	RAB18, member RAS oncogene family	1.2
426	Unnamed, BAC11041	0.001
427	Hyp protein LOC55172 Chr 14	0
428	--	
429	PAPSS1 - paps sunthetase	3.00E-94
430	--	
431	Na,K-ATPase beta subunit	2.00E-55
432	Pred similar to mucin11, GP80	0.58
433	VPS41 protein	21
434	Neuronal apoptosis inhibitory protein	21
336	A Kinase PRKA anchor protein	9.00E-102
339	Protocadherin alpha 6 isoform	6.5
340	Ub-conjugating enzyme E2G	4.00E-104
341	NECAP1 protein	4.00E-172
342	Pred. similar to LDLR-related protein 5	2.7
343	XP_373772 - Pred. hyp. protein	1.2
344	LOC51647 - hyp protein	4.00E-116
345	ESRM828	9
401	Glucosamine-fructose-6-phosphate aminotransferase	0.55
402	C11orf2 protein	17
404	Solute carrier family 19 member 2	0.08
405	Neighbor of COX4	2.00E-150
406	--	
407	--	
408	--	
409	Chloride channel protein	16

410	Methyl-CpG binding domain prot.1	5.7
411	Cubilin = intrinsic factor vit B12 R	6.00E-114
412	Mucin 16	2.6
413	Small nuclear ribonucleoprotein polypeptide D2	12
281	Choline dehydrogenase	3.00E-146
295	NADH dehydrogenase subunit 2	12
299	SLC22A7 protein	3.5
300	OS9 - amplified in osteosarcoma	3.7
304	ATPase, Na/K transporting, beta1	5.00E-78
306	PTPRT - protein tyrosine phosphatase, receptor type, T	2.7
307	--	
310	Protein phosphatase 1, regulatory (inhibitor) subunit 3F	2.2
312	Recoverin	8.7
314	AAL55847 - unknown	2.00E-23
320	Acetyl-CoA carboxylase alpha	1.00E-28
322	Cytidine 5'-monophosphate N-acetylneuraminic acid synthetase variant	2.00E-104
328	Fibrillin 15	12
329	OTTHUMP00000028903	2.00E-04
330	Filamin A, alpha	2.8
331	LOC163782 hyp protein	4.8
332	G-protein coupled receptor	0.11
333	BAC87517 - unnamed	2.7
334	Doublesex and mab-3 related TF1c	0.002
335	BAC11041 - unnamed	0.004
435	BAC86879 - unnamed and others	1.00E-10
436	cubilin	2.00E-71
437	NADH dehydrogenase subunit 1	1.00E-09
438	NADH dehydrogenase subunit 1	1.00E-09
439	NADH dehydrogenase subunit 1	6.00E-13
440	T-cell R alpha-chain, V-region	2.1
441	C1orf16	7
442	--	
443	PEG10	3.6
444	--	
445	--	
446	Nictric oxide synthase 1	6.6
447	CAB66718 - Hyp protein	6.5
448	BAC86958 - unnamed	0.002
449	Ribulose-5-phosphate-3-epimerase	7.00E-165
450	Chemokine C-X3-C motif receptor1	6.7
461	Interleukin 3 precursor	1.2
462	LOC388739 - hyp prot	29
463	Rab11 family interacting protein 4	1.5
464	Semaphorin III family homolog	29
107	--	
116	BAC87120 - unnamed	9.00E-06
120	CGI-128 protein = LOC51647 -hyp	4.00E-116
173	DNA topoisomerase II	2
241	NADH dehydrogenase subunit I	9.00E-16
245	T1 protein, NIK and IKKbeta-binding protein	8.00E-90
246	A-kinase anchor protein 13 isoform 2	9.1

247	Pred similar to mucin 11	1
248	BAC87517 - unnamed	2.7
249	NADH dehydrogenase subunit 1	2.00E-21
250	--	
294	Synaptotagmin XV	3
305	Niemann-Pick ds, type C2 precursor	2.00E-62
308	Cubilin, intrinsic factor vit B12 R	6.00E-68
350	BAC86300 - unnamed	0.061
481	Heat shock protein	6.00E+116
482	Scavenger receptor hlg	0.004
483	Ig heavy chain variable region	0.63
484	Cytochrome C oxidase subunit I	9.00E-26
485	Lutheran blood group glycoprotein	0.43
486	RGS12TS isoform 2	11
487	BAB71696 -unnamed	2.00E-52
488	WDR6 protein	3.6
490	PLCG1 variant	0.33
491	NADH dehydrogenase subunit 1	5.00E-29
492	SGT1	0.62
493	TAR (HIV) binding protein 1	16
494	Phospholipase A2 activating protein	1.5
495	Promyelocytic leukemia zinc finger protein	3.6
496	--	
497	--	
498	--	
499	FTO protein	8.00E-25
500	Cytochrome oxidase subunit 2	2.00E-39
541	Neuronal PAS domain protein 2	1.6
542	TPA:NOD14	3.9
543.2	CAC21648 - hyp protein	0.39
543	CAC21648 - hyp protein	0.39
544	Rab11-family interacting protein 4	2.6
545	PI glycan, class M	0.5
546	Pred sim. to LDLR-related protein 5	2.7
547	TM7SF2	1.1
549	Centaurin, gamma-like fam, memb4	12
550	Na/K ATPase beta 3 subunit	3.00E-44
118	CUB and sushi multiple domains	0.86
153	BAC85869 unnamed	3.4
226	MCM3	7.00E-04
254	Doublesex and mab-3 related TF 1c	0.48
255	KIAA0342	2
272	KIAA1409	0.042
273	PSAP prosaposin, cerebroside sulfate activator protein	2.00E-70
283	2'-phosphodiesterase	1.00E-54
289	Scavenger receptor hlg	0.005
293	BAC85706 unnamed	2
309	Tumor endothelial marker 5 precursor, G protein-coupled receptor 124	0.12
311	Cubilin	6.00E-101
313	Niemann-Pick dz, type C2 precursor	4.00E-75
316	BAC85863 unnamed	1.00E-08

318	BAC87519 unnamed	16
323	Similar to plasma hyaluronidase	6.6
346	Immunoglobulin heavy chain variable region	0.83
347	KIAA1127	0.35
348	Putative endothelin receptor type B-like protein	0.42
349	ATP1B1	0
403	RAN binding protein 9 (RANBP9)	0
414	ATP1B1	5.00E-95
489	RAB11 family interacting protein 4 (class II)	2.7
553	Uromodulin (UMOD)	1.00E-24
556	Similar to mucin11, gp80	0.58
559	Similar to TAR DNA binding protein	0.18
560	LOC55172 Hyp protein, C14orf104	0
351	--	
352	Similar to mucin11, gp80	0.58
353	HSPC163 protein variant	5
354	ABT1-associated protein	0.85
355	Immunoglobulin heavy chain variable region	1.5
356	EEF1A1 protein – elongation factor	0
357	PSAP prosaposin	2.00E-70
358	--	
359	CELSR1 protein – cadherin EGF LAG seven-pass G-type receptor 1	3
360	Haptoglobin-related protein	0.006
361	NADH dehyrdogenase subunit 2	2.00E-04
362	Na/Ca exchanger 2	17
363	HLA-A*0204	5.00E-45
364	Putative p150	1.00E-07
365	Cytochrome c oxidase subunit I	1.00E-35
366	--	
367	Kallikrein precursor	6.8
368	BTB and CNC homology 1 isoform A	1.3
369	ATP-binding cassette, sub-family A, member 6, isoform a	0.25
370	recoverin	4.1
371	Poly(rC)-binding protein 2 isoform a	5.00E-127
372	Ryanodine receptor 2	2
373	Melastatin 1, transient receptor potential cation channel	1.5
374	Peptidylglycine alpha-amidating monooxygenase isoform a	0.35
375	Solute carrier family 40 (iron-regulated transporter)	71
376	Fibrillin 15	12
377	Serpin A11 precursor	3.6
378	Doublesex and mab-3 related TF 1c	0.48
379	BAB13911	2.00E-12
380	Fibrillin 15	13
381	BAC86209	0.98
382	Cytochrome c oxidase subunit 1	1.00E-19
384	ANGEL2 protein	5.00E-05
385	--	
386	Heart alpha-kinase	12
387	ANGEL2 protein	0.033
388	Mutant desmin	22
390	BAC86912	7.00E-04

391	LOC65996	2.00E-25
392	CAD62601	1.00E-09
393	Meiotic recombination 11 homolog A isoform 2	12
394	Amyloid lambda light chain variable region	0.5
395	Similar to mucin11 and gp80	0.58
396	LOC23131	0.82
397	ATP1B1	0
398	BAC85647	0.86
399	CAC85341	0.58
400	BAC86849	0.081

A.3 STRETCH-INDUCED CAPACITANCE CHANGES

To determine whether uroplakin proteins are required for fusiform vesicle exocytosis, capacitance was monitored as a measure of surface area in stretched knockout mouse bladder tissue. The tissue's capacitance was calculated by fitting the data to a model of the epithelium that includes apical and basolateral resistance and capacitance values, and a series resistance [159], as described in the Methods. The capacitance changes in response to stretch for uroplakin III, uroplakin II, double knockout, and strain-matched control mouse bladders were compared.

For each mouse strain, the capacitance of stretched versus control bladder tissue was compared at each time point (Figure A.2, A-D). It is important to note that for stretched tissues at the 20- and 60-minute time points (indicated by red boxes in Figure A.2), the tissue's resistance dropped due to the administration of Krebs buffer. Resistance gradually increased over the later time points as the tissue accommodated the increase in pressure induced by the stretch stimulus. At the 20- and 60-minute time points, the R^2 value of the non-linear regression, a measure of the goodness of the fit of the model's curve compared to the data, indicated that these data did not fit the model as well as other time points. Typically regression yielded R^2 values > 0.98, while data

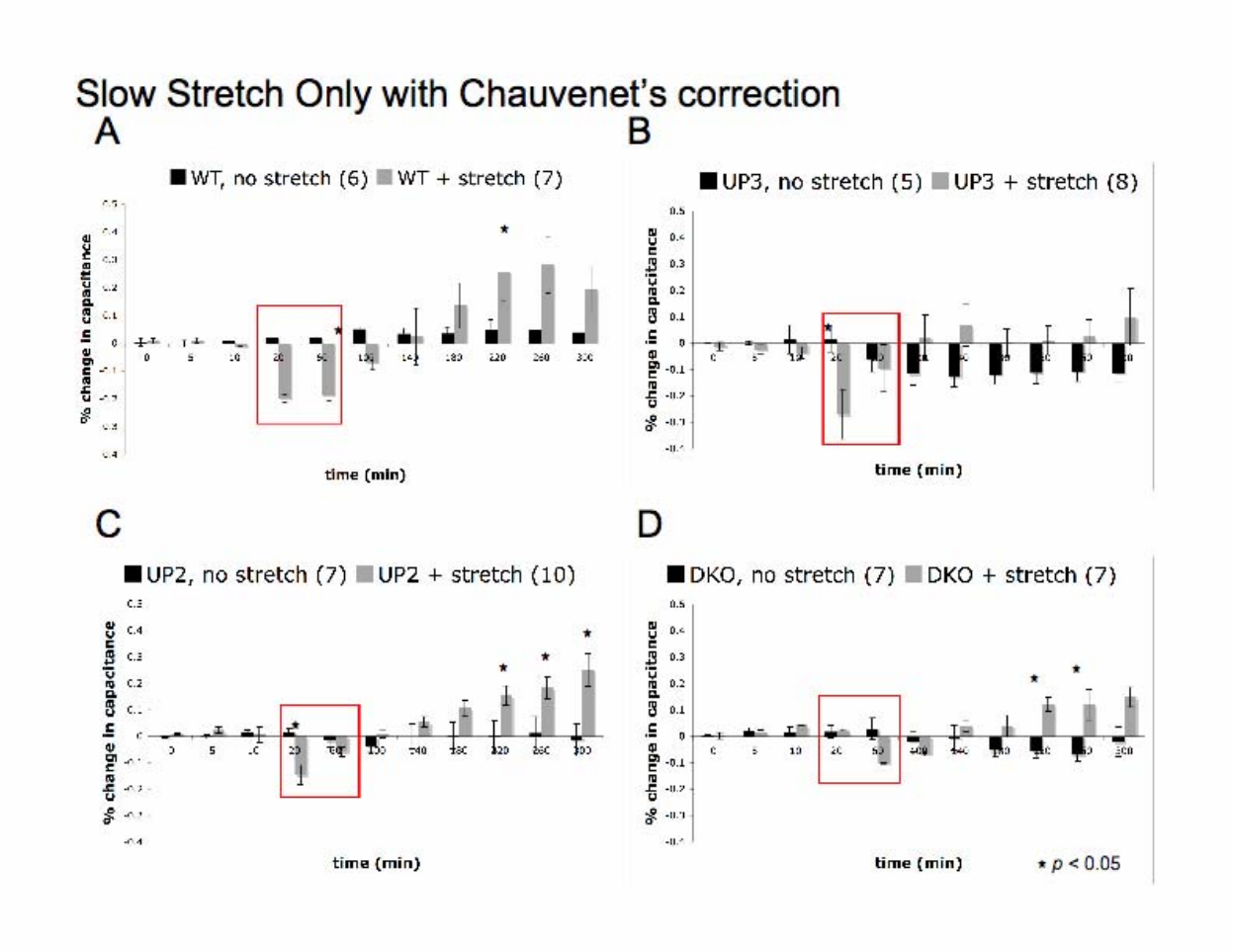

Figure A.2: Stretch versus control capacitance changes for each UP knockout mouse strain

UP knockout and control mouse bladders were mounted in Ussing stretching chambers and subjected to 5 h control unstretch or stretch treatments, as described in the methods. Comparisons of control versus stretch capacitance values for each time point are shown in control (A), UPIII (B), UPII (C), and UPII/III (D) mouse strains. The red box indicates time points that were difficult to curve fit using the double exponential model due to decreased resistance values during stretch; these points had lower R^2 values than the others.

from 20- and 60-minute time points yielded R^2 values of ~ .93 - .97. The ability of the model to fit the data at these time points may be affected by underlying tissues, such as smooth muscle or underlying nervous and connective tissue present on the undissected mouse bladder tissue, which contribute electrical properties that were not accounted for in the model of the epithelium used to analyze this data. The contributions of these tissues may have greater impact when the resistance is lower due to increased hydrostatic pressure during stretch. These tissues may respond independently of the epithelium, for example by muscle contraction or relaxation, which impact the tissue's overall surface area. Future study of these early events will rely on the development of an equivalent electrical model that incorporates the contribution of each of these present tissue types.

There was a significant difference in capacitance change ($p < 0.05$) between stretched and control bladders in uroplakin II knockout tissue at time points > 220 minutes. Additionally, capacitance was significantly different between stretched and control bladders at 220 minutes in strain-matched control tissue. There were significant differences between stretched and control tissues at 20 or 60 minutes in all mouse strains, although the quality of the non-linear regression analysis is lower at these time points, as discussed above.

There was no significant change in capacitance in control, non-stretched tissue from each of the four strains over 5 hours (Figure A.3E). The differences among the strains were not significant (at $p < 0.05$) at any time point, as calculated by one-way analysis of variance with Bonferroni post-test.

Next, comparisons of capacitance in response to stretch were made among the strains (Figure A.3F). When the control tissue was stretched, there was an ~ 30% increase in capacitance over 5 hours. Bladder tissue lacking uroplakin II exhibited an ~ 24% increase, tissue

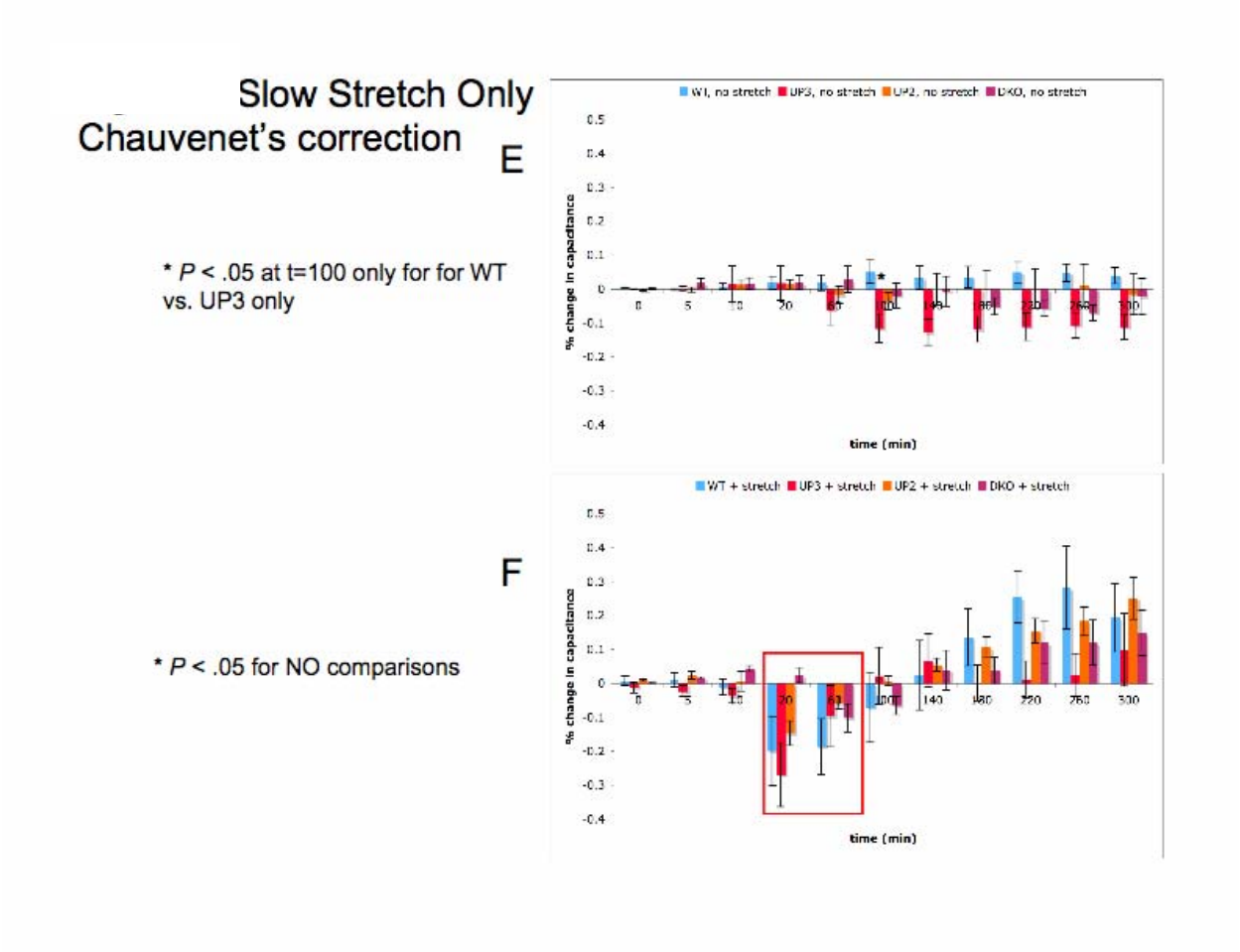

Figure A.3: Summary of control and stretch capacitance studies using control, UPII, UPIII, and UPII/UPIII knockout mouse bladders

UP knockout and control mouse bladders were mounted in Ussing stretching chambers and subjected to 5 h control unstretch (E) or stretch (F) treatments, as described in the methods. The red box indicates time points that were difficult to curve fit using the double exponential model due to decreased resistance values during stretch; these points had lower R^2 values than the others.

lacking uroplakin III increased by ~ 11%, and samples lacking both uroplakin II and III increased by ~ 14% at the 5 hour time point. Again, the differences among the strains were not significant (at $p < 0.05$) at any time point, as calculated by one-way analysis of variance with Bonferroni post-test. While the capacitance changes in response to stretch were not statistically significantly different among the strains, there is an apparent reduction in the surface area increase response in bladder tissue lacking uroplakin III and both uroplakin II/III proteins. This suggests that uroplakin III may have some role in facilitating fusiform vesicle membrane trafficking events, though the data indicate that these uroplakin proteins are not absolutely required for apical surface expansion.

While uroplakin KO mice appear to have increased permeability to water and urea, the capacitance studies suggest that a deficiency of uroplakin proteins does not significantly affect the ability of the apical surface to expand in the face of increased hydrostatic pressure, in contrast to results obtained from control mice (C57 strain) shown in Figure A.4. This suggests that the apparent small spherical vesicles that lack uroplakin proteins and underlie the apical membrane may still be competent for fusion with the apical surface to allow surface expansion. It is important to note that these small spherical vesicles are not unique to mice lacking uroplakin proteins. They also appear to be present in strain-matched control bladder tissue (see Figure 5 in [163]), in addition to the typical fusiform vesicles found below the apical umbrella cell surface. Perhaps the spherical vesicles represent a second type of membrane pool that is able to fuse with the apical surface upon stretch. Alternatively, it is possible that these are in fact fusiform vesicles simply oriented in a plane such that their fusiform shape is not appreciated.

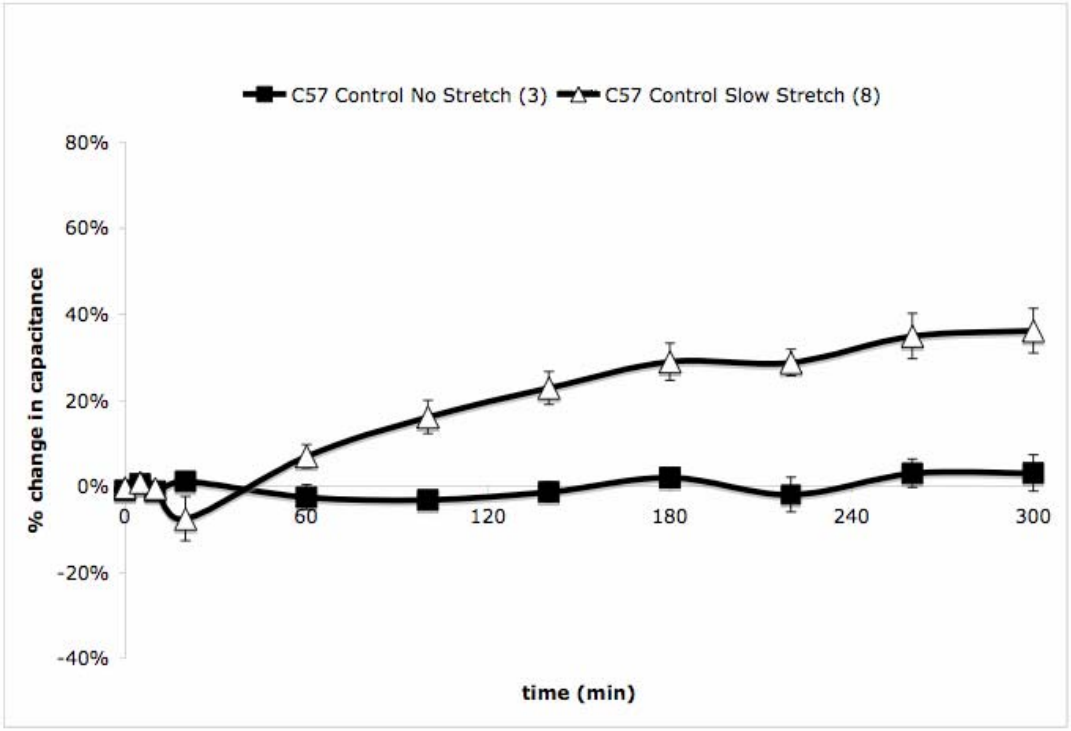

Figure A.4: Capacitance changes in C57 control mouse bladders

C57 control mouse bladders were mounted in Ussing stretching chambers and subjected to 5 h stretch or no stretch, as described in the methods.

APPENDIX B

DIFFERENTIAL TWO-DIMENSIONAL GEL ELECTROPHORESIS

Differential two-dimensional gel electrophoresis was performed to compare 5-h stretched rabbit bladder tissue lysates with that of unstretched control tissue, as described in the Methods section.

B.1 IDENTIFICATION OF GEL DIFFERENCES

Visual inspection of a two-frame looping QuickTime movie of the Cy3 and Cy5 gel images was performed to detect protein differences. The Cy3 and Cy5 images from a single gel are depicted in Figure B1.

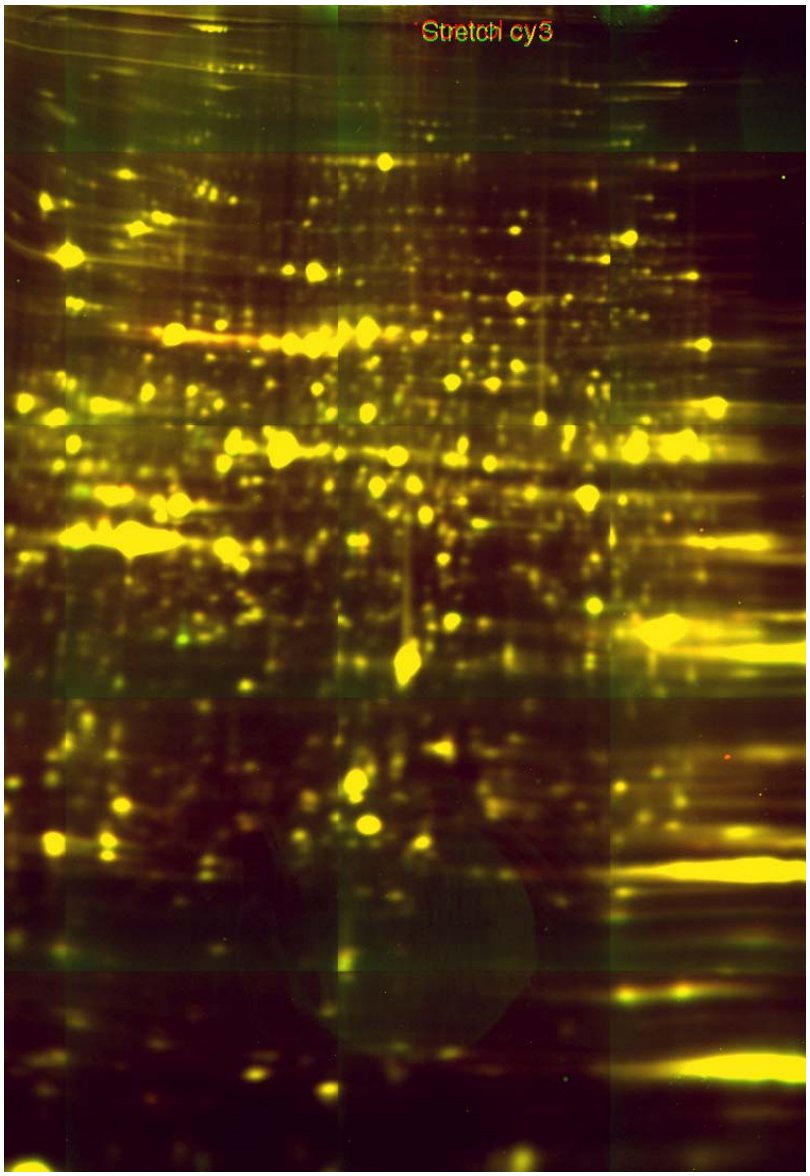

Figure B.1: Differential gel electrophoresis image

The two-dimensional gels comparing control unstretched protein lysate (Cy3, red) and stretched protein lysate (Cy5, green) were imaged, and the resulting images were overlayed such that matching proteins appear yellow and differences appear red or green, according to the sample in which they predominate.

B.2 PROTEIN IDENTIFICATION

MALDI-MS/MS analysis was performed by the University of Pittsburgh's Genomics and Proteomics Core Laboratory. The following proteins were identified as being up/down-regulated by 5 h stretch in rabbit uroepithelium (Table B.1).

Table B.1: Results of MALDI-MS/MS analysis of DIGE samples.
GPS Explorer TM Software (Applied Biosystems, Foster City, CA) was used to analyze the combined MS results. The Spot Label specifies the well containing the excised protein spot as numbered during the experiment. The protein mass and PI are used to match the protein identity with the original position of the excised spot in the gel. The # Peaks describes the number of peptide peaks used to match spectra. The Protein Score is calculated by the Mascot program (Matrix Science Inc., Boston, MA) using a probability-based implementation of the Mowse scoring algorithm. The score is reported as $-10*LOG_{10}(P)$, where P is the probability that the observed match is a random event, thus a high score indicates a confident identification. For scores that are significant (at $p < 0.05$), the percent sequence coverage of the matched protein identity is listed.

Spot Label	Protein Name	Accession Number	Protein MW	Protein PI	# Peaks	Protein Score	% Coverage
A1	ORF1 [Rattus sp.]	gi|2462658	942.4	5.3	1	12.9	
A10	PREDICTED: hypothetical protein [Pan troglodytes]	gi|114607928	10161.2	11.9	3	23.8	
A11	mutant NADH-cytochrome b5 reductase [Homo sapiens]	gi|40067426	6538.5	10.0	3	26.3	
A12	Chain E, Crystal Structure Of A New Rexinoid Bound To The Rxralpha Ligand Binding Doamin In The Rxr	gi|56965942	2363.3	8.6	3	36.9	
A13	CEP290 protein [Homo sapiens]	gi|14250413	19336.8	5.5	6	35.1	
A14	hCG38498, isoform CRA_d [Homo sapiens]	gi|119596676	6239.2	12.2	3	36.8	
A15	cationic trypsinogen [Homo sapiens]	gi|1616766	9199.9	9.5	1	28.6	
A16	ANA immunoglobulin heavy chain variable region [Mus musculus]	gi|41352115	13677.6	9.0	3	26.8	
A17	SMT3A protein [Homo sapiens]	gi|1770517	11703.8	5.9	4	31.4	
A18	SMT3A protein [Homo sapiens]	gi|1770517	11703.8	5.9	4	31.4	
A19	hypothetical protein LOC384198	gi|85702013	11790.1	9.7	4	35.1	

	[Mus musculus]						
A2	PREDICTED: hypothetical protein [Rattus norvegicus]	gi|109458423	7172.8	4.5	3	20.5	
A20	hypothetical protein LOC384198 [Mus musculus]	gi|85702013	11790.1	9.7	4	32.5	
A21	S-cone pigment gene/opsin [Aotus trivirgatus]	gi|4262108	2323.0	4.1	2	25.7	
A22	Unknown gene product [Homo sapiens]	gi|3417294	47882.9	9.1	8	41.8	
A23	immunoglobulin heavy chain variable region [Lama glama]	gi|83764228	12208.1	9.1	3	28.4	
A24	T-cell receptor V alpha chain 3 [Homo sapiens]	gi|6690320	3241.6	9.1	3	38.2	
A3	PREDICTED: similar to keratin 1 isoform 1 [Macaca mulatta]	gi|109096835	59017.2	6.9	7	66.9	10%
A4	unnamed protein product [Homo sapiens]	gi|22760270	26886.6	10.9	5	35.3	
A5	T-cell receptor beta chain [Homo sapiens]	gi|11527717	3750.9	8.2	2	23.8	
A6	T-cell receptor beta chain [Homo sapiens]	gi|11527717	3750.9	8.2	2	23.7	
A7	T-cell receptor beta chain [Homo sapiens]	gi|11527717	3750.9	8.2	2	23.3	
A8	PREDICTED: similar to ATP-binding cassette, sub-family F (GCN20), member 2 [Mus musculus]	gi|94394836	12151.3	9.0	4	29.2	
A9	PREDICTED: hypothetical protein [Bos taurus]	gi|119921319	4403.0	4.4	2	24.5	
B1	unnamed protein product [Macaca fascicularis]	gi|90079261	4562.5	10.3	3	30.4	
B10	hCG2033193 [Homo sapiens]	gi|119587815	13504.8	8.6	5	41.9	
B12	PREDICTED: similar to Glyceraldehyde-3-phosphate dehydrogenase (GAPDH) [Canis familiaris]	gi|74007414	37618.8	7.2	3	35.7	
B13	40S ribosomal protein S20 [Sus scrofa]	gi|45269031	11947.6	10.2	7	44.5	
B15	PREDICTED: similar to N-acetylglucosamine-1-phosphotransferase, gamma subunit, partial [Macaca mula	gi|109129603	11398.0	7.2	4	36.1	
B16	PREDICTED: similar to autism susceptibility candidate 2 [Rattus norvegicus]	gi|109495660	34131.0	10.8	6	32.2	
B17	Unknown (protein for IMAGE:3950510) [Homo sapiens]	gi|116283316	38192.3	8.0	6	29.9	
B18	unnamed protein product [Macaca fascicularis]	gi|90081036	2907.6	10.0	3	29.1	
B19	MHC class II beta chain [Otolemur garnettii]	gi|3980181	10746.3	7.9	4	38.6	
B2	Glycogen phosphorylase, brain form	gi|1730559	96854.4	6.2	4	45.1	
B20	GRAF [Homo sapiens]	gi|20198950	5859.0	6.0	3	31.5	
B21	hCG2033193 [Homo sapiens]	gi|119587815	13504.8	8.6	5	41.9	
B22	type 2A protein phosphatase catalytic subunit [Canis familiaris]	gi|50978726	36183.6	5.3	5	56.8	
B23	argininosuccinate synthetase	gi|553871	13487.8	5.3	4	33.6	
B24	argininosuccinate synthetase	gi|553871	13487.8	5.3	4	44.7	
B3	PREDICTED: similar to ribosomal protein L14 [Rattus	gi|109499636	22920.7	11.0	7	31.9	

	norvegicus]						
B4	hCG2033193 [Homo sapiens]	gi|119587815	13504.8	8.6	5	41.9	
B5	hCG2033193 [Homo sapiens]	gi|119587815	13504.8	8.6	5	42.2	
B6	hCG2033193 [Homo sapiens]	gi|119587815	13504.8	8.6	5	42.5	
B9	hCG2033193 [Homo sapiens]	gi|119587815	13504.8	8.6	4	32.7	
C1	PREDICTED: similar to GTPase activating protein testicular GAP1 [Rattus norvegicus]	gi|109515215	5276.6	5.1	3	29.8	
C10	hCG2033193 [Homo sapiens]	gi|119587815	13504.8	8.6	5	42.8	
C11	PREDICTED: similar to THAP domain containing 11 isoform 2 [Bos taurus]	gi|76640192	33737.1	9.0	5	24.5	
C12	hCG2033193 [Homo sapiens]	gi|119587815	13504.8	8.6	5	43.1	
C13	MHC class II beta chain [Otolemur garnettii]	gi|3980181	10746.3	7.9	4	38.0	
C14	hCG2033193 [Homo sapiens]	gi|119587815	13504.8	8.6	5	41.8	
C15	hCG2033193 [Homo sapiens]	gi|119587815	13504.8	8.6	4	32.5	
C16	hCG2033193 [Homo sapiens]	gi|119587815	13504.8	8.6	4	32.7	
C17	PREDICTED: similar to KRT8 protein isoform 1 [Pan troglodytes]	gi|114620283	30761.3	4.8	2	37.4	
C18	unnamed protein product [Mus musculus]	gi|74177777	54545.5	5.8	5	70.3	12%
C19	PREDICTED: similar to keratin 10 isoform 2 [Pan troglodytes]	gi|114667513	56862.9	5.1	4	63.5	
C2	Aldehyde dehydrogenase, cytosolic 2 (ALDH class 1) (Non-lens ALDH1) (ALDH1-NL)	gi|2494067	26840.5	7.7	3	45.2	
C20	PREDICTED: similar to Nuclear envelope pore membrane protein POM 121 (Pore membrane protein of 121	gi|113416611	38545.5	9.7	5	29.7	
C21	hCG2033193 [Homo sapiens]	gi|119587815	13504.8	8.6	5	42.2	
C22	hCG2033193 [Homo sapiens]	gi|119587815	13504.8	8.6	5	43.1	
C23	unnamed protein product [Macaca fascicularis]	gi|90081036	2907.6	10.0	3	28.9	
C24	PREDICTED: similar to macrophage actin-associated-tyrosine-phosphorylated protein [Bos taurus]	gi|119916336	39184.4	8.5	5	24.8	
C3	hCG2033193 [Homo sapiens]	gi|119587815	13504.8	8.6	4	32.5	
C4	PREDICTED: hypothetical protein [Mus musculus]	gi|94405917	9470.2	11.2	5	37.8	
C5	p14ARF protein [Ateles fusciceps]	gi|18642362	6200.5	12.1	3	30.8	
C6	hCG2033193 [Homo sapiens]	gi|119587815	13504.8	8.6	4	32.5	
C7	PREDICTED: hypothetical protein [Pan troglodytes]	gi|114623845	9316.7	6.8	4	34.1	
C8	hCG2033193 [Homo sapiens]	gi|119587815	13504.8	8.6	5	41.9	
C9	hCG2033193 [Homo sapiens]	gi|119587815	13504.8	8.6	5	43.1	
D1	tryptophan rich basic protein, isoform CRA_d [Homo sapiens]	gi|119630053	14018.3	9.4	4	26.2	
D10	unnamed protein product [Macaca fascicularis]	gi|90081036	2907.6	10.0	3	28.0	
D11	PREDICTED: similar to NADH dehydrogenase (ubiquinone) 1 alpha subcomplex, 2, 8kDa isoform 1 [Macaca	gi|109078941	11360.0	10.1	3	27.1	
D12	immunoglobulin heavy chain variable region [Homo sapiens]	gi|112699781	11109.4	8.6	3	37.2	
D13	Chain A, Solution Structure Of The Third Ig-Like Domain Of	gi|118137533	11074.5	6.9	4	31.9	

	Human Kiaa1556 Protein						
D14	PREDICTED: hypothetical protein [Pan troglodytes]	gi|114623845	9316.7	6.8	3	29.7	
D15	peptidyl arginine deiminase type IV [Homo sapiens]	gi|50299753	11066.8	9.2	3	24.1	
D16	PREDICTED: similar to acyl-Coenzyme A dehydrogenase family, member 9 isoform 2 [Canis familiaris]	gi|73984512	16068.3	8.9	5	34.1	
D17	neuronatin [Bos taurus]	gi|30315674	6158.4	11.3	4	43.2	
D18	PREDICTED: hypothetical protein [Macaca mulatta]	gi|109066762	5819.1	10.4	4	37.7	
D19	PREDICTED: similar to Gamma-aminobutyric-acid receptor alpha-3 subunit precursor (GABA(A) receptor)	gi|114691162	7969.1	8.9	3	28.2	
D2	PREDICTED: similar to TGFB-induced factor 2 [Rattus norvegicus]	gi|109469118	22056.4	7.8	5	36.6	
D20	Chain A, Solution Structure Of Rna Binding Domain In Hypothetical Protein Loc91801	gi|83754752	12304.3	8.8	3	29.0	
D21	EndoA' cytokeratin (5' end put.); putative	gi|309215	53209.7	5.4	3	40.4	
D22	keratin type II	gi|511654	54277.3	5.4	5	82.2	12%
D23	Ig heavy chain V region [Mus musculus]	gi|2606047	4668.4	9.5	3	40.1	
D24	cytokeratin 18 [Oryctolagus cuniculus]	gi|21217434	13263.8	4.5	4	34.1	
D3	PREDICTED: cytosolic malic enzyme 1 isoform 1 [Macaca mulatta]	gi|109071882	51423.8	8.0	4	49.3	
D4	PREDICTED: cytosolic malic enzyme 1 isoform 1 [Macaca mulatta]	gi|109071882	51423.8	8.0	3	37.9	
D5	unnamed protein product [Macaca fascicularis]	gi|9280281	10107.4	10.1	3	23.2	
D6	hCG2033193 [Homo sapiens]	gi|119587815	13504.8	8.6	4	33.2	
D7	Chain A, Crystal Structure Of A Human Malic Enzyme	gi|78101464	60778.4	5.6	4	120.0	12%
D8	PREDICTED: cytosolic malic enzyme 1 isoform 1 [Macaca mulatta]	gi|109071882	51423.8	8.0	4	95.3	13%
D9	hCG2045847 [Homo sapiens]	gi|119631741	5450.3	12.7	4	34.2	
E1	PREDICTED: similar to Actin, cytoplasmic 1 (Beta-actin 1) [Canis familiaris]	gi|57043600	42231.9	5.3	6	60.5	
E10	PREDICTED: GrpE-like 2, mitochondrial (E. coli) [Macaca mulatta]	gi|109079280	25691.5	8.2	5	31.1	
E11	PREDICTED: GrpE-like 2, mitochondrial (E. coli) [Macaca mulatta]	gi|109079280	25691.5	8.2	5	31.3	
E12	Hypothetical protein MGC16384 [Homo sapiens]	gi|14550486	5350.8	12.0	3	35.4	
E13	PREDICTED: hypothetical protein [Mus musculus]	gi|94386124	21171.4	12.1	6	48.0	
E14	PREDICTED: hypothetical protein [Mus musculus]	gi|94386124	21171.4	12.1	5	34.6	
E15	T-cell receptor beta chain [Homo sapiens]	gi|4028212	4884.7	12.3	3	26.0	
E16	PREDICTED: similar to ribosomal protein L14 [Rattus	gi|109499636	22920.7	11.0	7	37.1	

	norvegicus]						
E17	peroxisomal Ca-dependent solute carrier [Oryctolagus cuniculus]	gi|2352427	53200.4	6.9	5	122.0	13%
E18	peroxisomal Ca-dependent solute carrier [Oryctolagus cuniculus]	gi|2352427	53200.4	6.9	4	74.9	16%
E19	unnamed protein product [Macaca fascicularis]	gi|90081036	2907.6	10.0	4	44.0	
E2	PREDICTED: similar to Actin, cytoplasmic 1 (Beta-actin 1) [Canis familiaris]	gi|57043600	42231.9	5.3	5	86.0	12%
E20	unnamed protein product [Macaca fascicularis]	gi|90081036	2907.6	10.0	3	31.1	
E21	Annexin A1 (Annexin I) (Lipocortin I) (Calpactin II) (Chromobindin-9) (p35) (Phospholipase A2 inhib	gi|1703316	38996.1	6.3	3	83.7	17%
E22	Chain B, Solution Structure Of The C-Terminal Domain Of Human Rpa32 Complexed With Ung2(73-88)	gi|11513779	1820.1	12.5	2	23.8	
E23	Retinal dehydrogenase 1 (RalDH1) (RALDH 1) (Aldehyde dehydrogenase family 1 member A1) (Aldehyde de	gi|42558920	54933.0	7.0	3	51.5	
E24	PREDICTED: hypothetical protein [Bos taurus]	gi|119891359	16889.4	4.9	4	28.4	
E3	KRT8 protein [Homo sapiens]	gi|62913980	41082.7	4.9	7	109.0	20%
E4	KRT8 protein [Homo sapiens]	gi|62913980	41082.7	4.9	7	132.0	20%
E5	Serum albumin precursor	gi|44889024	70861.0	5.9	5	43.6	
E6	Serum albumin precursor	gi|44889024	70861.0	5.9	5	56.7	
E7	Liver carboxylesterase 2	gi|462025	59248.8	5.7	4	51.4	
E8	Liver carboxylesterase 2	gi|462025	59248.8	5.7	4	49.7	
E9	hCG2033193 [Homo sapiens]	gi|119587815	13504.8	8.6	4	32.5	
F1	PREDICTED: similar to THAP domain protein 1 isoform 1 [Canis familiaris]	gi|57097749	21721.9	9.2	4	28.3	
F10	Aldo-keto reductase family 1 member C4 (Chlordecone reductase) (CDR) (3-alpha-hydroxysteroid dehydr	gi|67460579	37492.2	7.1	5	47.5	
F11	Ppp2cb protein [Mus musculus]	gi|17512397	32550.9	5.5	5	144.0	23%
F12	type 2A protein phosphatase catalytic subunit [Canis familiaris]	gi|50978726	36183.6	5.3	6	178.0	23%
F13	Annexin A8 (Annexin VIII)	gi|75069379	36941.6	5.5	4	43.4	
F14	Annexin A8 (Annexin VIII)	gi|75069379	36941.6	5.5	6	45.0	
F15	unnamed protein product [Mus musculus]	gi|74139512	36474.6	5.6	3	35.9	
F16	unnamed protein product [Mus musculus]	gi|74151637	20048.4	7.8	3	63.9	
F17	26S proteasome p40.5 subunit [Bos taurus]	gi|66792850	43124.2	5.4	5	157.0	23%
F18	26S proteasome p40.5 subunit [Bos taurus]	gi|66792850	43124.2	5.4	5	171.0	23%
F19	unnamed protein product [Macaca fascicularis]	gi|90084567	4188.0	9.2	3	31.7	
F2	PREDICTED: similar to GTPase activating protein testicular GAP1 [Rattus norvegicus]	gi|109515215	5276.6	5.1	3	30.2	
F20	unnamed protein product [Macaca fascicularis]	gi|90081036	2907.6	10.0	3	28.1	
F21	PREDICTED: similar to guanylate binding protein family,	gi|109009942	17375.8	9.3	5	27.6	

	member 6 [Macaca mulatta]						
F22	PREDICTED: hypothetical protein [Mus musculus]	gi|94405917	9470.2	11.2	4	29.6	
F23	PREDICTED: similar to Histone H1.2 (H1d) [Macaca mulatta]	gi|109069925	22314.3	11.0	6	25.2	
F24	aldolase A [Ovis aries]	gi|7331107	15432.0	7.0	3	25.7	
F3	MHC class II antigen beta chain [Aotus nancymaae]	gi|78172278	10406.0	5.1	3	28.3	
F4	protein kinase C alpha isoform [Canis familiaris]	gi|3818626	5618.9	10.0	3	29.5	
F5	putative protein product of HMFT2263 [Homo sapiens]	gi|51555812	5686.0	4.6	3	34.6	
F6	unnamed protein product [Mus musculus]	gi|26337401	31028.8	7.6	5	33.2	
F7	PREDICTED: aldo-keto reductase family 1, member C4 isoform 5 [Pan troglodytes]	gi|114629172	37552.2	6.5	5	48.5	
F8	PREDICTED: similar to guanylate binding protein family, member 6 [Macaca mulatta]	gi|109009942	17375.8	9.3	6	40.6	
F9	PREDICTED: similar to GEM-interacting protein (GMIP), partial [Macaca mulatta]	gi|109139720	6949.4	4.4	3	28.1	

BIBLIOGRAPHY

1. Lavelle, J., Meyers, S., Ramage, R., Bastacky, S., Doty, D., Apodaca, G., and Zeidel, M.L. (2002). Bladder permeability barrier: recovery from selective injury of surface epithelial cells. Am J Physiol Renal Physiol *283*, F242-253.

2. Birder, L.A. (2005). More than just a barrier: urothelium as a drug target for urinary bladder pain. Am J Physiol Renal Physiol *289*, F489-495.

3. Lavelle, J.P., Meyers, S.A., Ruiz, W.G., Buffington, C.A., Zeidel, M.L., and Apodaca, G. (2000). Urothelial pathophysiological changes in feline interstitial cystitis: a human model. Am J Physiol Renal Physiol *278*, F540-553.

4. Netter, F.H. (2002). Atlas of Human Anatomy, Third Edition, (Philadelphia, PA: Saunders).

5. Sadler, T.W. (2006). Langman's Medical Embryology, 10th Edition Edition, (Philadelphia, PA: Lippincott Williams & Wilkins).

6. Redman, J. (2001). Anatomy of the urogenital tract, (New York, NY: McGraw-Hill).

7. de Groat, W.C., and Yoshimura, N. (2001). Pharmacology of the lower urinary tract. Annu Rev Pharmacol Toxicol *41*, 691-721.

8. Williamson-Kirkland (1980). Neurological aspect of rehabilitation. In University of Washington orthopaedic resident lecture series. (Seattle: University of Washington).

9. Andersson, K.E. (2002). Bladder activation: afferent mechanisms. Urology *59*, 43-50.

10. Gabella, G., and Davis, C. (1998). Distribution of afferent axons in the bladder of rats. Journal of neurocytology *27*, 141-155.

11. Wiseman, O.J., Fowler, C.J., and Landon, D.N. (2003). The role of the human bladder lamina propria myofibroblast. BJU Int *91*, 89-93.

12. Apodaca, G. (2004). The uroepithelium: not just a passive barrier. Traffic (Copenhagen, Denmark) *5*, 117-128.

13. Lewis, S.A. (2000). Everything you wanted to know about the bladder epithelium but were afraid to ask. Am J Physiol Renal Physiol *278*, F867-874.

14. Staehelin, L.A., Chlapowski, F.J., and Bonneville, M.A. (1972). Lumenal plasma membrane of the urinary bladder. I. Three-dimensional reconstruction from freeze-etch images. J Cell Biol *53*, 73-91.

15. Deng, F.M., Liang, F.X., Tu, L., Resing, K.A., Hu, P., Supino, M., Hu, C.C., Zhou, G., Ding, M., Kreibich, G., et al. (2002). Uroplakin IIIb, a urothelial differentiation marker, dimerizes with uroplakin Ib as an early step of urothelial plaque assembly. J Cell Biol *159*, 685-694.

16. Wu, X.R., Lin, J.H., Walz, T., Haner, M., Yu, J., Aebi, U., and Sun, T.T. (1994). Mammalian uroplakins. A group of highly conserved urothelial differentiation-related membrane proteins. J Biol Chem *269*, 13716-13724.

17. Tu, L., Sun, T.T., and Kreibich, G. (2002). Specific heterodimer formation is a prerequisite for uroplakins to exit from the endoplasmic reticulum. Mol Biol Cell *13*, 4221-4230.

18. Hu, C.C., Liang, F.X., Zhou, G., Tu, L., Tang, C.H., Zhou, J., Kreibich, G., and Sun, T.T. (2005). Assembly of urothelial plaques: tetraspanin function in membrane protein trafficking. Mol Biol Cell *16*, 3937-3950.

19. Min, G., Wang, H., Sun, T.T., and Kong, X.P. (2006). Structural basis for tetraspanin functions as revealed by the cryo-EM structure of uroplakin complexes at 6-A resolution. J Cell Biol *173*, 975-983.

20. Hicks, R.M., Ketterer, B., and Warren, R.C. (1974). The ultrastructure and chemistry of the luminal plasma membrane of the mammalian urinary bladder: a structure with low permeability to water and ions. Philos Trans R Soc Lond B Biol Sci *268*, 23-38.

21. Hu, P., Deng, F.M., Liang, F.X., Hu, C.M., Auerbach, A.B., Shapiro, E., Wu, X.R., Kachar, B., and Sun, T.T. (2000). Ablation of uroplakin III gene results in small urothelial plaques, urothelial leakage, and vesicoureteral reflux. J Cell Biol *151*, 961-972.

22. Wu, X.R., and Sun, T.T. (1993). Molecular cloning of a 47 kDa tissue-specific and differentiation-dependent urothelial cell surface glycoprotein. Journal of cell science *106 (Pt 1)*, 31-43.

23. Born, M., Pahner, I., Ahnert-Hilger, G., and Jons, T. (2003). The maintenance of the permeability barrier of bladder facet cells requires a continuous fusion of discoid vesicles with the apical plasma membrane. European journal of cell biology *82*, 343-350.

24. Chen, Y., Guo, X., Deng, F.M., Liang, F.X., Sun, W., Ren, M., Izumi, T., Sabatini, D.D., Sun, T.T., and Kreibich, G. (2003). Rab27b is associated with fusiform vesicles and may be involved in targeting uroplakins to urothelial apical membranes. Proceedings of the National Academy of Sciences of the United States of America *100*, 14012-14017.

25. Veranic, P., Romih, R., and Jezernik, K. (2004). What determines differentiation of urothelial umbrella cells? European journal of cell biology *83*, 27-34.

26. Acharya, P., Beckel, J., Ruiz, W.G., Wang, E., Rojas, R., Birder, L., and Apodaca, G. (2004). Distribution of the tight junction proteins ZO-1, occludin, and claudin-4, -8, and -12 in bladder epithelium. Am J Physiol Renal Physiol *287*, F305-318.

27. Taylor, J. (1982). Introduction to Error Analysis: The Study of Uncertainties in Physical Measurements, (New York, NY: University Science Books).

28. Negrete, H.O., Lavelle, J.P., Berg, J., Lewis, S.A., and Zeidel, M.L. (1996). Permeability properties of the intact mammalian bladder epithelium. Am J Physiol *271*, F886-894.

29. Chang, A., Hammond, T.G., Sun, T.T., and Zeidel, M.L. (1994). Permeability properties of the mammalian bladder apical membrane. Am J Physiol *267*, C1483-1492.

30. Buckley, M., Xin, P., Washington, S., Herb, N., Erickson, D., and Bhavanandan, V.P. (2000). Lectin histochemical examination of rabbit bladder glycoproteins and characterization of a mucin isolated from the bladder mucosa. Arch Biochem Biophys *375*, 270-277.

31. Hirao, Y., Izumi, K., and Oyasu, R. (1980). The effect of normal rat urine on mucosal regeneration in heterotopic urinary bladder. Lab Invest *42*, 76-84.

32. Chodak, G.W., Shing, Y., Borge, M., Judge, S.M., and Klagsbrun, M. (1986). Presence of heparin binding growth factor in mouse bladder tumors and urine from mice with bladder cancer. Cancer Res *46*, 5507-5510.

33. Hayashi, O., Noguchi, S., and Oyasu, R. (1987). Transferrin as a growth factor for rat bladder carcinoma cells in culture. Cancer Res *47*, 4560-4564.

34. Nguyen, M., Watanabe, H., Budson, A.E., Richie, J.P., and Folkman, J. (1993). Elevated levels of the angiogenic peptide basic fibroblast growth factor in urine of bladder cancer patients. Journal of the National Cancer Institute *85*, 241-242.

35. Yura, Y., Hayashi, O., Kelly, M., and Oyasu, R. (1989). Identification of epidermal growth factor as a component of the rat urinary bladder tumor-enhancing urinary fractions. Cancer Res *49*, 1548-1553.

36. Fisher, D.A., Salido, E.C., and Barajas, L. (1989). Epidermal growth factor and the kidney. Annu Rev Physiol *51*, 67-80.

37. Birder, L.A., Apodaca, G., De Groat, W.C., and Kanai, A.J. (1998). Adrenergic- and capsaicin-evoked nitric oxide release from urothelium and afferent nerves in urinary bladder. Am J Physiol *275*, F226-229.

38. Burnstock, G. (2001). Purine-mediated signalling in pain and visceral perception. Trends in pharmacological sciences *22*, 182-188.

39. Chess-Williams, R. (2004). Potential therapeutic targets for the treatment of detrusor overactivity. Expert opinion on therapeutic targets *8*, 95-106.

40. Ferguson, D.R., Kennedy, I., and Burton, T.J. (1997). ATP is released from rabbit urinary bladder epithelial cells by hydrostatic pressure changes--a possible sensory mechanism? The Journal of physiology *505 (Pt 2)*, 503-511.

41. Wang, E.C., Lee, J.M., Ruiz, W.G., Balestreire, E.M., von Bodungen, M., Barrick, S., Cockayne, D.A., Birder, L.A., and Apodaca, G. (2005). ATP and purinergic receptor-dependent membrane traffic in bladder umbrella cells. J Clin Invest *115*, 2412-2422.

42. Yu, W., Zacharia, L.C., Jackson, E.K., and Apodaca, G. (2006). Adenosine Receptor Expression and Function in Bladder Uroepithelium. Am J Physiol Cell Physiol.

43. Messing, E.M. (1990). Clinical implications of the expression of epidermal growth factor receptors in human transitional cell carcinoma. Cancer Res *50*, 2530-2537.

44. Bradbury, N.A., and Bridges, R.J. (1994). Role of membrane trafficking in plasma membrane solute transport. Am J Physiol *267*, C1-24.

45. Pandita, R.K., and Andersson, K.E. (2002). Intravesical adenosine triphosphate stimulates the micturition reflex in awake, freely moving rats. J Urol *168*, 1230-1234.

46. Hawthorn, M.H., Chapple, C.R., Cock, M., and Chess-Williams, R. (2000). Urothelium-derived inhibitory factor(s) influences on detrusor muscle contractility in vitro. British journal of pharmacology *129*, 416-419.

47. Truschel, S.T., Wang, E., Ruiz, W.G., Leung, S.M., Rojas, R., Lavelle, J., Zeidel, M., Stoffer, D., and Apodaca, G. (2002). Stretch-regulated exocytosis/endocytosis in bladder umbrella cells. Mol Biol Cell *13*, 830-846.

48. Sakakibara, K., Sato, K., Yoshino, K., Oshiro, N., Hirahara, S., Mahbub Hasan, A.K., Iwasaki, T., Ueda, Y., Iwao, Y., Yonezawa, K., et al. (2005). Molecular identification and characterization of Xenopus egg uroplakin III, an egg raft-associated transmembrane protein that is tyrosine-phosphorylated upon fertilization. J Biol Chem *280*, 15029-15037.

49. Takahashi, M., Ishida, T., Traub, O., Corson, M.A., and Berk, B.C. (1997). Mechanotransduction in endothelial cells: temporal signaling events in response to shear stress. J Vasc Res *34*, 212-219.

50. Alexander, L.D., Alagarsamy, S., and Douglas, J.G. (2004). Cyclic stretch-induced cPLA2 mediates ERK 1/2 signaling in rabbit proximal tubule cells. Kidney Int *65*, 551-563.

51. Apodaca, G. (2002). Modulation of membrane traffic by mechanical stimuli. Am J Physiol Renal Physiol *282*, F179-190.

52. Huang, H., Kamm, R.D., and Lee, R.T. (2004). Cell mechanics and mechanotransduction: pathways, probes, and physiology. Am J Physiol Cell Physiol *287*, C1-11.

53. Lewis, S.A., and de Moura, J.L. (1984). Apical membrane area of rabbit urinary bladder increases by fusion of intracellular vesicles: an electrophysiological study. J Membr Biol *82*, 123-136.

54. Amano, O., Kataoka, S., and Yamamoto, T.Y. (1988). Derivation and termination of fusiform vesicles in the transitional epithelium of the rat urinary bladder. The Tohoku journal of experimental medicine *156*, 417-418.

55. Hicks, R.M. (1966). The function of the golgi complex in transitional epithelium. Synthesis of the thick cell membrane. J Cell Biol *30*, 623-643.

56. Lewis, S.A., and de Moura, J.L. (1982). Incorporation of cytoplasmic vesicles into apical membrane of mammalian urinary bladder epithelium. Nature *297*, 685-688.

57. Minsky, B.D., and Chlapowski, F.J. (1978). Morphometric analysis of the translocation of lumenal membrane between cytoplasm and cell surface of transitional epithelial cells during the expansion-contraction cycles of mammalian urinary bladder. J Cell Biol *77*, 685-697.

58. Wang, E., Truschel, S., and Apodaca, G. (2003). Analysis of hydrostatic pressure-induced changes in umbrella cell surface area. Methods *30*, 207-217.

59. Levin, R.M., and Wein, A.J. (1982). Response of the in vitro whole bladder (rabbit) preparation to autonomic agonists. J Urol *128*, 1087-1090.

60. Kerr, D.E., Liang, F., Bondioli, K.R., Zhao, H., Kreibich, G., Wall, R.J., and Sun, T.T. (1998). The bladder as a bioreactor: urothelium production and secretion of growth hormone into urine. Nature biotechnology *16*, 75-79.

61. Deng, F.M., Ding, M., Lavker, R.M., and Sun, T.T. (2001). Urothelial function reconsidered: a role in urinary protein secretion. Proceedings of the National Academy of Sciences of the United States of America *98*, 154-159.

62. Apodaca, G. (2001). Endocytic traffic in polarized epithelial cells: role of the actin and microtubule cytoskeleton. Traffic (Copenhagen, Denmark) *2*, 149-159.

63. Gottlieb, T.A., Ivanov, I.E., Adesnik, M., and Sabatini, D.D. (1993). Actin microfilaments play a critical role in endocytosis at the apical but not the basolateral surface of polarized epithelial cells. J Cell Biol *120*, 695-710.

64. Valentijn, K., Valentijn, J.A., and Jamieson, J.D. (1999). Role of actin in regulated exocytosis and compensatory membrane retrieval: insights from an old acquaintance. Biochem Biophys Res Commun *266*, 652-661.

65. Sarikas, S.N., and Chlapowski, F.J. (1989). The effect of thioglycolate on intermediate filaments and membrane translocation in rat urothelium during the expansion-contraction cycle. Cell and tissue research *258*, 393-401.

66. Lewis, S.A., and Lewis, J.R. (2006). Kinetics of urothelial ATP release. Am J Physiol Renal Physiol *291*, F332-340.

67. Alberts, B. (2002). Molecular biology of the cell, 4th Edition, (New York: Garland Science).

68. Birder, L.A., Ruan, H.Z., Chopra, B., Xiang, Z., Barrick, S., Buffington, C.A., Roppolo, J.R., Ford, A.P., de Groat, W.C., and Burnstock, G. (2004). Alterations in P2X and P2Y purinergic receptor expression in urinary bladder from normal cats and cats with interstitial cystitis. Am J Physiol Renal Physiol *287*, F1084-1091.

69. Birder, L.A., Barrick, S.R., Roppolo, J.R., Kanai, A.J., de Groat, W.C., Kiss, S., and Buffington, C.A. (2003). Feline interstitial cystitis results in mechanical hypersensitivity and altered ATP release from bladder urothelium. Am J Physiol Renal Physiol *285*, F423-429.

70. Keay, S., Kleinberg, M., Zhang, C.O., Hise, M.K., and Warren, J.W. (2000). Bladder epithelial cells from patients with interstitial cystitis produce an inhibitor of heparin-binding epidermal growth factor-like growth factor production. J Urol *164*, 2112-2118.

71. Tominaga, M., Wada, M., and Masu, M. (2001). Potentiation of capsaicin receptor activity by metabotropic ATP receptors as a possible mechanism for ATP-evoked pain and hyperalgesia. Proceedings of the National Academy of Sciences of the United States of America *98*, 6951-6956.

72. Bishop, B.L., Duncan, M.J., Song, J., Li, G., Zaas, D., and Abraham, S.N. (2007). Cyclic AMP-regulated exocytosis of Escherichia coli from infected bladder epithelial cells. Nature medicine *13*, 625-630.

73. Zhou, G., Mo, W.J., Sebbel, P., Min, G., Neubert, T.A., Glockshuber, R., Wu, X.R., Sun, T.T., and Kong, X.P. (2001). Uroplakin Ia is the urothelial receptor for uropathogenic Escherichia coli: evidence from in vitro FimH binding. Journal of cell science *114*, 4095-4103.

74. Balestreire, E.M., and Apodaca, G. (2007). Apical epidermal growth factor receptor signaling: regulation of stretch-dependent exocytosis in bladder umbrella cells. Mol Biol Cell *18*, 1312-1323.

75. Karnaky, K.J., Jr. (1998). Regulating epithelia from the apical side: new insights. Focus on "Differential signaling and regulation of apical vs. basolateral EGFR in polarized epithelial cells". Am J Physiol *275*, C1417-1418.

76. Tschumperlin, D.J., Dai, G., Maly, I.V., Kikuchi, T., Laiho, L.H., McVittie, A.K., Haley, K.J., Lilly, C.M., So, P.T., Lauffenburger, D.A., et al. (2004). Mechanotransduction through growth-factor shedding into the extracellular space. Nature *429*, 83-86.

77. Holbro, T., and Hynes, N.E. (2004). ErbB receptors: directing key signaling networks throughout life. Annu Rev Pharmacol Toxicol *44*, 195-217.

78. Barbieri, M.A., Roberts, R.L., Gumusboga, A., Highfield, H., Alvarez-Dominguez, C., Wells, A., and Stahl, P.D. (2000). Epidermal growth factor and membrane trafficking. EGF receptor activation of endocytosis requires Rab5a. J Cell Biol *151*, 539-550.

79. Harris, R.C., Chung, E., and Coffey, R.J. (2003). EGF receptor ligands. Exp Cell Res *284*, 2-13.

80. Singh, A.B., and Harris, R.C. (2005). Autocrine, paracrine and juxtacrine signaling by EGFR ligands. Cell Signal *17*, 1183-1193.

81. Olayioye, M.A., Neve, R.M., Lane, H.A., and Hynes, N.E. (2000). The ErbB signaling network: receptor heterodimerization in development and cancer. Embo J *19*, 3159-3167.

82. Pearson, G., Robinson, F., Beers Gibson, T., Xu, B.E., Karandikar, M., Berman, K., and Cobb, M.H. (2001). Mitogen-activated protein (MAP) kinase pathways: regulation and physiological functions. Endocr Rev *22*, 153-183.

83. Wiley, L.M., Wu, J.X., Harari, I., and Adamson, E.D. (1992). Epidermal growth factor receptor mRNA and protein increase after the four-cell preimplantation stage in murine development. Dev Biol *149*, 247-260.

84. Gonnella, P.A., Siminoski, K., Murphy, R.A., and Neutra, M.R. (1987). Transepithelial transport of epidermal growth factor by absorptive cells of suckling rat ileum. J Clin Invest *80*, 22-32.

85. Chen, M.C., Solomon, T.E., Kui, R., and Soll, A.H. (2002). Apical EGF receptors regulate epithelial barrier to gastric acid: endogenous TGF-alpha is an essential facilitator. Am J Physiol Gastrointest Liver Physiol *283*, G1098-1106.

86. Kuwada, S.K., Lund, K.A., Li, X.F., Cliften, P., Amsler, K., Opresko, L.K., and Wiley, H.S. (1998). Differential signaling and regulation of apical vs. basolateral EGFR in polarized epithelial cells. Am J Physiol *275*, C1419-1428.

87. Chow, N.H., Liu, H.S., Yang, H.B., Chan, S.H., and Su, I.J. (1997). Expression patterns of erbB receptor family in normal urothelium and transitional cell carcinoma. An immunohistochemical study. Virchows Arch *430*, 461-466.

88. Rotterud, R., Nesland, J.M., Berner, A., and Fossa, S.D. (2005). Expression of the epidermal growth factor receptor family in normal and malignant urothelium. BJU Int *95*, 1344-1350.

89. Mellon, J.K., Cook, S., Chambers, P., and Neal, D.E. (1996). Transforming growth factor alpha and epidermal growth factor levels in bladder cancer and their relationship to epidermal growth factor receptor. Br J Cancer *73*, 654-658.

90. Freeman, M.R., Yoo, J.J., Raab, G., Soker, S., Adam, R.M., Schneck, F.X., Renshaw, A.A., Klagsbrun, M., and Atala, A. (1997). Heparin-binding EGF-like growth factor is an autocrine growth factor for human urothelial cells and is synthesized by epithelial and smooth muscle cells in the human bladder. J Clin Invest *99*, 1028-1036.

91. Rezzonico, R., Cayatte, C., Bourget-Ponzio, I., Romey, G., Belhacene, N., Loubat, A., Rocchi, S., Van Obberghen, E., Girault, J.A., Rossi, B., et al. (2003). Focal adhesion kinase pp125FAK interacts with the large conductance calcium-activated hSlo potassium channel in human osteoblasts: potential role in mechanotransduction. J Bone Miner Res *18*, 1863-1871.

92. Yano, S., Komine, M., Fujimoto, M., Okochi, H., and Tamaki, K. (2004). Mechanical stretching in vitro regulates signal transduction pathways and cellular proliferation in human epidermal keratinocytes. J Invest Dermatol *122*, 783-790.

93. Hecht, D., and Zick, Y. (1992). Selective inhibition of protein tyrosine phosphatase activities by H2O2 and vanadate in vitro. Biochem Biophys Res Commun *188*, 773-779.

94. Helin, K., Velu, T., Martin, P., Vass, W.C., Allevato, G., Lowy, D.R., and Beguinot, L. (1991). The biological activity of the human epidermal growth factor receptor is positively regulated by its C-terminal tyrosines. Oncogene *6*, 825-832.

95. Mitamura, T., Higashiyama, S., Taniguchi, N., Klagsbrun, M., and Mekada, E. (1995). Diphtheria toxin binds to the epidermal growth factor (EGF)-like domain of human heparin-binding EGF-like growth factor/diphtheria toxin receptor and inhibits specifically its mitogenic activity. J Biol Chem *270*, 1015-1019.

96. Baskin, L.S., Sutherland, R.S., Thomson, A.A., Hayward, S.W., and Cunha, G.R. (1996). Growth factors and receptors in bladder development and obstruction. Lab Invest *75*, 157-166.

97. Nguyen, H.T., Adam, R.M., Bride, S.H., Park, J.M., Peters, C.A., and Freeman, M.R. (2000). Cyclic stretch activates p38 SAPK2-, ErbB2-, and AT1-dependent signaling in bladder smooth muscle cells. Am J Physiol Cell Physiol *279*, C1155-1167.

98. Cheng, J., Huang, H., Zhang, Z.T., Shapiro, E., Pellicer, A., Sun, T.T., and Wu, X.R. (2002). Overexpression of epidermal growth factor receptor in urothelium elicits urothelial hyperplasia and promotes bladder tumor growth. Cancer Res *62*, 4157-4163.

99. Bindels, E.M., van der Kwast, T.H., Izadifar, V., Chopin, D.K., and de Boer, W.I. (2002). Functions of epidermal growth factor-like growth factors during human urothelial reepithelialization in vitro and the role of erbB2. Urol Res *30*, 240-247.

100. Krepinsky, J.C., Li, Y., Chang, Y., Liu, L., Peng, F., Wu, D., Tang, D., Scholey, J., and Ingram, A.J. (2005). Akt mediates mechanical strain-induced collagen production by mesangial cells. J Am Soc Nephrol *16*, 1661-1672.

101. Iwasaki, H., Eguchi, S., Ueno, H., Marumo, F., and Hirata, Y. (2000). Mechanical stretch stimulates growth of vascular smooth muscle cells via epidermal growth factor receptor. Am J Physiol Heart Circ Physiol *278*, H521-529.

102. Sanchez-Esteban, J., Wang, Y., Gruppuso, P.A., and Rubin, L.P. (2004). Mechanical stretch induces fetal type II cell differentiation via an epidermal growth factor receptor-extracellular-regulated protein kinase signaling pathway. Am J Respir Cell Mol Biol *30*, 76-83.

103. Kudoh, S., Komuro, I., Hiroi, Y., Zou, Y., Harada, K., Sugaya, T., Takekoshi, N., Murakami, K., Kadowaki, T., and Yazaki, Y. (1998). Mechanical stretch induces hypertrophic responses in cardiac myocytes of angiotensin II type 1a receptor knockout mice. J Biol Chem *273*, 24037-24043.

104. Lax, I., Bellot, F., Howk, R., Ullrich, A., Givol, D., and Schlessinger, J. (1989). Functional analysis of the ligand binding site of EGF-receptor utilizing chimeric chicken/human receptor molecules. Embo J *8*, 421-427.

105. Daub, H., Weiss, F.U., Wallasch, C., and Ullrich, A. (1996). Role of transactivation of the EGF receptor in signalling by G-protein-coupled receptors. Nature *379*, 557-560.

106. Milenkovic, I., Weick, M., Wiedemann, P., Reichenbach, A., and Bringmann, A. (2003). P2Y receptor-mediated stimulation of Muller glial cell DNA synthesis: dependence on EGF and PDGF receptor transactivation. Invest Ophthalmol Vis Sci *44*, 1211-1220.

107. Mount, C.D., Lukas, T.J., and Orth, D.N. (1985). Purification and characterization of epidermal growth factor (beta-urogastrone) and epidermal growth factor fragments from large volumes of human urine. Arch Biochem Biophys *240*, 33-42.

108. Sun, Y., Keay, S., De Deyne, P.G., and Chai, T.C. (2001). Augmented stretch activated adenosine triphosphate release from bladder uroepithelial cells in patients with interstitial cystitis. J Urol *166*, 1951-1956.

109. Li, C., and Xu, Q. (2000). Mechanical stress-initiated signal transductions in vascular smooth muscle cells. Cell Signal *12*, 435-445.

110. Ruwhof, C., and van der Laarse, A. (2000). Mechanical stress-induced cardiac hypertrophy: mechanisms and signal transduction pathways. Cardiovascular research *47*, 23-37.

111. Zwick, E., Hackel, P.O., Prenzel, N., and Ullrich, A. (1999). The EGF receptor as central transducer of heterologous signalling systems. Trends in pharmacological sciences *20*, 408-412.

112. Wang, E.C., Lee, J.M., Johnson, J.P., Kleyman, T.R., Bridges, R., and Apodaca, G. (2003). Hydrostatic pressure-regulated ion transport in bladder uroepithelium. Am J Physiol Renal Physiol *285*, F651-663.

113. Sun, Y., Chen, M., Lowentritt, B.H., Van Zijl, P.S., Koch, K.R., Keay, S., Simard, J.M., and Chai, T.C. (2007). EGF and HB-EGF modulate inward potassium current in human bladder urothelial cells from normal and interstitial cystitis patients. Am J Physiol Cell Physiol *292*, C106-114.

114. Boonstra, J., Moolenaar, W.H., Harrison, P.H., Moed, P., van der Saag, P.T., and de Laat, S.W. (1983). Ionic responses and growth stimulation induced by nerve growth factor and epidermal growth factor in rat pheochromocytoma (PC12) cells. J Cell Biol *97*, 92-98.

115. Shen, J.P., and Cotton, C.U. (2003). Epidermal growth factor inhibits amiloride-sensitive sodium absorption in renal collecting duct cells. Am J Physiol Renal Physiol *284*, F57-64.

116. Bryant, J.A., Finn, R.S., Slamon, D.J., Cloughesy, T.F., and Charles, A.C. (2004). EGF activates intracellular and intercellular calcium signaling by distinct pathways in tumor cells. Cancer biology & therapy *3*, 1243-1249.

117. Gutkind, J.S. (1998). Cell growth control by G protein-coupled receptors: from signal transduction to signal integration. Oncogene *17*, 1331-1342.

118. Park, J.M., Borer, J.G., Freeman, M.R., and Peters, C.A. (1998). Stretch activates heparin-binding EGF-like growth factor expression in bladder smooth muscle cells. Am J Physiol *275*, C1247-1254.

119. Harrell, P.C., McCawley, L.J., Fingleton, B., McIntyre, J.O., and Matrisian, L.M. (2005). Proliferative effects of apical, but not basal, matrix metalloproteinase-7 activity in polarized MDCK cells. Exp Cell Res *303*, 308-320.

120. Prenzel, N., Zwick, E., Daub, H., Leserer, M., Abraham, R., Wallasch, C., and Ullrich, A. (1999). EGF receptor transactivation by G-protein-coupled receptors requires metalloproteinase cleavage of proHB-EGF. Nature *402*, 884-888.

121. Eguchi, S., Dempsey, P.J., Frank, G.D., Motley, E.D., and Inagami, T. (2001). Activation of MAPKs by angiotensin II in vascular smooth muscle cells. Metalloprotease-dependent EGF receptor activation is required for activation of ERK and p38 MAPK but not for JNK. J Biol Chem *276*, 7957-7962.

122. Kansra, S., Stoll, S.W., Johnson, J.L., and Elder, J.T. (2004). Autocrine extracellular signal-regulated kinase (ERK) activation in normal human keratinocytes: metalloproteinase-mediated release of amphiregulin triggers signaling from ErbB1 to ERK. Mol Biol Cell *15*, 4299-4309.

123. Ohtsu, H., Dempsey, P.J., and Eguchi, S. (2006). ADAMs as mediators of EGF receptor transactivation by G protein-coupled receptors. Am J Physiol Cell Physiol *291*, C1-10.

124. Erickson, D.R., Kunselman, A.R., Bentley, C.M., Peters, K.M., Rovner, E.S., Demers, L.M., Wheeler, M.A., and Keay, S.K. (2007). Changes in urine markers and symptoms after bladder distention for interstitial cystitis. J Urol *177*, 556-560.

125. Martinez-Arca, S., Bech-Serra, J.J., Hurtado-Kuttner, M., Borroto, A., and Arribas, J. (2005). Recycling of cell surface pro-transforming growth factor-{alpha} regulates epidermal growth factor receptor activation. J Biol Chem *280*, 36970-36977.

126. Callegari, C., Laborde, N.P., Buenaflor, G., Nascimento, C.G., Brasel, J.A., and Fisher, D.A. (1988). The source of urinary epidermal growth factor in humans. Eur J Appl Physiol Occup Physiol *58*, 26-31.

127. Liang, F., Kachar, B., Ding, M., Zhai, Z., Wu, X.R., and Sun, T.T. (1999). Urothelial hinge as a highly specialized membrane: detergent-insolubility, urohingin association, and in vitro formation. Differentiation *65*, 59-69.

128. Lim, K.I., and Yin, J. (2005). Localization of receptors in lipid rafts can inhibit signal transduction. Biotechnology and bioengineering *90*, 694-702.

129. Roepstorff, K., Thomsen, P., Sandvig, K., and van Deurs, B. (2002). Sequestration of epidermal growth factor receptors in non-caveolar lipid rafts inhibits ligand binding. J Biol Chem *277*, 18954-18960.

130. Pike, L.J., and Casey, L. (2002). Cholesterol levels modulate EGF receptor-mediated signaling by altering receptor function and trafficking. Biochemistry *41*, 10315-10322.

131. N'Dow, J., Pearson, J.P., Bennett, M.K., Neal, D.E., and Robson, C.N. (2000). Mucin gene expression in human urothelium and in intestinal segments transposed into the urinary tract. J Urol *164*, 1398-1404.

132. Ramsauer, V.P., Carraway, C.A., Salas, P.J., and Carraway, K.L. (2003). Muc4/sialomucin complex, the intramembrane ErbB2 ligand, translocates ErbB2 to the apical surface in polarized epithelial cells. J Biol Chem *278*, 30142-30147.

133. Gendler, S.J. (2001). MUC1, the renaissance molecule. Journal of mammary gland biology and neoplasia *6*, 339-353.

134. Klein, P., Mattoon, D., Lemmon, M.A., and Schlessinger, J. (2004). A structure-based model for ligand binding and dimerization of EGF receptors. Proceedings of the National Academy of Sciences of the United States of America *101*, 929-934.

135. Bouyain, S., Longo, P.A., Li, S., Ferguson, K.M., and Leahy, D.J. (2005). The extracellular region of ErbB4 adopts a tethered conformation in the absence of ligand. Proceedings of the National Academy of Sciences of the United States of America *102*, 15024-15029.

136. Ferguson, K.M., Berger, M.B., Mendrola, J.M., Cho, H.S., Leahy, D.J., and Lemmon, M.A. (2003). EGF activates its receptor by removing interactions that autoinhibit ectodomain dimerization. Molecular cell *11*, 507-517.

137. Habel, M. (2002). Understanding Urinalysis. (Sierra Vista, AZ: RnCeus Interactive, LLC).

138. Moro, L., Venturino, M., Bozzo, C., Silengo, L., Altruda, F., Beguinot, L., Tarone, G., and Defilippi, P. (1998). Integrins induce activation of EGF receptor: role in MAP kinase induction and adhesion-dependent cell survival. Embo J *17*, 6622-6632.

139. Clark, E.A., and Brugge, J.S. (1995). Integrins and signal transduction pathways: the road taken. Science (New York, N.Y *268*, 233-239.

140. Low, S.Y., and Taylor, P.M. (1998). Integrin and cytoskeletal involvement in signalling cell volume changes to glutamine transport in rat skeletal muscle. The Journal of physiology *512 (Pt 2)*, 481-485.

141. Yarden, Y. (2001). The EGFR family and its ligands in human cancer. signalling mechanisms and therapeutic opportunities. Eur J Cancer *37 Suppl 4*, S3-8.

142. Varley, C.L., Garthwaite, M.A., Cross, W., Hinley, J., Trejdosiewicz, L.K., and Southgate, J. (2006). PPARgamma-regulated tight junction development during human urothelial cytodifferentiation. J Cell Physiol *208*, 407-417.

143. Singh, A.B., and Harris, R.C. (2004). Epidermal growth factor receptor activation differentially regulates claudin expression and enhances transepithelial resistance in Madin-Darby canine kidney cells. J Biol Chem *279*, 3543-3552.

144. Rebel, J.M., De Boer, W.I., Thijssen, C.D., Vermey, M., Zwarthoff, E.C., and Van der Kwast, T.H. (1994). An in vitro model of urothelial regeneration: effects of growth factors and extracellular matrix proteins. The Journal of pathology *173*, 283-291.

145. Messing, E.M., Hanson, P., Ulrich, P., and Erturk, E. (1987). Epidermal growth factor--interactions with normal and malignant urothelium: in vivo and in situ studies. J Urol *138*, 1329-1335.

146. (2006). Cancer Facts and Figures - 2006. In Cancer Facts and Figures - 2006, A.C. Society, ed. (Atlanta, Georgia).

147. Chow, N.H., Liu, H.S., Lee, E.I., Chang, C.J., Chan, S.H., Cheng, H.L., Tzai, T.S., and Lin, J.S. (1997). Significance of urinary epidermal growth factor and its receptor expression in human bladder cancer. Anticancer research *17*, 1293-1296.

148. Messing, E.M. (1992). Growth factors and bladder cancer: clinical implications of the interactions between growth factors and their urothelial receptors. Seminars in surgical oncology *8*, 285-292.

149. Neal, D.E., and Mellon, K. (1992). Epidermal growth factor receptor and bladder cancer: a review. Urologia internationalis *48*, 365-371.

150. Messing, E.M., and Murphy-Brooks, N. (1994). Recovery of epidermal growth factor in voided urine of patients with bladder cancer. Urology *44*, 502-506.

151. Popov, Z., Gil-Diez-De-Medina, S., Ravery, V., Hoznek, A., Bastuji-Garin, S., Lefrere-Belda, M.A., Abbou, C.C., and Chopin, D.K. (2004). Prognostic value of EGF receptor and tumor cell proliferation in bladder cancer: therapeutic implications. Urol Oncol *22*, 93-101.

152. Kenny, P.A., and Bissell, M.J. (2007). Targeting TACE-dependent EGFR ligand shedding in breast cancer. J Clin Invest *117*, 337-345.

153. Zucker, S., Hymowitz, M., Conner, C., Zarrabi, H.M., Hurewitz, A.N., Matrisian, L., Boyd, D., Nicolson, G., and Montana, S. (1999). Measurement of matrix metalloproteinases and tissue inhibitors of metalloproteinases in blood and tissues. Clinical and experimental applications. Annals of the New York Academy of Sciences *878*, 212-227.

154. Ongusaha, P.P., Kwak, J.C., Zwible, A.J., Macip, S., Higashiyama, S., Taniguchi, N., Fang, L., and Lee, S.W. (2004). HB-EGF is a potent inducer of tumor growth and angiogenesis. Cancer Res *64*, 5283-5290.

155. Kim, J., Adam, R.M., and Freeman, M.R. (2005). Trafficking of nuclear heparin-binding epidermal growth factor-like growth factor into an epidermal growth factor receptor-dependent autocrine loop in response to oxidative stress. Cancer Res *65*, 8242-8249.

156. O-Charoenrat, P., Modjtahedi, H., Rhys-Evans, P., Court, W.J., Box, G.M., and Eccles, S.A. (2000). Epidermal growth factor-like ligands differentially up-regulate matrix metalloproteinase 9 in head and neck squamous carcinoma cells. Cancer Res *60*, 1121-1128.

157. Nutt, J.E., and Lunec, J. (1996). Induction of metalloproteinase (MMP1) expression by epidermal growth factor (EGF) receptor stimulation and serum deprivation in human breast tumour cells. Eur J Cancer *32A*, 2127-2135.

158. Kassouf, W., Dinney, C.P., Brown, G., McConkey, D.J., Diehl, A.J., Bar-Eli, M., and Adam, L. (2005). Uncoupling between epidermal growth factor receptor and downstream signals defines resistance to the antiproliferative effect of Gefitinib in bladder cancer cells. Cancer Res *65*, 10524-10535.

159. Lewis, S.A.C., Chris; Willis, N.K. (1996). Impedance analysis of Epithelia. In Epithelial Transport: A Guide to Methods and Experimental Analysis, L.R. Nancy K. Wills, and Simon A. Lewis, ed. (New York: Chapman & Hall), pp. 118-145.

160. Apodaca, G., Katz, L.A., and Mostov, K.E. (1994). Receptor-mediated transcytosis of IgA in MDCK cells is via apical recycling endosomes. J Cell Biol *125*, 67-86.

161. Truschel, S.T., Ruiz, W.G., Shulman, T., Pilewski, J., Sun, T.T., Zeidel, M.L., and Apodaca, G. (1999). Primary uroepithelial cultures. A model system to analyze umbrella cell barrier function. J Biol Chem *274*, 15020-15029.

162. Viswanathan, S., Unlu, M., and Minden, J.S. (2006). Two-dimensional difference gel electrophoresis. Nature protocols *1*, 1351-1358.

163. Kong, X.T., Deng, F.M., Hu, P., Liang, F.X., Zhou, G., Auerbach, A.B., Genieser, N., Nelson, P.K., Robbins, E.S., Shapiro, E., et al. (2004). Roles of uroplakins in plaque formation, umbrella cell enlargement, and urinary tract diseases. J Cell Biol *167*, 1195-1204.